

# JOURNAL OF MATHEMATICAL SCIENCES AND MODELLING

---

ISSN: 2636-8692

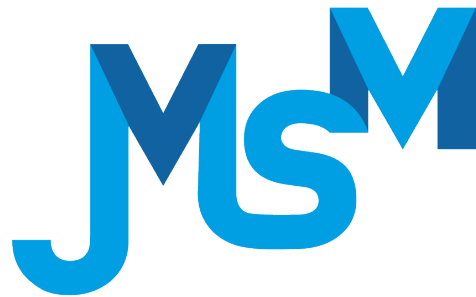
VOLUME VI  
ISSUE II

JMS<sup>M</sup>

VOLUME VI ISSUE II  
ISSN 2636-8692

August 2023  
<http://dergipark.gov.tr/jmsm>

# JOURNAL OF MATHEMATICAL SCIENCES AND MODELLING



---

## Editor in Chief

---

Mahmut Akyiğit  
Department of Mathematics,  
Faculty of Science, Sakarya University,  
Sakarya-TÜRKİYE  
makyigit@sakarya.edu.tr

---

## Assistant Editor

---

Emrah Evren Kara  
Department of Mathematics,  
Faculty of Science and Arts, Düzce University,  
Düzce-TÜRKİYE  
eevrenkara@duzce.edu.tr

---

## Editorial Board of Journal of Mathematical Sciences and Modelling

---

Ioannis Dassios  
University College Dublin,  
IRELAND

Galip Oturanç  
Karamanoglu Mehmet Bey University,  
TÜRKİYE

Mujahid Abbas  
University of Pretoria,  
SOUTH AFRICA

Dağıştan Şimşek  
Konya Technical University,  
TÜRKİYE

Olena Sierikova  
National University of Civil Protection of Ukraine,  
UKRAINE

İrem Bağlan  
Kocaeli University,  
TÜRKİYE

---

## Statistics Editor

---

Melek Eriş Büyükkaya  
Karadeniz Technical University,  
TÜRKİYE

---

---

## **Language Editor**

---

Tolga Aktürk  
Yıldız Technical University,  
TÜRKİYE

---

## **Technical Editor**

---

Ayla Erdur Kara  
Tekirdag Namık Kemal University,  
TÜRKİYE

# Contents

- 1 Reduced Order Modelling of Shigesada–Kawasaki–Teramoto Cross-Diffusion Systems  
*Gülden MÜLAYİM* 42–48
- 2 Application of Fractional SPR Psychological Disease Model in Turkey and Stability Analysis  
*Zafer ÖZTÜRK, Halil BİLGİL, Sezer SORGUN* 49–55
- 3 Dynamical Analysis of a Local Lengley–Epstein System Coupled with Fractional Delayed Differential Equations  
*Ercan BALCI* 56–64
- 4 Qualitative Study of A Discrete–Time Harvested Fishery Model in the Presence of Toxicity  
*Debasis MUKHERJEE* 65–75
- 5 Quantitative Aeroelastic Stability Prediction of Wings Exhibiting Nonlinear Restoring Forces  
*Aykut TAMER* 76–86

# Reduced Order Modelling of Shigesada-Kawasaki-Teramoto Cross-Diffusion Systems

Gülden Mülayim<sup>1</sup>

<sup>1</sup>Department of Mathematics, Faculty of Science and Arts, Adıyaman University, Adıyaman, Türkiye

## Article Info

**Keywords:** Discrete empirical interpolation method, Discontinuous Galerkin method, Proper orthogonal decomposition, Shigesada-Kawasaki-Teramoto equation.

**2010 AMS:** 37N25, 35K57, 35K61, 65M06, 65L05, 34C20

**Received:** 14 January 2023

**Accepted:** 6 March 2023

**Available online:** 9 May 2023

## Abstract

Shigesada-Kawasaki-Teramoto (SKT) is the most known equation in population ecology for nonlinear cross-diffusion systems. The full order model (FOM) of the SKT system is constructed using symmetric interior penalty discontinuous Galerkin method (SIPG) in space and the semi-implicit Euler method in time. The reduced order models (ROMs) are solved using proper orthogonal decomposition (POD) Galerkin projection. Discrete empirical interpolation method (DEIM) is used to solve the nonlinearities of the SKT system. Numerical simulations show the accuracy and efficiency of the POD and POD-DEIM reduced solutions for the SKT system.

## 1. Introduction

The nonlinear cross-diffusion systems has a general form which is given by  $z = (z_1, \dots, z_M) : \Omega \times [0, T] \rightarrow \mathbb{R}^M$  such that

$$\begin{aligned} \frac{\partial \mathbf{z}}{\partial t} &= \Delta \beta(\mathbf{z}) + f(\mathbf{z}) \quad \text{in } \Omega \times (0, T] \\ \frac{\partial \beta(\mathbf{z})}{\partial n} &= 0 \quad \text{on } \partial \Omega \times (0, T) \\ \mathbf{z}(\cdot, 0) &= \mathbf{z}^0 \quad \text{in } \Omega, \end{aligned} \quad (1.1)$$

where  $\Omega \subset \mathbb{R}^d$ ; ( $d = 1, 2$ ) is a bounded domain,  $\partial \Omega$  is a smooth boundary,  $T$  is a positive constant,  $z^0 = (z_1^0, \dots, z_M^0) : \Omega \rightarrow \mathbb{R}^M$  are population densities,  $\beta = (\beta_1, \dots, \beta_M)$ ,  $f = (f_1, \dots, f_M) : \mathbb{R}^M \rightarrow \mathbb{R}^M$  are nonlinear functions of population densities, and  $n$  is the unit outward normal vector to the boundary  $\partial \Omega$  [1].

The most known and popular nonlinear cross-diffusion system is the Shigesada-Kawasaki-Teramato (SKT) equation with Lotka-Volterra kinetics [2] in population ecology. The SKT system represents the spatial and temporal behavior of two species under population pressure due to intra and interspecific interference. The interaction of two species may cause different diffusion rates. This leads to destabilization of the constant steady-state and occurs a pattern formation like labyrinth, spot and stripe. The SKT system with Lotka-Volterra kinetics is defined as [3]

$$\frac{\partial z_1}{\partial t} = \Delta \underbrace{(a_1 + b_1 z_1 + c_1 z_2)}_{\beta_1} z_1 + \Gamma \underbrace{(\mu_1 - \gamma_{11} z_1 - \gamma_{12} z_2)}_{f_1} z_1, \quad (1.2)$$

$$\frac{\partial z_2}{\partial t} = \Delta \underbrace{(a_2 + b_2 z_2 + c_2 z_1)}_{\beta_2} z_2 + \Gamma \underbrace{(\mu_2 - \gamma_{21} z_1 - \gamma_{22} z_2)}_{f_2} z_2 \quad (1.3)$$

where  $\beta_1, \beta_2$  are the nonlinear cross-diffusion and  $f_1, f_2$  are the Lotka-Volterra kinetics, and  $a_i, b_i, c_i, \gamma_{ij}$  ( $i, j = 1, 2$ ) are nonnegative constants. The constants  $\mu_i$  denote the intrinsic growth rates,  $\gamma_{ii}$  the intraspecific competition coefficients, and  $\gamma_{ij}$  ( $i \neq j$ ) the interspecific

competition rates. The  $i^{th}$  species keeps away from high-density areas of the  $j^{th}$  species due to cross-diffusion terms. The parameter  $\Gamma$  represents the relative strength of the reaction terms. SKT systems are not a simple nonlinear problem when it comes to dealing with the cross-diffusivities. Therefore, it is more useful for the analysis of SKT systems to remove the cross-diffusion component. Murakawa [1, 4] proposed an approximation to the SKT system (1.2) by a semilinear reaction-diffusion system. In this approximation, the system has a simple reaction and linear diffusion terms. Nonlinear problems are difficult to solve compared to semilinear problems. Various methods can be considered for discretizing semilinear systems, such as the finite element approximation [5], the finite difference method [6], and the finite volume approximation [7].

In this paper, symmetric interior penalty discontinuous Galerkin finite elements (SIPG) method [8] for spatial discretization and semi-implicit Euler method for temporal discretization [1, 3, 9] are considered. The SIPG approximation uses discontinuous polynomials and captures singularities locally. Even though fully implicit methods provide better accuracy and stability, they are not easy to implement when dealing with semilinear reaction-diffusion systems. The semi-implicit Euler method is easy to implement and is a stable numerical method. Recently, model order reduction techniques are developed for the dimension reduction of large dynamic systems in engineering and science. The main idea of reduced order modelling is to construct basis functions in a low-dimensional reduced space and then project the full order model equation onto the reduced space to obtain a reduced order system. The most known and most commonly used technique is proper orthogonal decomposition (POD) [10, 11]. In POD method, the Galerkin projection is used to approximate reduced solutions. POD is a useful method for linear problems, but for nonlinear problems, the dimension of the solutions of the reduced order model (ROM) has the same dimension as the solutions of the full order model (FOM) [12]. To reduce the computational cost of the nonlinear terms in the reduced order model, some methods have been developed. The empirical interpolation method (EIM) [13] and the discrete empirical interpolation method (DEIM) [14] are the most commonly used methods. The DEIM method is introduced for nonlinear functions. The nonlinear kinetics depends on single variables in the finite difference method while it depends on the mesh and the degree of the polynomial in the finite element methods. Therefore, the POD-DEIM is developed for efficiency [15, 16]. The reduced basis functions in POD-DEIM are computed in the offline phase by applying singular value decomposition (SVD) to large snapshot matrices. Randomized singular value decomposition (rSVD) [17, 18] is used as a fast and accurate method. By using rSVD in the offline phase, the computational cost is reduced. This paper is divided into the following sections: In Section 2, the full discrete solution of the SKT system in space and time discretization is obtained. The model order reduction methods POD and DEIM are described in Section 3. Numerical simulations are presented for the SKT equation in two-dimensional case in Section 4.

## 2. Full Order Model

The SKT system (1.2- 1.3) has a nonlinear diffusion part. To remove the nonlinear diffusion part, a semi-linear reaction-diffusion system is proposed to approximate (1.2- 1.3) [9]:

$$\begin{aligned} \frac{\partial \mathbf{u}}{\partial t} &= \frac{1}{\nu} \Delta \mathbf{u} - \frac{1}{\varepsilon} (\mathbf{u} - \beta(\nu \mathbf{u} + \mathbf{v})) + \frac{1}{\varepsilon} f(\nu \mathbf{u} + \mathbf{v}) \quad \text{in } \Omega \times (0, T), \\ \frac{\partial \mathbf{v}}{\partial t} &= \frac{\nu}{\varepsilon} \mathbf{u} - \beta(\nu \mathbf{u} + \mathbf{v}), \quad \text{in } \Omega \times (0, T), \\ \frac{\partial \mathbf{u}}{\partial n} &= 0, \quad \text{on } \partial \Omega \times (0, T), \\ \mathbf{u}(\cdot, 0) &= \mathbf{u}^{0, \varepsilon}, \quad \mathbf{v}(\cdot, 0) = \mathbf{v}^{0, \varepsilon} \quad \text{in } \Omega. \end{aligned} \tag{2.1}$$

where  $u$  and  $v$  are the population densities and  $z = u + v$  is taken in equation (1.2). Then, the weak solutions  $\mathbf{u}^\varepsilon$  and  $\mathbf{v}^\varepsilon$  are approximations to  $\beta(\mathbf{z})$  and  $(\mathbf{z} - \nu \beta(\mathbf{z}))$ , where  $\nu$  and  $\varepsilon$  are positive parameters. The initial conditions are approximated as  $\mathbf{u}^{0, \varepsilon} \approx \beta(\mathbf{z}^0)$  and  $\mathbf{v}^{0, \varepsilon} \approx (\mathbf{z}^0 - \nu \beta(\mathbf{z}^0))$ . In (2.1), the system (1.1) is approximated by a system of  $M$  semilinear PDEs coupled with  $M$  ordinary differential equations (ODEs), which has the advantage of solving semi-linear problems instead of nonlinear systems.

The semi-discrete systems (2.1) is discretized by semi-implicit Euler method in time [1]:

$$\begin{aligned} \frac{U_i^n - U_i^{n-1}}{\tau} &= \frac{1}{\mu} \Delta U_i^n - \frac{1}{\varepsilon} (U_i^{n-1} - \beta(\mu U_i^{n-1} + V_i^{n-1})) + \frac{1}{\mu} f(\mu U_i^{n-1} + V_i^{n-1}) \quad \text{in } \Omega \\ \frac{\partial U_i^n}{\partial \nu} &= 0 \quad \text{on } \partial \Omega \\ \frac{V_i^n - V_i^{n-1}}{\tau} &= \frac{\mu}{\varepsilon} (U_i^{n-1} - \beta(\mu U_i^{n-1} + V_i^{n-1})) \quad \text{in } \Omega \end{aligned}$$

where the time step size  $\tau$  is given by  $\frac{T}{N_T}$  and  $n = 1, 2, \dots, N_T$ ,  $i = 1, 2$ . The scheme can be rewritten by setting  $Z_i^n = \mu U_i^n + V_i^n$ , choosing  $\varepsilon = \tau$  and adding  $\mu U_i^n$  on both sides to the third relation, then the following semi-linear scheme is obtained

$$\begin{aligned} U_i^n - \frac{\tau}{\mu} \Delta U_i^n &= \beta(Z_i^{n-1}) + \frac{\tau}{\mu} f(Z_i^{n-1}) \quad \text{in } \Omega, \\ \frac{\partial U_i^n}{\partial \nu} &= 0 \quad \text{on } \partial \Omega, \\ Z_i^n &= Z_i^{n-1} + \mu (U_i^n - \beta(Z_i^{n-1})) \quad \text{in } \Omega, \end{aligned} \tag{2.2}$$

where  $Z_i^n$  and  $U_i^n$  solutions are approximations to  $z(\cdot, n\tau)$  and  $\beta(z(\cdot, n\tau))$ , respectively. A simple system of equations is obtained to solve. Here  $M$  independent linear equations is solved in  $U_i^n$  and then  $Z_i^n$  is calculated.

Symmetric interior penalty Galerkin (SIPG) method is used to obtain a fully discrete system to (1.2) in space discretization. The continuous weak solutions (2.2) solve the variational formulation

$$(U_i^n, w_i) + a\left(\frac{\tau}{\mu}; U_i^n, w_i\right) = (\beta(Z_i^{n-1}), w_i) + \left(\frac{\tau}{\mu}; Z_i^{n-1}, w_i\right)$$

where the  $L^2$  inner product is defined as  $(\cdot, \cdot) = (\cdot, \cdot)_\Omega$  on the domain  $\Omega$ , and  $a\left(\frac{\tau}{\mu}; U_i^n, w_i\right) = (d\nabla u, \nabla w)$  is the bilinear form.

$\{\mathcal{T}_h\}$  is a disjoint partition of the domain  $\Omega$  with triangles  $\{T_i\}_{i=1}^{N_{el}} \in \mathcal{T}_h$  where  $N_{el}$  is the number of elements in the partition. The space of discrete solution and test functions is defined as

$$D_h = \{w \in L^2(\Omega) : w_K \in \mathbb{P}_d(K), \quad \forall K \in \mathcal{T}_h\},$$

where  $\mathbb{P}_d(K)$  is the set of polynomials defined on  $K \in \mathcal{T}_h$  of degree at most  $d$ . (2.2) is multiplied by test functions  $w_i$ , integrated over each mesh element, Green's theorem is used and the variational formulation is obtained:

$$(U_{ih}^n, w_i) + a_h\left(\frac{\tau}{\mu}; U_{ih}^n, w_i\right) = (\beta(Z_{ih}^{n-1}), w_i) + \left(\frac{\tau}{\mu}; Z_{ih}^{n-1}, w_i\right) \quad (2.3)$$

with the SIPG bilinear form as follows

$$\begin{aligned} a_h\left(\frac{\tau}{\mu}; U^n, w\right) &= \sum_{K \in \mathcal{T}_h} \int_K \frac{\tau}{\mu} \nabla U \cdot \nabla w dx - \sum_{E \in \mathcal{E}_h^0 \cup \mathcal{E}_h^p} \int_E \left\{ \frac{\tau}{\mu} \nabla U \right\} \cdot [w] ds + \\ &\quad \sum_{E \in \mathcal{E}_h^0 \cup \mathcal{E}_h^p} \int_E \left\{ \frac{\tau}{\mu} \nabla w \right\} \cdot [U] + \sum_{E \in \mathcal{E}_h^0 \cup \mathcal{E}_h^p} \frac{\sigma}{h} \frac{\tau}{\mu} \int_E [u] \cdot [w] ds \end{aligned}$$

where  $h$  denotes the length of edge  $e$ ,  $\mathcal{E}_h^0$  denotes the set of interior faces (edges),  $[\cdot]$ , and  $\{\cdot\}$  denotes the jump and the average, respectively. The semi-discrete solutions are given as

$$U_{ih} = \sum_{k=1}^{n_e} \sum_{m=1}^{n_l} u_m^k(t) \varphi_m^k(x), \quad i = 1, 2,$$

where  $u_m^k$  is the unknown vectors,  $\varphi_m^k$  are the basis functions in  $D_h$ , for  $k = 1, 2, \dots, n_e$ , and  $m = 1, 2, \dots, n_l$ . The number  $n_e$  is the number of triangles in  $\mathcal{T}_h$ , and  $n_l$  is the local dimension on each element given by  $n_l = (d+1)(d+2)/2$ , where  $d$  is the degree of polynomial order. Then the SIPG system (2.3) leads to a full order solution (FOM):

$$MU + \frac{\tau}{\mu} AU = \beta_1(Z_1^{n-1}) + \frac{\tau}{\mu} f(Z_1^{n-1}) \quad (2.4)$$

$$MZ_1^n = MZ_1^{n-1} + \mu(MU^n - \beta_1(Z_1^{n-1})) \quad (2.5)$$

$$MV + \frac{\tau}{\mu} AV = \beta_2(Z_2^{n-1}) + \frac{\tau}{\mu} g(Z_2^{n-1}) \quad (2.6)$$

$$MZ_2^n = MZ_2^{n-1} + \mu(MV^n - \beta_2(Z_2^{n-1})),$$

where  $M \in \mathbb{R}^{N \times N}$  is the mass matrix, and  $A \in \mathbb{R}^{N \times N}$  is the stiffness matrix. The number  $N = N_{loc} \times N_{el}$  indicates the degree of freedom in the DG method, where  $N_{loc}$  is the number of local dimensions in each triangle and  $N_{el}$  represents the number of elements. Moreover,  $F(Z) = \beta_1(Z^{n-1}) + \frac{\tau}{\mu} f(Z^{n-1})$  and  $G(Z) = \beta_2(Z^{n-1}) + \frac{\tau}{\mu} g(Z^{n-1}) \in \mathbb{R}^N$  are nonlinear forms. Then the solutions of 2.4 and 2.6 have the following form:

$$U(t) = \sum_{i=1}^N u_i(t) \varphi_i(x) = \boldsymbol{\varphi} \mathbf{u}(t), \quad V(t) = \sum_{i=1}^N v_i(t) \varphi_i(x) = \boldsymbol{\varphi} \mathbf{v}(t) \quad (2.7)$$

where  $u_i(t), v_i(t)$  are the unknown coefficients and  $\varphi_i$  are the DG basis functions.

### 3. Reduced Order Model

In this section, the reduced order model (ROM) is introduced for nonlinear cross-diffusion systems. Proper orthogonal decomposition (POD) method with Galerkin projection [12] and the discrete empirical interpolation method (DEIM) for nonlinear reaction terms are considered for the SKT system.

#### 3.1. Proper orthogonal decomposition

The FOM solutions  $U(t)$  and  $V(t)$  (2.4) approximate the ROM solutions of dimension  $k \ll N$  onto subspaces spanned by a set of  $L^2$ -orthogonal basis functions  $\{\psi_u\}_{i=1}^k$  and  $\{\psi_v\}_{i=1}^k$

$$U(t) = \sum_{i=1}^k \tilde{U}_i(t) \psi_u, \quad V(t) = \sum_{i=1}^k \tilde{V}_i(t) \psi_v \quad (3.1)$$

where  $\tilde{U}(t) = (\tilde{U}_1(t), \dots, \tilde{U}_k(t))$  and  $\tilde{V}(t) = (\tilde{V}_1(t), \dots, \tilde{V}_k(t))$  are the coefficient vectors of the ROM solutions. The reduced basis functions  $\{\psi_u\}_{i=1}^k$  and  $\{\psi_v\}_{i=1}^k$  are in the form of linear combination of the DG basis functions  $\{\varphi_i\}_{i=1}^N$

$$\Psi_{u,i} = \sum_{j=1}^N \Psi_{u,j,i} \varphi_j(x), \quad \Psi_{v,i} = \sum_{j=1}^N \Psi_{v,j,i} \varphi_j(x) \quad (3.2)$$

The coefficient vectors of the reduced basis function  $\Psi_{u,i}$  and  $\Psi_{v,i}$  are in the columns of the matrices  $\Psi_u = [\Psi_{u,.,1}, \dots, \Psi_{u,.,k}]$  and  $\Psi_v = [\Psi_{v,.,1}, \dots, \Psi_{v,.,k}]$ .

The reduced basis functions are calculated by applying randomized singular value decomposition (rSVD) to the snapshot matrix

$$S_1 = [U_1, \dots, U_N], \quad S_2 = [V_1, \dots, V_N]$$

where each component of  $S_1$  and  $S_2$  corresponds to the coefficient vectors of the discrete solutions of the FOM (2.4). The FOM and the ROM coefficient vectors have a relation using the expansion (2.7),(3.1),(3.2)

$$\mathbf{U} = \Psi_u \tilde{\mathbf{U}}, \quad \mathbf{V} = \Psi_v \tilde{\mathbf{V}} \quad (3.3)$$

$k$ -dimensional ROM is constructed by substituting (3.3) and projected onto the reduced subspace leading to the system

$$\begin{aligned} \tilde{M}_u \mathbf{U}^n + \frac{\tau}{\mu} \tilde{A}_u \mathbf{U}^n &= \Psi_u^T (\beta_1(\mathbf{z}_1^{n-1}) + \frac{\tau}{\mu} f_1(\mathbf{z}_1^{n-1})) \\ \tilde{M}_{z_1} \mathbf{z}_1^n &= \tilde{M}_{z_1} \mathbf{z}_1^{n-1} + \mu (\mathbf{U}^n - \Psi_u^T \beta_1(\mathbf{z}_1^{n-1})) \\ \tilde{M}_v \mathbf{V}^n + \frac{\tau}{\mu} \tilde{A}_v \mathbf{V}^n &= \Psi_v^T (\beta_2(\mathbf{z}_2^{n-1}) + \frac{\tau}{\mu} f_2(\mathbf{z}_2^{n-1})) \\ \tilde{M}_{z_2} \mathbf{z}_2^n &= \tilde{M}_{z_2} \mathbf{z}_2^{n-1} + \mu (\mathbf{V}^n - \Psi_v^T \beta_2(\mathbf{z}_2^{n-1})) \end{aligned}$$

with the reduced matrices

$$\begin{aligned} \tilde{M}_u &= \Psi_u^T M \Psi_u, & \tilde{A}_u &= \Psi_u^T A \Psi_u, & \tilde{M}_{z_1} &= \Psi_{z_1}^T M \Psi_{z_1}, \\ \tilde{M}_v &= \Psi_v^T M \Psi_v, & \tilde{A}_v &= \Psi_v^T A \Psi_v, & \tilde{M}_{z_2} &= \Psi_{z_2}^T M \Psi_{z_2}, \end{aligned}$$

### 3.2. Discrete empirical interpolation method

Though the reduced system has a smaller dimension than the full system, the dimension of the nonlinear vectors is the same as the dimension of the full system. DEIM is used to approximate the nonlinear vectors  $f(z(t)) = \Psi^T f(\Psi Z^{n-1})$  and  $\beta(z(t)) = \Psi^T \beta(\Psi Z^{n-1})$  from a subspace generated by the nonlinear functions.  $\mathcal{F} = [f_1, f_2, \dots, f_j] \in \mathbb{R}^{N \times J}$  and  $\mathcal{B} = [\beta_1, \beta_2, \dots, \beta_j] \in \mathbb{R}^{n \times J}$  represent the snapshot matrices of the nonlinear functions. rSVD is applied to the matrices  $\mathcal{F}$  and  $\mathcal{B}$ , and find  $m \ll N$  orthogonal basis functions  $\{Q_i\}_{i=1}^m$ . Then the approximation of the nonlinear functions is given by  $Q = [Q_1, Q_2, \dots, Q_m] \in \mathbb{R}^{N \times m}$

$$f(\Psi Z(t)) \approx Qh(t), \quad \beta(\Psi Z(t)) \approx Qh(t) \quad (3.4)$$

with the coefficient vector  $h(t)$ . The system (3.4) is overdetermined.  $m$  distinguished rows is taken from the system  $Qh(t)$  for the computation of  $h(t)$  through the projection matrix  $P = [e_{\rho_1}, \dots, e_{\rho_m}] \in \mathbb{R}^{N \times m}$  with  $e_{\rho_i} = [0, \dots, 0, \underbrace{1}_{\rho_i}, 0, \dots, 0] \in \mathbb{R}^N$ . Since  $P^T Q$  is nonsingular, the

coefficient vector  $h(t)$  can be written as with the projection:

$$h(t) = (P^T Q)^{-1} P^T f(\Psi_u Z(t)), \quad h(t) = (P^T Q)^{-1} P^T \beta(\Psi_u Z(t)) \quad (3.5)$$

Using the equations (3.4),(3.5) the nonlinear vectors can be approximated as follows

$$f(z(t)) \approx WF, \quad \beta(z(t)) \approx WB$$

where the matrix  $W = \Psi_u^T Q (P^T Q)^{-1} \in \mathbb{R}^{k \times m}$  is precomputable and  $F = P^T f(\Psi_u Z(t)) \in \mathbb{R}^m$  and  $B = P^T \beta(\Psi_u Z(t)) \in \mathbb{R}^m$  are the  $m$ -dimensional nonlinear vectors.

## 4. Numerical results

In this section, the numerical results for two-dimensional SKT system (1.2- 1.3) are presented. The solutions of FOM and ROM are compared with the results of POD and POD-DEIM.

The initial conditions are taken as a random perturbation around the stationary solutions  $(u_0, v_0) = (1.67, 0.92)$  given by using MATLAB function rand, uniformly distributed pseudo-random numbers. The parameters are set as follows

$$\begin{aligned} a_1 &= 0.01, & a_2 &= 0.001, & b &= 7.264, & b_2 &= 1.1, & c_1 &= 0.1, & c_2 &= 0.2 \\ \mu_1 &= 1.2, & \gamma_{11} &= 0.5, & \gamma_{12} &= 0.4, & \mu_2 &= 1, & \gamma_{21} &= 0.38, & \gamma_{22} &= 0.4, & \Gamma &= 28.05. \end{aligned}$$

The spatial interval is set to  $\Omega = [0, \sqrt{2\pi}] \times [0, 2\pi]$ . The time step size is taken as  $dt = 0.01$ .

In Figure 4.1, the FOM solutions of components  $Z_1$  and  $Z_2$  are plotted which are very close to those in [19]. In Figure 4.2, normalized singular values are plotted for each component and the nonlinear components. The singular values decrease very fast at the beginning. In Figure 4.3, the ROM solutions are obtained by using 3-POD and 24 and 21 DEIM basis functions for each component, respectively. The ROM solutions are almost the same as the FOM solutions. In Table 4.1, the  $L^2$ - relative errors for the POD and POD-DEIM solutions are presented. The results are acceptable since POD-DEIM is applied to the nonlinear part. CPU time and speed-up factors  $C_{POD}$  and  $C_{DEIM}$  are calculated for POD and POD-DEIM. The results show the increasing of the speed-up factors which represents the efficiency of POD-DEIM.

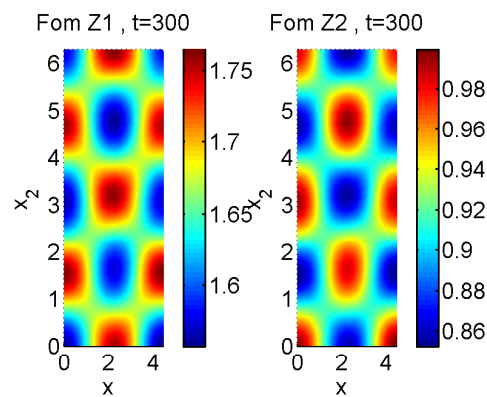


Figure 4.1: FOM solutions for the component  $Z_1$  and  $Z_2$ .

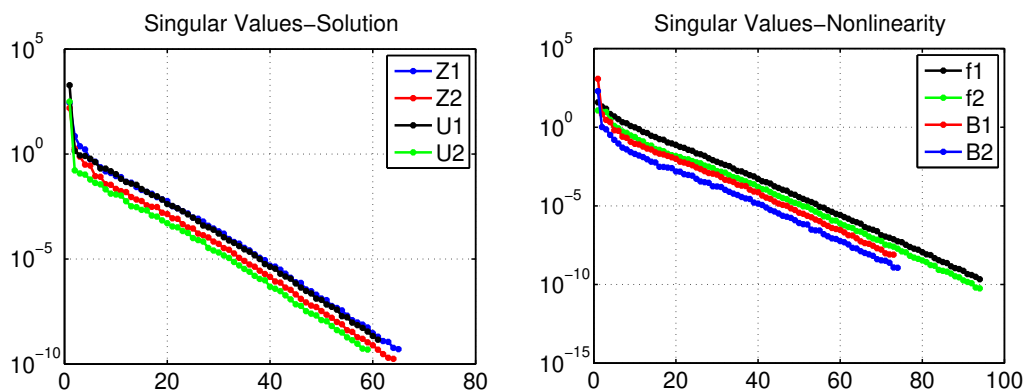


Figure 4.2: Decay of normalized singular values for the state components  $Z_1, Z_2, U_1$  and  $U_2$

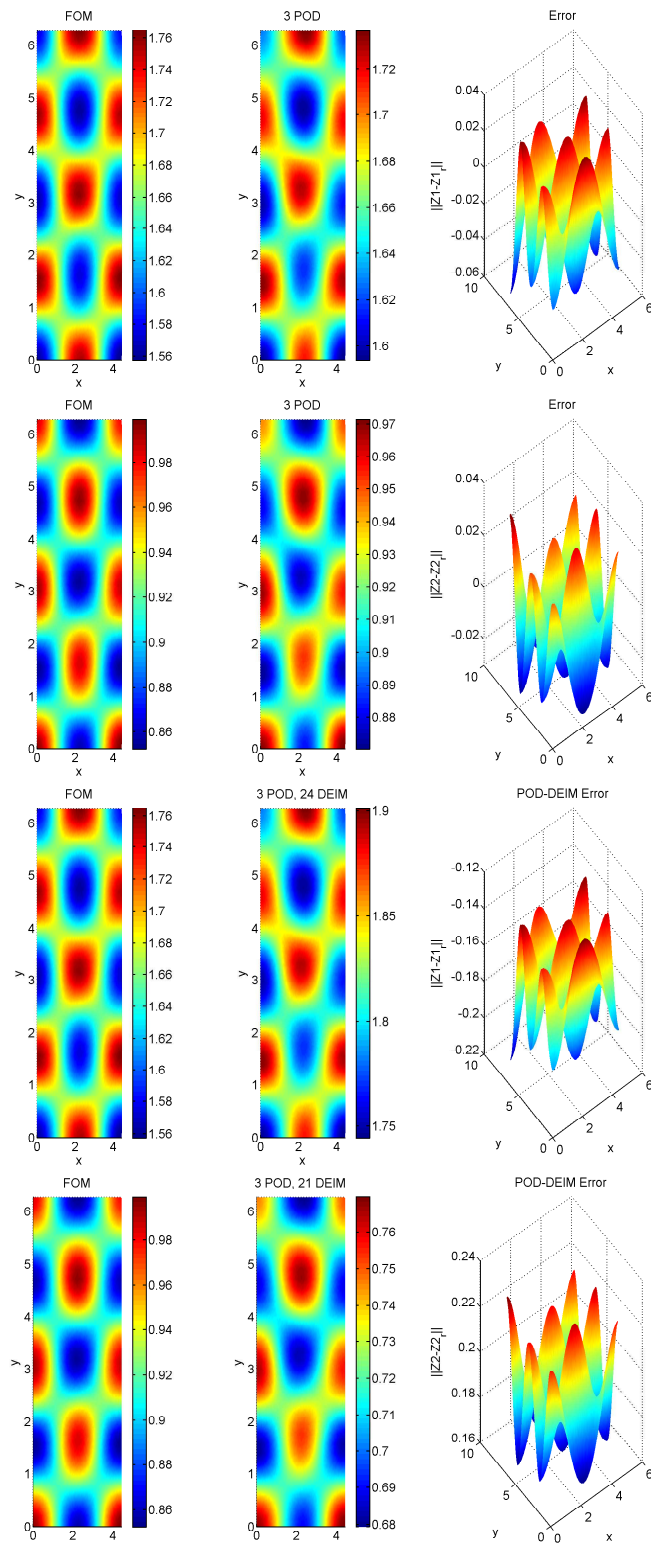


Figure 4.3: FOM and ROM solutions with the error for the component  $Z_1$  (upper),  $Z_2$  (bottom).

	Error $Z_1$	Error $Z_2$	CPU Time	Speed-up
FOM	-	-	2382.09	-
POD	1.16e-02	1.37e-02	329.55	7.23
POD-DEIM	4.72e-02	1.04e-01	135.60	17.57

Table 4.1: Relative errors and speed up factors.

### Article Information

**Acknowledgements:** The authors would like to express their sincere thanks to the editor and the anonymous reviewers for their helpful comments and suggestions.

**Author's contributions:** All authors contributed equally to the writing of this paper. All authors read and approved the final manuscript.

**Conflict of Interest Disclosure:** No potential conflict of interest was declared by the author.

**Copyright Statement:** Authors own the copyright of their work published in the journal and their work is published under the CC BY-NC 4.0 license.

**Supporting/Supporting Organizations:** No grants were received from any public, private or non-profit organizations for this research.

**Ethical Approval and Participant Consent:** It is declared that during the preparation process of this study, scientific and ethical principles were followed and all the studies benefited from are stated in the bibliography.

**Plagiarism Statement:** This article was scanned by the plagiarism program. No plagiarism detected.

**Availability of data and materials:** Not applicable.

## References

- [1] H. Murakawa, *A linear scheme to approximate nonlinear cross-diffusion systems*, Esaim Math. Model. Numer. Anal., **45**(6) (2011), 1141-1161.
- [2] N. Shigesada, K. Kawasaki, E. Teramoto, *Spatial segregation of interacting species*, J. Theor. Biol., **79** (1) (1979), 83-99.
- [3] H. Murakawa, *A linear finite volume method for nonlinear cross-diffusion systems*, Numer. Math., **136** (1) (2017), 1-26.
- [4] H. Murakawa, *A solution of nonlinear diffusion problems by semilinear reaction-diffusion systems*, Kybernetika, **45** (4) (2009), 580-590.
- [5] W. J. Barrett, F. J. Blowey, *Finite element approximation of a nonlinear cross-diffusion population model*, Numer. Math., **98** (2) (2004), 195-221.
- [6] L. Chen, A. Jüngel, *Analysis of a parabolic cross-diffusion population model without self-diffusion*, J. Differ. Equ., **224** (1) (2006), 39-59.
- [7] B. Andreianov, M. Bendahmane, R. Ruiz-Baier, *Analysis of a finite volume method for a cross-diffusion model in population dynamics*, Math. Models Methods Appl. Sci. **21** (02) (2011), 307-344.
- [8] B. Riviere, *Galerkin Methods for Solving Elliptic and Parabolic Equations: Theory and Implementation*, SIAM, 2008.
- [9] H. Murakawa, *Cross-diffusion systems: RDS approximation and numerical analysis*, Publications of the Research Institute for Mathematical Sciences, **1924** (2014), 21-29.
- [10] K. Kunisch, S. Volkwein, *Galerkin proper orthogonal decomposition methods for parabolic problems*, Numer. Math., **90** (1) (2001), 117-148.
- [11] S. Volkwein, *Proper orthogonal decomposition: Theory and reduced order modelling*, Lecture Notes, University of Konstanz, **4** (4) (2013), 1-29.
- [12] B. Karasözen, G. Mülayim, M. Uzunca, S. Yildiz, *Reduced order modelling of nonlinear cross-diffusion systems*, Appl. Math. Comput., **401** (2021), 126058.
- [13] M. Barrault, Y. Maday, N. C. Nguyen, A. T. Patera, *An empirical interpolation method: application to efficient reduced-basis discretization of partial differential equations*, Comptes Rendus Math., **339** (9) (2004), 667-672.
- [14] S. Chaturantabut, D. C. Sorensen, *Nonlinear model reduction via discrete empirical interpolation*, SIAM J. Sci. Comput., **32** (5) (2010), 2737-2764.
- [15] S. Chaturantabut, D. C. Sorensen, *A state space error estimate for POD-DEIM nonlinear model reduction*, SIAM J. Numer. Anal., **50** (1) (2012), 46-63.
- [16] B. Karasözen, T. Küçükseyhan, M. Uzunca, *Structure preserving integration and model order reduction of skew-gradient reaction-diffusion systems*, Ann. Oper. Res., **258** (1) (2017), 79-106.
- [17] N. Halko, P. G. Martinsson, J. A. Tropp, *Finding structure with randomness: Probabilistic algorithms for constructing approximate matrix decompositions*, SIAM Review, **53** (2) (2011), 217-288.
- [18] M. W. Mahoney, *Randomized algorithms for matrices and data*, Found. Trends Mach. Learn., **3** (2) (2011), 123-224.
- [19] G. Gambino, M. Lombardo, M. Sammartino, *Pattern formation driven by cross-diffusion in a 2D domain*, Nonlinear Anal. Real World Appl., **14** (3) (2013), 1755-1779.

# Application of Fractional *SPR* Psychological Disease Model in Turkey and Stability Analysis

Zafer Öztürk<sup>1\*</sup>, Halis Bilgili<sup>2</sup> and Sezer Sorgun<sup>3</sup>

<sup>1</sup>Institute of Science, Nevşehir Hacı Bektaş Veli University, 50300, Nevşehir, Türkiye

<sup>2</sup>Department of Mathematics, Aksaray University, 68100, Aksaray, Türkiye

<sup>3</sup>Department of Mathematics, Nevşehir Hacı Bektaş Veli University, 50300, Nevşehir, Türkiye

\*Corresponding author

## Article Info

**Keywords:** Caputo Derivative, Euler Method, Fractional Psychological Disease Model, Mathematical Modeling, Stability analysis.

**2010 AMS:** 60G25, 34B60, 68U01

**Received:** 31 October 2022

**Accepted:** 31 December 2022

**Available online:** 9 May 2023

## Abstract

Psychological diseases and their treatment are problems related to public health. According to data from the World Health Organization, about a billion people have either mental illness or substance use disorder problems in 2017. Mental, neurological diseases and substance use disorders account for 30 percent of the global non-fatal disease burden and 10 percent of the global disease burden. It is noted that in the world Dec 2005 and 2015, the incidence of mental health diseases increased by about 16 percent. In this study, we have created a fractional-order mathematical modeling of the population of individuals suffering from psychological diseases in a society. In this model, the total population was divided into three compartments: individuals who did not receive psychological treatment (*S*), individuals who received psychological support (*P*) and individuals who recovered after completing psychological treatment (*R*). As a fractional derivative, we used the Caputo derivative definitions. Numerical solutions were obtained with the help of the Euler method by performing stability analysis related to the fractional *SPR* model created for the mathematical model of psychological patients. Thus, it was interpreted by creating dynamics for the number of individuals with psychological problems in a population.

## 1. Introduction

Psychological diseases are the general name given for psychological disorders that prevent a person from living a healthy lifestyle that he should lead in a healthy way. Psychological diseases affect people mentally, as well as the negative situations that they have created manifest themselves physically. This condition affects the person's lifestyle quite a lot. Psychological disorders, obsessive-compulsive disorder, Depression, social phobia, panic disorder, post-traumatic stress disorder, bipolar disorder, eating disorders, Adult attention deficit and hyperactivity disorder, substance abuse, anxiety disorder, in the form of nicotine dependence can be sorted [1].

Genetic factors, brain injuries, traumatic experiences, problems that arise during childbirth, intensive substance abuse, intense drug use, eating enough people, recent natural disasters, poor living conditions, death, and mourning process, the high expectations of the community, the person to live alone, sexual abuse or emotional abuse, social cohesion, the difficulty of living, evolving technology, the pace of work intensive, universal problems, economic problems, family problems, such as psychological cause diseases [2].

Mathematical modeling of individuals undergoing psychological treatment in society has been studied using ordinary differential equation (ODE) systems [2]-[4]. It is well known that psychological diseases are a common condition in today's world. We also know that mental illnesses extremely affect the social behavior of people in a population. The causes of psychological illness are also an important issue for us. Such situations sometimes arise independently of each other. In some cases, psychological diseases occur in connection with each other. For example, bodily reactions also occur in people with intense traumatic lives. Or traumatic life also triggers a panic attack condition. But in some cases, psychological diseases occur alone. At this point, we need to consider the genetic factors and environmental factors of people. From another point of view, the existing genetic factor reappears due to living conditions. A disease with a recessive gene can occur due

to intense anxiety in the later processes. Traumatic experiences are very important in this regard. A person who does not have an anxiety problem experiences an anxiety disorder as a result of an earthquake he is experiencing. Such situations also arise with past lives [3]. The main purpose of mathematical modeling is to explain the functioning of processes by expressing real-life problems mathematically. Mathematical models have been developed to help explain a system, study the effects of its various components, and make predictions about its behavior. Recently, fractional derivatives have been used in several areas, such as mechanics, cancer therapy, ecology, neural networking, image processing, epidemiology [5]-[33].

Fractional derivative models give better results in the theory of various physical and biological processes and the control of dynamic systems than integer digit models. One of the most important reasons for this is that fractional order derivative and integral definitions have a memory property. Another important reason is that although the model is the same, the fractional orders of the equations change with each real application studied, giving specific and precise results to the relevant problem. In population models, the future status of a population depends on its past status. This is called the memory effect. The memory effect of the population can be studied by adding a delay term or using a fractional derivative in the model [5]-[33].

This paper consists of four parts. In the first chapter, the importance of fractional mathematical modeling and information about psychological diseases were given. In the second part, the formation of a fractional *SPR* psychological model, the generalized Euler Method and the stability analysis of the created model were performed. In the third part, numerical results were obtained and graphs were drawn by making a new application of the fractional *SPR* psychological model. In the fourth part, the results were given.

## 2. Fractional Derivation and Fractional *SPR* Psychological Disease Model

The most commonly used definitions of the fractional derivative are Riemann-Liouville, Caputo, Atangana-Baleanu and the Conformable derivative. In this study, because the classical initial conditions are easily applicable and provide ease of calculation, the Caputo derivative operator was preferred and modeling was created. The definition of the Caputo fractional derivative is given below.

**Definition 2.1.** [4] Let  $f(t)$  be a function that can be continuously differentiable  $n$  times. The value of the function  $f(t)$  for the value of  $\alpha$  that satisfies the condition  $n - 1 < \alpha < n$ . The Caputo fractional derivative of  $\alpha$ -th order  $f(t)$  is defined by  $D_t^\alpha f(t) = \frac{1}{\Gamma(n-\alpha)} \int_a^t (t-x)^{(n-\alpha-1)} f^{(n)}(x) dx$ .

**Definition 2.2.** [4] The Riemann-Liouville (RL) fractional-order integral of a function  $A(t) \in C_n$  ( $n \geq -1$ ) is given by

$$J^\gamma A(t) = \frac{1}{\Gamma(\alpha)} \int_0^t (t-s)^{(\alpha-1)} A(s) ds, \quad J^0 A(t) = A(t). \quad (2.1)$$

**Definition 2.3.** [4] The series expansion of two-parametrized form of Mittag-Leffler function for  $a, b > 0$  is given by

$$E_{a,b}(t) = \sum_{i=0}^{\infty} \frac{t^i}{\Gamma(ai+b)}. \quad (2.2)$$

### 2.1. The fractional *SPR* psychological disease model

The fractional *SPR* model of psychological illness basically divides a community into three main groups. The first are individuals who do not receive psychological treatment, individuals who receive psychological support, and individuals who recover by completing psychological treatment. The expression of the *SPR* psychological disease model as a system of fractional differential equations is as follows [1, 2].

$$\begin{aligned} \frac{d^\alpha S}{dt^\alpha} &= \mu N - \mu S - \beta S \\ \frac{d^\alpha P}{dt^\alpha} &= \beta S - \mu P - \sigma P - \theta P \\ \frac{d^\alpha R}{dt^\alpha} &= \sigma P - \mu R \end{aligned} \quad (2.3)$$

Where  $\frac{d^\alpha}{dt^\alpha}$  is the Caputo fractional derivative of  $\alpha$ -th order with respect to time  $t$ . All compartments and parameters are shown in Table 2.1 and Table 2.2. The initial values are defined as,

$$S(0) = S_0, \quad P(0) = P_0, \quad R(0) = R_0$$

$0 < \alpha \leq 1$ . Since society is divided into three compartments, it is  $S + P + R = N$  and all terms are derived with respect to time

$$\frac{d^\alpha N}{dt^\alpha} = \frac{d^\alpha S}{dt^\alpha} + \frac{d^\alpha P}{dt^\alpha} + \frac{d^\alpha R}{dt^\alpha}$$

it is clear that.

**Table 2.1:** Variables used in the model and their meanings

Variables used in the systems	Meaning
$S(t)$	$t$ the number of individuals who do not receive timely psychological treatment (annually)
$P(t)$	$t$ the number of individuals receiving psychological support on time (annually)
$R(t)$	the number of individuals who recovered at the time of $t$ (annually)
$N(t)$	Total population

Because fractional-order models have a memory feature in events related to a time variable, they show more realistic and accurate results than integer-order models [5]-[14]. Therefore, the established model was created as a fractional order. In the system of (2.3), the fractional-order differential equation for  $\alpha = 1$  is reduces to a full order differential equation.

**Table 2.2:** Parameters and their meanings

Parameters	Meaning
$\beta$	The annual rate of initiation of psychological therapy
$\mu$	Annual birth and natural mortality rate
$\sigma$	Annual rate of complete recovery
$\theta$	The annual mortality rate due to psychological diseases

All individuals are born into the sensitive class. Natural birth and death rates were considered equal in the model. All births are considered to have entered the sensitive class. A large proportion of individuals who have completed treatment for psychological diseases may again develop a psychological disease of the same or another type. The parameters defined in the model do not change with time. The  $N$  population was dimensioned and new variables were created as follows.

$$s = \frac{S}{N}, \quad p = \frac{P}{N}, \quad r = \frac{R}{N}$$

It is clear from here that  $s + p + r = 1$ . Thus, the new form of the fractional *SPR* model is written as follows.

$$\begin{aligned} D^\alpha s(t) &= \mu - \mu s(t) - \beta s(t), \\ D^\alpha p(t) &= \beta s(t) - \mu p(t) - \sigma p(t) - \theta p(t), \\ D^\alpha r(t) &= \sigma p(t) - \mu r(t). \end{aligned} \tag{2.4}$$

**2.2. Generalized Euler method**

In this paper, we used the Generalized Euler method to solve the initial value problem with the Caputo fractional derivative. Many of the mathematical models consist of nonlinear systems and finding solutions to these systems can be quite difficult. In most cases, analytical solutions cannot be found and a numerical approach should be considered for this. One of these approaches is the Generalized Euler method [15].  $D^\alpha y(t) = f(t, y(t)), y(0) = y_0, 0 < \alpha \leq 1, 0 < t < \alpha$  for the initial value problem,  $h = \frac{a}{n}$  impending  $[t_j, t_{j+1}]$  is divided into  $n$  sub with  $j = 0, 1, \dots, n - 1$ . Suppose that  $y(t), D^\alpha y(t)$  and  $D^{2\alpha} y(t)$  are continuous in range  $[0, a]$  and using the generalized Taylor’s formula, the following equation is obtained [15].

$$y(t_1) = y(t_0) + \frac{h^\alpha}{\Gamma(\alpha + 1)} f(t_0, y(t_0))$$

This process will be repeated to create an array. Let  $t_j = t_{j+1} + h$  such that

$$y(t_{j+1}) = y(t_j) + \frac{h^\alpha}{\Gamma(\alpha + 1)} f(t_j, y(t_j))$$

$j = 0, 1, \dots, n - 1$  the generalized formula in the form is obtained. For every  $k = 0, 1, \dots, n - 1$

$$\begin{aligned} S(k + 1) &= S(k) + \frac{h^\alpha}{\Gamma(\alpha + 1)} (\mu N - \mu S(k) - \beta S(k)), \\ P(k + 1) &= P(k) + \frac{h^\alpha}{\Gamma(\alpha + 1)} (\beta S(k) - \mu P(k) - \sigma P(k) - \theta P(k)), \\ R(k + 1) &= R(k) + \frac{h^\alpha}{\Gamma(\alpha + 1)} (\sigma P(k) - \mu R(k)) \end{aligned} \tag{2.5}$$

is obtained.

**2.3. Analysis of the diseased equilibrium point and stability of the fractional *SPR* psychological model**

In order to find the equilibrium point (2.4) in the system ,  $D^\alpha s = 0$  ,  $D^\alpha p = 0$  ,  $D^\alpha r = 0$  it is considered to be.

$$\begin{aligned} D^\alpha s(t) &= \mu - \mu s(t) - \beta s(t), \\ D^\alpha p(t) &= \beta s(t) - \mu p(t) - \sigma p(t) - \theta p(t), \\ D^\alpha r(t) &= \sigma p(t) - \mu r(t). \end{aligned}$$

To determine the psychologically diseased equilibrium point of the system,  $p(t) \neq 0$  is taken.  $E_0 = (s_0, p_0, r_0)$  including,

$$E_0 = \left( \frac{\mu}{(\mu + \beta)}, \frac{\beta \mu}{(\mu + \beta)(\mu + \sigma + \theta)}, \frac{\sigma \beta}{(\mu + \beta)(\mu + \sigma + \theta)} \right) \tag{2.6}$$

the psychologically diseased equilibrium point is achieved. The Jacobian matrix at the equilibrium point of the system

$$J(E_0) = \begin{bmatrix} -\mu - \beta & 0 & 0 \\ \beta & -\mu - \sigma - \theta & 0 \\ 0 & \sigma & -\mu \end{bmatrix} \quad (2.7)$$

it is obtained. The eigenvalues obtained from the Jacobian matrix (2.7) are given below.

$$\begin{aligned} \lambda_1 &= -\mu - \beta, \\ \lambda_2 &= -\mu - \sigma - \theta, \\ \lambda_3 &= -\mu \end{aligned}$$

where  $\beta, \mu, \sigma, \theta$  are the parameters of positively defined real numbers. It is clear that  $\lambda_1 < 0$ ,  $\lambda_2 < 0$  and  $\lambda_3 < 0$ . The equilibrium point of the system is locally asymptotically stable.

**Theorem 2.4.** For all  $t \geq 0$ ,  $S(0) = S_0 \geq 0$ ,  $P(0) = P_0 \geq 0$ ,  $R(0) = R_0 \geq 0$ , the solutions of the system in (2.3) with initial conditions  $(S(t), P(t), R(t)) \in \mathbb{R}_+^3$  are not negative.

### 3. Numerical simulation of the fractional *SPR* psychological disease model for Turkey

In this section, numerical simulation and graphs of the fractional *SPR* psychological disease model for Turkey data for 2019 will be shown. Now let us obtain a numerical simulation of the fractional *SPR* model using the Generalized Euler method. Let us consider the following parameters according to the data in [18].  $S = 67.850.000$ ,  $P = 15.000.000$ ,  $R = 150.000$ ,  $\beta = 0.05$ ,  $\sigma = 0.01$ ,  $\mu = 0.022$ ,  $\theta = 0.15$  and let's take size of step  $h = 0.1$ . Hence we get the following results and tables. Using the Euler method, we obtain the following tables for given.

**Table 3.1:** The values of  $S$ ,  $P$  and  $R$  at the moment  $t \alpha = 1$ .

$t$	$S(t)$	$P(t)$	$R(t)$
0	68750000,00	15000000,00	150000,00
1	68437600,00	15070750,00	164670,00
2	68127449,28	15138650,35	179378,47
3	67819531,64	15203764,16	194122,49
4	67513831,01	15266153,31	208899,18
5	67210331,43	15325878,47	223705,76
6	66909017,04	15382999,14	238539,48
7	66609872,12	15437573,64	253397,70
8	66312881,04	15489659,16	268277,80
9	66018028,30	15539311,77	283177,24
10	65725298,49	15586586,44	298093,57
11	65434676,34	15631537,06	313024,35
12	65146146,67	15674216,46	327967,23
13	64859694,42	15714676,46	342919,92
14	64575304,62	15752967,82	357880,17

**Table 3.2:** The values of  $S$ ,  $P$  and  $R$  at the moment  $t \alpha = 0.9$ .

$t$	$S(t)$	$P(t)$	$R(t)$
0	68750000,00	15000000,00	150000,00
1	68341078,49	15092609,46	169202,55
2	67936010,89	15180336,34	188471,03
3	67534760,87	15263322,19	207798,86
4	67137292,47	15341704,93	227179,65
5	66743570,03	15415618,98	246607,23
6	66353558,26	15485195,30	266075,61
7	65967222,17	15550561,53	285579,01
8	65584527,14	15611842,02	305111,80
9	65205438,85	15669157,93	324668,56
10	64829923,29	15722627,33	344244,02
11	64457946,81	15772365,22	363833,10
12	64089476,05	15818483,67	383430,88
13	63724477,96	15861091,84	403032,59
14	63362919,82	15900296,11	422633,62

**Table 3.3:** The values of  $S$ ,  $P$  and  $R$  at the moment  $t \alpha = 0.8$ .

$t$	$S(t)$	$P(t)$	$R(t)$
0	68750000,00	15000000,00	150000,00
1	68218403,82	15120391,89	174963,23
2	67693320,72	15232532,29	200037,88
3	67174670,87	15336732,14	225209,49
4	66662375,47	15433292,11	250464,17
5	66156356,66	15522502,86	275788,62
6	65656537,54	15604645,42	301170,07
7	65162842,15	15679991,41	326596,28
8	64675195,46	15748803,45	352055,52
9	64193523,38	15811335,35	377536,54
10	63717752,69	15867832,44	403028,57
11	63247811,09	15918531,83	428521,31
12	62783627,17	15963662,67	454004,89
13	62325130,38	16003446,41	479469,87
14	61872251,04	16038097,03	504907,21

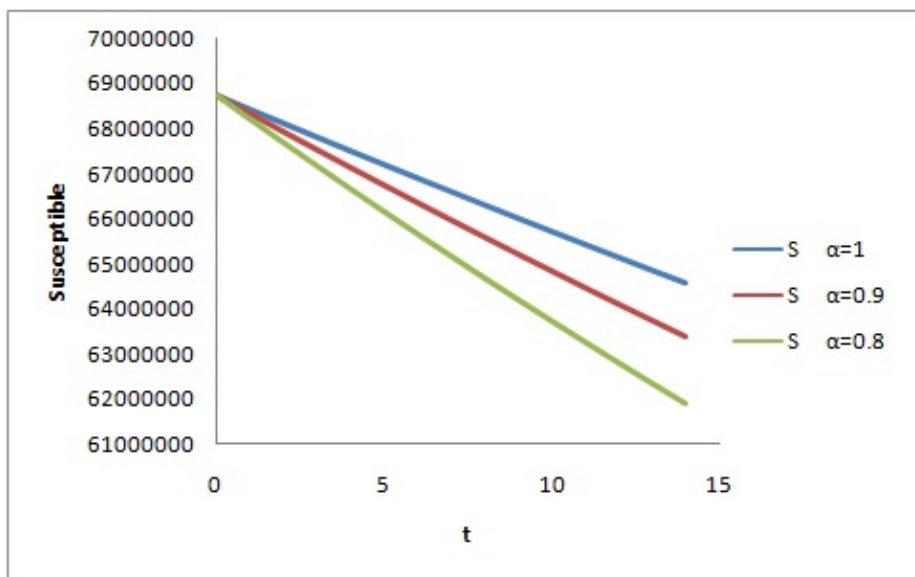


**Figure 3.1:** The graph of change of the  $S$  compartment model.

It is clear that, the most effective and manageable parameter of the model is  $\beta$ . Controlling the factors effecting human psychology, especially economic problems, will reduce the value of the  $\beta$  parameter. According to the observed value of the  $\beta$  parameter, it is seen Figure 3.1 that the number of individuals who have not yet received psychological support in Turkey is gradually decreasing. In parallel, it is clear that there will be an increase in the number of individuals in other compartments.

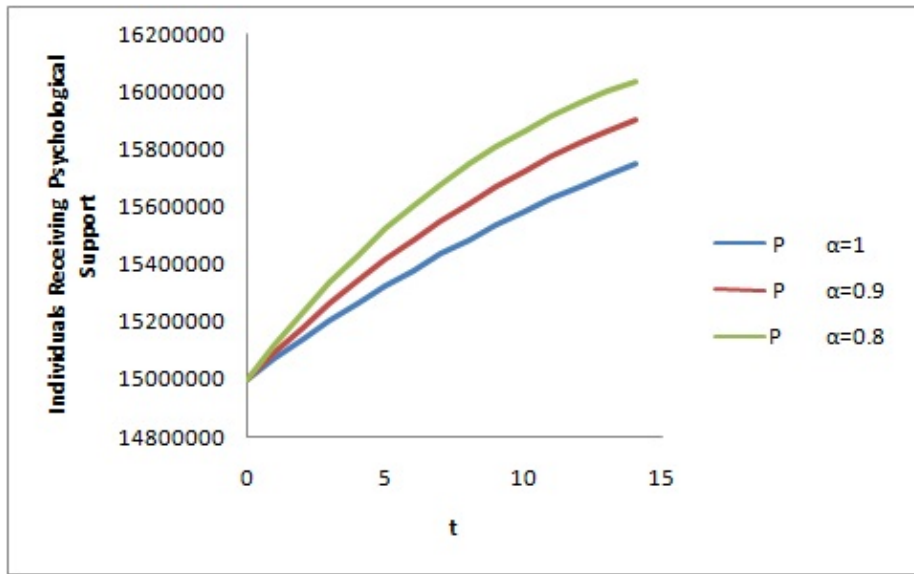


Figure 3.2: The graph of change of the  $P$  compartment model.

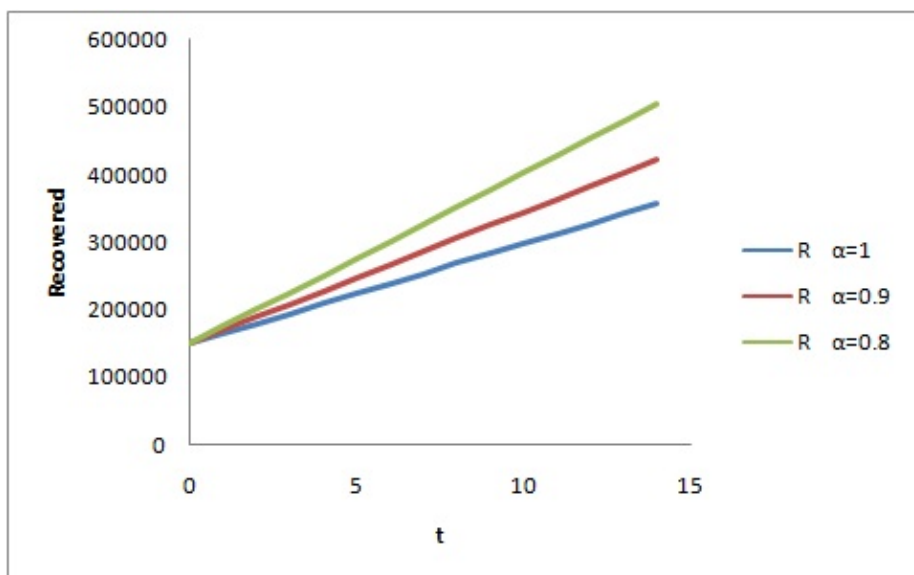


Figure 3.3: The graph of change of the  $R$  compartment model.

In Table 3.1, Table 3.2 and Table 3.3, the changes of  $S$ ,  $P$  and  $R$  are observed for different states of  $\alpha$ . By the above figures, we observe the following highlights:

- \* It is observed that the number of individuals who do not receive psychological treatment decreases over time (Figure 3.1).
- \* It is observed that the number of individuals receiving psychological support has increased over time (Figure 3.2).
- \* It is observed that the number of recovered individuals increases over time (Figure 3.3).
- \* According to the parameter values taken in this study, it is possible to reach the disease-free equilibrium point given in equation (2.6) only if the vast majority of the population is affected by the disease and receives treatment. In order to turn this negative scenario into a positive one, country managers and families should take the necessary measures and look for ways to reduce the  $\beta$  parameter.

#### 4. Conclusions and Comments

In this paper, a new application of the fractional  $SPR$  psychological disease model was made taking into account the psychological disease data of Turkey since 2019 [18] and graphs were drawn with the help of the numerical results obtained. The psychological diseased equilibrium point of the fractional  $SPR$  model was obtained and stability analysis was performed. In the graphs obtained, it was observed that the number of individuals who did not receive psychological treatment decreased over time, the number of individuals who received psychological support increased over time and the number of individuals who recovered increased over time.

## Article Information

**Acknowledgements:** The authors would like to express their sincere thanks to the editor and the anonymous reviewers for their helpful comments and suggestions.

**Author's contributions:** All authors contributed equally to the writing of this paper. All authors read and approved the final manuscript.

**Conflict of Interest Disclosure:** No potential conflict of interest was declared by the author.

**Copyright Statement:** Authors own the copyright of their work published in the journal and their work is published under the CC BY-NC 4.0 license.

**Supporting/Supporting Organizations:** No grants were received from any public, private or non-profit organizations for this research.

**Ethical Approval and Participant Consent:** It is declared that during the preparation process of this study, scientific and ethical principles were followed and all the studies benefited from are stated in the bibliography.

**Plagiarism Statement:** This article was scanned by the plagiarism program. No plagiarism detected.

**Availability of data and materials:** Not applicable.

## References

- [1] J. T. Townsend, D. E. Landon, *Mathematical models of recognition and confusion in psychology*, Math. Soc. Sci., **4**(1) (1983), 25-71.
- [2] W. K. Estes, *Mathematical models in psychology*, A Handbook for Data Analysis in the Behavioral Sciences: Volume 1: Methodological Issues, Volume 2: Statistical Issues, **3** (2014).
- [3] D. Wodarz, M. A. Nowak, *Mathematical models of HIV pathogenesis and treatment*, BioEssays, **24**(12) (2002), 1178-1187.
- [4] I. Podlubny, *Fractional Differential Equations*, Academy Press, San Diego CA, 1999.
- [5] F. Brauer, C. Castillo-Chavez, Z. Feng, *Mathematical models in epidemiology*, Springer, New York, 2019.
- [6] H. Bilgili, A. Yousef, A. Erciyes, Ü. Erdinç, Z. Öztürk, *A fractional-order mathematical model based on vaccinated and infected compartments of SARS-CoV-2 with a real case study during the last stages of the epidemiological event*, J. Comput. Appl. Math., (2022), 115015.
- [7] N. T. Bailey, *The Mathematical Theory of Infectious Diseases and its Applications*, Charles Griffin & Company Ltd, 5a Crendon Street, High Wycombe, Bucks HP13 6LE, 1975.
- [8] H. Hethcote, M. Zhién, L. Shengbing, *Effects of quarantine in six endemic models for infectious diseases*, Math. Biosci., **180**(1-2) (2002), 141-160.
- [9] S. Wang, Y. Ding, H. Lu, S. Gong, *Stability and bifurcation analysis of SIQR for the COVID-19 epidemic model with time delay*, Math. Biosci. Eng., **18**(5) (2021), 5505-5524.
- [10] B. K. Mishra, N. Jha, *SEIQRS model for the transmission of malicious objects in computer network*, Appl. Math. Model., **34**(3) (2010), 710-715.
- [11] X. Liu, T. Yasuhiro, I. Shingo, *SVIR epidemic models with vaccination strategies*, J. Theor. Biol., **253**(1) (2008), 1-11.
- [12] M. B. Trawicki, *Deterministic seirs epidemic model for modeling vital dynamics, vaccinations, and temporary immunity*, Mathematics, **5**(1) (2017), 7.
- [13] Z. Öztürk, S. Sorgun, H. Bilgili, *SIQRV Modeli ve Nümerik Uygulaması*, Avrupa Bilim ve Teknoloji Dergisi, **28** (2021), 573-578.
- [14] W. O. Kermack, A. G. McKendrick, *A contribution to the mathematical theory of epidemics*, In: Proc. R. Soc. Lond., Series A, Containing Papers of a Mathematical and Physical Character, **115**(772) (1927), 700-721.
- [15] D. Yaro, S. K. Omari-Sasu, P. Harvim, A. W. Saviour, B. A. Obeng, *Generalized Euler method for modeling measles with fractional differ ential equations*, Int. J. Innov. Res. Dev., **4** (2015).
- [16] Z. Öztürk, S. Sorgun, H. Bilgili, Ü. Erdinç, *New exact solutions of conformable time-fractional bad and good modified Boussinesq equations*, J. New Theory, **37** (2021), 8-25.
- [17] M. Braun, M. Golubitsky, *Differential Equations and their Applications*, Springer-Verlag, New York, 1983.
- [18] <https://tuikweb.tuik.gov.tr/UstMenu.do>.
- [19] P. Kumar, V. S. Erturk, H. Vellappandi, H. Trinh, V. Govindaraj, *A study on the maize streak virus epidemic model by using optimized linearization-based predictor-corrector method in Caputo sense*, Chaos Solit. Fractals, **158** (2022), 112067.
- [20] P. Kumar, V. S. Erturk, H. Abboubakar, K. S. Nisar, *Prediction studies of the epidemic peak of coronavirus disease in Brazil via new generalised Caputo type fractional derivatives*, Alex. Eng. J., **60**(3) (2021), 3189-3204.
- [21] P. Kumar, V. Govindaraj, V. S. Erturk, *A novel mathematical model to describe the transmission dynamics of tooth cavity in the human population*, Chaos Solit. Fractals, **161** (2022), 112370.
- [22] M. Vellappandi, P. Kumar, V. Govindaraj, *Role of fractional derivatives in the mathematical modeling of the transmission of Chlamydia in the United States from 1989 to 2019*, Nonlinear Dyn., (2022), 1-15.
- [23] S. Abbas, S. Tyagi, P. Kumar, V. S. Erturk, S. Momani, *Stability and bifurcation analysis of a fractional-order model of cell-to-cell spread of HIV-1 with a discrete time delay*, Math. Meth. App. Sci., **45**(11) (2022), 7081-7095.
- [24] V. S. Erturk, E. Godwe, D. Baleanu, P. Kumar, J. Asad, A. Jajarmi, *Novel fractional-order Lagrangian to describe motion of beam on nanowire*, Acta Phys. Pol. A, **140**(3) (2021), 265-272.
- [25] P. Kumar, V. S. Erturk, A. Yusuf, S. Kumar, *Fractional time-delay mathematical modeling of Oncolytic Virotherapy*, Chaos Solit. Fractals, **150** (2021), 111123.
- [26] A. Din, F. M. Khan, Z. U. Khan, A. Yusuf, T. Munir, *The mathematical study of climate change model under nonlocal fractional derivative*, Partial Differential Equations in Applied Mathematics, **5** (2022), 100204.
- [27] E. Viera-Martin, J. F. Gomez-Aguilar, J. E. Solis-Perez, J. A. Hernandez-Perez, R. F. Escobar-Jimenez, *Artificial neural networks: a practical review of applications involving fractional calculus*, Eur. Phys. J. Spec. Top., (2022), 1-37.
- [28] V. S. Erturk, A. Ahmadkhanlu, P. Kumar, V. Govindaraj, *Some novel mathematical analysis on a corneal shape model by using Caputo fractional derivative*, Optik, **261** (2022), 169086.
- [29] V. S. Erturk, A. K. Alomari, P. Kumar, M. Murillo-Arcila, *Analytic solution for the strongly nonlinear multi-order fractional version of a BVP occurring in chemical reactor theory*, Discrete Dyn. Nat. Soc., **2022** (2022), 8655340.
- [30] Q. Yang, D. Chen, T. Zhao, Y. Chen, *Fractional calculus in image processing: a review*, Fract. Calc. Appl. Anal., **19**(5) (2016), 1222-1249.
- [31] P. Kumar, V. Govindaraj, V. S. Erturk, M. H. Abdellattif, *A study on the dynamics of alkali-silica chemical reaction by using Caputo fractional derivative*, Pramana, **96**(3) (2022), 1-19.
- [32] Z. Öztürk, H. Bilgili, Ü. Erdinç, *An optimized continuous fractional grey model for forecasting of the time dependent real world cases*, Hacettepe J. Math. Stat., **51**(1) (2022), 308-326.
- [33] Ü. Erdinç, H. Bilgili, Z. Öztürk, *A novel fractional forecasting model for time dependent real world cases*, Accepted: Revstat Stat. J., (2022).

# Dynamical Analysis of a Local Lengley-Epstein System Coupled with Fractional Delayed Differential Equations

Ercan Balci

Department of Mathematics, Faculty of Science, Erciyes University, Kayseri, Turkey

## Article Info

**Keywords:** Caputo fractional derivative, Fractional delayed differential equations, Hopf bifurcation, Lengyel-Epstein equation

**2010 AMS:** 34A08, 34K20

**Received:** 21 December 2022

**Accepted:** 13 April 2023

**Available online:** 20 July 2023

## Abstract

We consider a system of fractional delayed differential equations. The ordinary differential version of the system without delay is introduced in the Lengyel-Epstein reaction-diffusion system. We evaluate the system with and without delay and explore the stability of the unique positive equilibrium. We also prove the existence of Hopf bifurcation for both cases. Furthermore, the impacts of Caputo fractional order parameter and time delay parameter on the dynamics of the system are investigated with numerical simulations. It is also concluded that for different values of time delay parameter, the decrement of the Caputo fractional order parameter has opposite effects on the system in terms of stability.

## 1. Introduction

Fractional calculus is considered as a generalization of ordinary calculus to non-integer orders. Fractional derivative operator is a non-local operator in nature. As a result, fractional differential equations are associated with memory and hereditary attributes, which are present in many real processes. Thus, there are many applications of fractional differential equations in various research fields such as chemistry [1, 2], physics [3, 4], biology [5, 6], epidemic modelling [7–9] mechanical engineering [10] and network theory [11]. The best-known definitions of fractional order derivative are Riemann-Liouville and Caputo definitions. These definitions are more reliable in terms of non-locality and uncovering memory effects despite the fact that there are relatively new approaches like conformable fractional derivative, Caputo-Fabrizio derivative etc. [12] On the other hand, Riemann-Liouville fractional derivative requires fractional initial conditions due to fact that Riemann-Liouville derivative of a constant is not zero. This is not the case for Caputo sense fractional differential equations which requires standard initial conditions same as in ordinary differential equations (ODEs). This property makes Caputo definition more appealing while modelling physical or biological facts. The Caputo fractional derivative of order  $\alpha > 0$  of a real valued function  $h$  is defined as

$$D^\alpha h(s) = \frac{1}{\Gamma(k-\alpha)} \int_0^s (s-\zeta)^{k-\alpha-1} h^{(k)}(\zeta) d\zeta,$$

where  $k$  is an integer and  $k-1 < \alpha < k$ .

Time delay is another useful tool to describe processes that also depends on the past data [13], which exist in many real systems such as chemical processes, technical processes, biosciences, economics and other branches [14, 15]. Since both time delays and fractional derivatives allow past data to affect the current state, fractional delayed differential equations (FDDEs) are very effective for constructing strongly realistic models of systems with memory and hereditary properties. There are some works on stability conditions of FDDEs. But, the existing stability conditions for FDDEs do not comprise effective algebraic criteria or algorithms for testing of stability of FDDEs [14, 16, 17]. Some studies on dynamical analysis of FDDEs can be found in [11, 18–20]. In [11], authors worked on fractional complex-valued neural network with delays and provided a detailed numerical analysis. Li et al. [18] investigated the dynamical behaviours of a prey-predator model with double delays and proved the existence of Hopf bifurcation depending on the time delay parameter. In [19], authors also considered a prey-predator model with incorporating the dispersal of prey and analyzed numerically the relation between the fractional order and the time delay parameters.

In this work, we study Caputo fractional order version of the following system of delay differential equations

$$\begin{cases} u' = a - u - 4 \frac{uv(t-\tau)}{1+u^2}, \\ v' = \sigma b \left( u - \frac{uv(t-\tau)}{1+u^2} \right) \end{cases} \tag{1.1}$$

where  $\tau \geq 0$  is the delay parameter. When  $\tau = 0$ , the system (1.1) reduces to local Lengyel-Epstein system which is reaction-diffusion system that is used to describe chlorite-iodide malonic-acid (CIMA) chemical reaction [21, 22]. Here,  $u(t)$  and  $v(t)$  represents concentrations of the activator iodine ( $I^-$ ) and the inhibitor chlorite ( $ClO_2^-$ ). The positive parameters  $a$  and  $b$  are correlated to the feed concentrations;  $\sigma > 0$  is a rescaling coefficient depending on the concentration of the starch.

For  $\tau = 0$ , both of this ODE and the associated PDE model are studied in [23]. Yi et al. derived the conditions about Turing instability and they proved the existence of Hopf bifurcation together with direction of bifurcation [23]. In [24], authors make Hopf bifurcation analysis of the system (1.1) by applying normal form theory given in [25]. In [26], authors consider the fractional version of Lengyel-Epstein system by replacing left hand side ordinary derivatives by Caputo sense fractional derivatives. They established the conditions necessary for local and global asymptotic stability of the steady state [26].

Time delays can have a major influence on the dynamic behavior of systems and may cause instability and chaos [15]. On the other hand, using time delays in fractional differential equations is a relatively recent topic which is the main interest of this work. The aim is to study fractional order version of the system (1.1) with  $\tau = 0$  and  $\tau > 0$ . Hopf bifurcation analysis is performed for both cases. Then, we give numerical simulations to illustrate and verify our theoretical results. We also focus on the relation between time delay parameter  $\tau$  and fractional order parameter  $\alpha$ .

## 2. Fractional Order System without Delay

Firstly, we take fractional order version of the system (1.1) with  $\tau = 0$  :

$$\begin{cases} D^\alpha u(t) = a - u - 4 \frac{uv}{1+u^2}, \\ D^\alpha v(t) = \sigma b \left( u - \frac{uv}{1+u^2} \right) \end{cases} \tag{2.1}$$

where  $\alpha \in (0, 1)$  is the order of the Caputo sense fractional derivative. In order to find equilibrium points of the system (2.1), we solve the following system:

$$\begin{cases} D^\alpha u(t) = 0 \\ D^\alpha v(t) = 0 \end{cases}$$

The system (2.1) has a unique positive equilibrium  $(u^*, v^*) = (\delta, 1 + \delta^2)$  with  $\delta = \frac{a}{5}$ .

**Theorem 2.1.** [27] Consider the  $n$ -dimensional system

$$D_\alpha^\alpha h(t) = f(t, x(t)), \quad x(t_0) = x_0,$$

where  $\alpha \in (0, 1)$ ,  $D_\alpha^\alpha$  represents the Caputo fractional derivative of order  $\alpha$ . Let  $x^*$  be the equilibrium point of the system and  $J(x^*)$  be the Jacobian matrix about the equilibrium point  $x^*$ . Then, the equilibrium point  $x^*$  is locally asymptotically stable if and only if all the eigenvalues  $\lambda_i, i = 1, 2, \dots, n$  of  $J(x^*)$  satisfy  $|\arg(\lambda_i)| > \frac{\alpha\pi}{2}$ .

**Theorem 2.2.** The equilibrium point  $(u^*, v^*) = (\delta, 1 + \delta^2)$  of the system (2.1) is locally asymptotically stable if one of the following conditions holds.

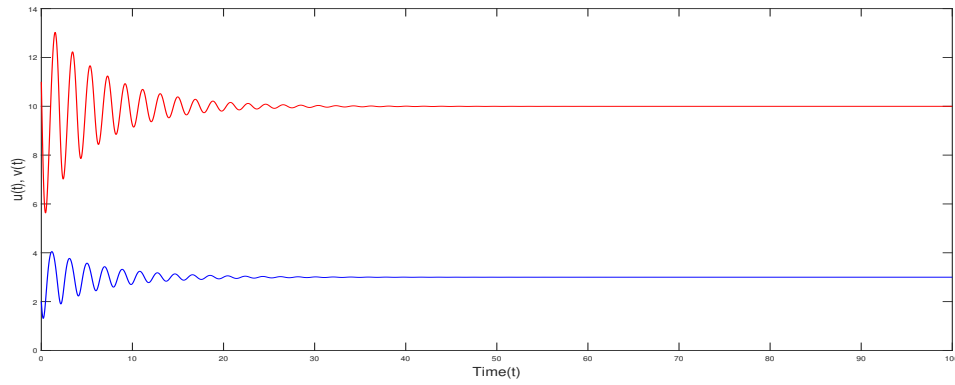
- i)  $\delta \leq \sqrt{\frac{5}{3}}$ ,
- ii)  $\delta > \sqrt{\frac{5}{3}}$  and  $b > \frac{-5+3\delta^2}{\delta\sigma}$ ,
- iii)  $\delta > \sqrt{\frac{5}{3}}, \frac{5+13\delta^2}{\delta\sigma} - 4\sqrt{\frac{10(1+\delta^2)}{\sigma^2}} < b < \frac{-5+3\delta^2}{\delta\sigma}$  and  $|\tan^{-1}(\frac{\sqrt{3\delta^2-5-\sigma b\delta} + \frac{20\sigma b\delta}{1+\delta^2}}{3\delta^2-5-\sigma b\delta})| > \frac{\alpha\pi}{2}$ .

*Proof.* The jacobian matrix of the system (2.1) evaluated at  $(u^*, v^*)$  is

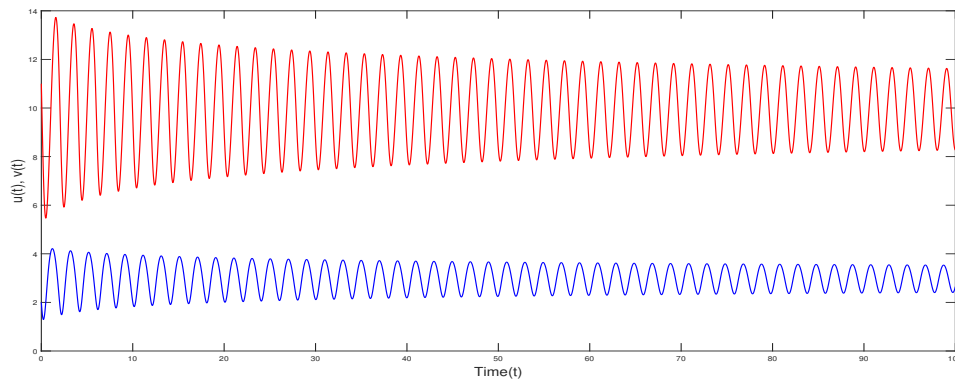
$$J(u^*, v^*) = \begin{pmatrix} \frac{3\delta^2-5}{1+\delta^2} & \frac{-4\delta}{1+\delta^2} \\ \frac{2\sigma b\delta^2}{1+\delta^2} & \frac{-\sigma b\delta}{1+\delta^2} \end{pmatrix}$$

and the corresponding characteristic polynomial is given by

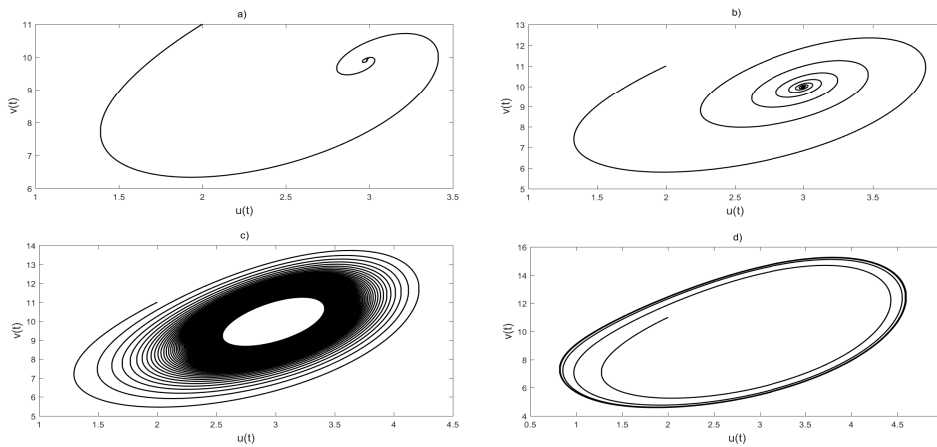
$$\lambda^2 + \rho_1\lambda + \rho_0 = 0$$



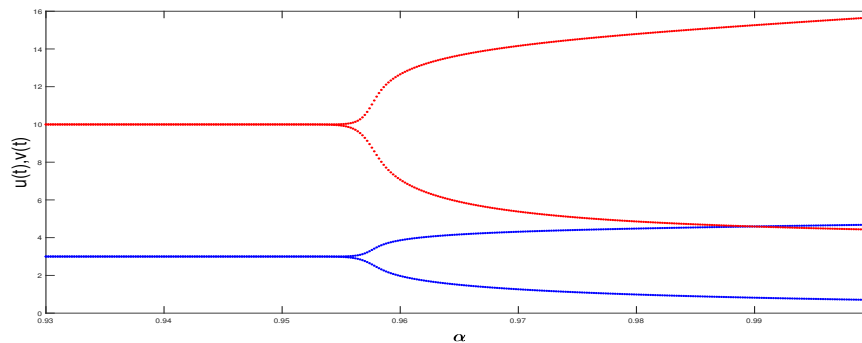
(a) Solution of system (2.1) where  $\alpha = 0.90$ ;  $u(t)$  and  $v(t)$  displayed by blue and red lines respectively with the initial condition (2, 11).



(b) Solution of system (2.1) where  $\alpha = \alpha^* = 0.9575$ ;  $u(t)$  and  $v(t)$  displayed as blue and red lines respectively with the initial condition (2, 11).



(c) Phase portraits of system (2.1) with varying the fractional order  $\alpha$  where  $\alpha = 0.80$  a),  $\alpha = 0.90$  b),  $\alpha = 0.9575$  c),  $\alpha = 0.99$  d) and initial condition (2, 11).



(d) Bifurcation diagram of (2.1) depending on  $\alpha$  with the initial condition (2, 11).

**Figure 2.1:** Numerical simulations of system (2.1)

where

$$\rho_1 = \frac{5 + \sigma b \delta - 3\delta^2}{1 + \delta^2}, \quad \rho_0 = \frac{5\sigma b \delta}{1 + \delta^2}.$$

Since all the parameters in the system (2.1) are positive,  $\rho_0 > 0$ . If the conditions i) or ii) holds we have that  $\rho_1 > 0$ . This implies that the eigenvalues  $\lambda_{1,2}$  of  $J(u^*, v^*)$  are negative real numbers or complex numbers with negative real part. So, they satisfy  $|\arg(\lambda_{1,2})| > \frac{\alpha\pi}{2}$ . Moreover, under the conditions  $\delta > \sqrt{\frac{5}{3}}, b < \frac{-5+3\delta^2}{\delta\sigma}, b > \frac{5+13\delta^2}{\delta\sigma} - 4\sqrt{\frac{10(1+\delta^2)}{\sigma^2}}$ , we have that  $\rho_1 < 0$  and  $\rho_1^2 - 4\rho_0 < 0$ . So, the eigenvalues  $\lambda_{1,2}$  of  $J(u^*, v^*)$  are complex numbers with positive real part. If  $|\arg(\lambda_{1,2})| = |\tan^{-1}(\frac{4\rho_0 - \rho_1^2}{\rho_1})| > \frac{\alpha\pi}{2}$ , the equilibrium point  $(u^*, v^*)$  is locally asymptotically stable and thus proving the theorem.  $\square$

**Theorem 2.3.** [17, 28] When the fractional order parameter  $\alpha$  passes through the critical value  $\alpha^* \in (0, 1)$ , Hopf bifurcation occurs for the system (2.1) around the equilibrium point if the followings satisfied:

- (a) The jacobian matrix of (2.1) at the equilibrium point has a pair of complex conjugate eigenvalues  $\lambda_{1,2} = \theta + i\gamma$ , where  $\theta > 0$ ;
- (b)  $m(\alpha^*) = 0$ , where  $m(\alpha) = \frac{\alpha\pi}{2} - \min_{1 \leq i \leq 2} |\arg(\lambda_i)|$ ;
- (c)  $\frac{dm(\alpha)}{d\alpha}|_{\alpha=\alpha^*} \neq 0$ . (transversality condition)

**Theorem 2.4.** Assume  $\delta > \sqrt{\frac{5}{3}}, b < \frac{-5+3\delta^2}{\delta\sigma}, b > \frac{5+13\delta^2}{\delta\sigma} - 4\sqrt{\frac{10(1+\delta^2)}{\sigma^2}}$ . Then the system (2.1) undergoes a Hopf bifurcation about the equilibrium point  $(u^*, v^*)$  when  $\alpha = \alpha^* = \frac{2}{\pi} \tan^{-1}(\frac{\sqrt{4\rho_0 - \rho_1^2}}{-\rho_1})$ .

*Proof.* We again consider the jacobian matrix  $J(u^*, v^*)$  (2.2) and the characteristic equation (2.2). The conditions  $\delta > \sqrt{\frac{5}{3}}$  and  $b < \frac{-5+3\delta^2}{\delta\sigma}$  ensures that  $\rho_1 < 0$ . Moreover the condition  $b > \frac{5+13\delta^2}{\delta\sigma} - 4\sqrt{\frac{10(1+\delta^2)}{\sigma^2}}$  guarantees that the eigenvalues  $\lambda_{1,2} = \frac{-\rho_1 \pm \sqrt{\rho_1^2 - 4\rho_0}}{2}$  of the  $J(u^*, v^*)$  are complex conjugates with positive real part. So,  $\min_{1 \leq i \leq 2} |\arg(\lambda_i)| = \tan^{-1}(\frac{\sqrt{4\rho_0 - \rho_1^2}}{-\rho_1})$ . For  $\alpha = \alpha^*, m(\alpha^*) = \frac{\alpha^*\pi}{2} - \min_{1 \leq i \leq 2} |\arg(\lambda_i)| = 0$ . Finally, the transversality condition  $\frac{dm(\alpha)}{d\alpha}|_{\alpha=\alpha^*} = \frac{\pi}{2} \neq 0$  is also satisfied, which proves the theorem.  $\square$

### 3. Fractional Order System with Delay

In this section, the fractional order version of the system (1.1) is considered with  $\tau > 0$ :

$$\begin{cases} D^\alpha u(t) = a - u - 4\frac{uv(t-\tau)}{1+u^2}, \\ D^\alpha v(t) = \sigma b \left( u - \frac{uv(t-\tau)}{1+u^2} \right). \end{cases} \tag{3.1}$$

Here  $\alpha \in (0, 1)$  is the order of the Caputo fractional derivative. We shall investigate the stability and Hopf bifurcation of the system (3.1) by setting the parameter  $\tau$  as a bifurcation parameter. We firstly note that, the system (3.1) with delay has also the same equilibrium point with the system (2.1) without delay, which is  $(u^*, v^*) = (\delta, 1 + \delta^2)$  where  $\delta = \frac{a}{5}$ .

**Theorem 3.1.** [29, 30] Consider the delayed, Caputo fractional fractional order system as

$$D^\alpha y(t) = Ay(t) + By(t-\tau), \quad y(t) = \Phi(t), t \in [-\tau, 0], \tag{3.2}$$

where  $\alpha \in (0, 1], y \in \mathbb{R}^n, A, B \in \mathbb{R}^{n \times n}$ , and  $\Phi(t) \in \mathbb{R}^{n \times n}$ . The characteristic equation of the system (3.2) is given as

$$\det |s^\alpha I - A - Be^{-s\tau}| = 0. \tag{3.3}$$

If all the roots of (3.3) have negative real parts, then the zero solution of system (3.2) is locally asymptotically stable.

By linearizing (3.1) about the positive equilibrium  $(u^*, v^*)$ , we obtain

$$\begin{cases} D^\alpha u(t) = \frac{3\delta^2 - 5}{1 + \delta^2} u(t) + \frac{4\delta}{1 + \delta^2} v(t-\tau), \\ D^\alpha v(t) = \frac{2\sigma b \delta^2}{1 + \delta^2} u(t) - \frac{\sigma b \delta}{1 + \delta^2} v(t-\tau). \end{cases} \tag{3.4}$$

The characteristic matrix of the system (3.4) is

$$J(u^*, v^*) = \begin{pmatrix} s - \frac{3\delta^2 - 5}{1 + \delta^2} & \frac{4\delta}{1 + \delta^2} e^{-s\tau} \\ \frac{-2\sigma b \delta^2}{1 + \delta^2} & s + \frac{\sigma b \delta}{1 + \delta^2} e^{-s\tau} \end{pmatrix}$$

and the corresponding characteristic equation is

$$s^{2\alpha} - ms^\alpha + (ns^\alpha + 5n)e^{-s\tau} = 0 \tag{3.5}$$

where

$$m = \frac{3\delta^2 - 5}{1 + \delta^2} \quad \text{and} \quad n = \frac{\sigma b \delta}{1 + \delta^2}.$$

**Theorem 3.2.** Assuming that the inequality (3.12) and the conditions of Theorem 2.2 are fulfilled, the following results hold for the fractional delayed system (3.1):

(i) The equilibrium point  $(u^*, v^*)$  is locally asymptotically stable for  $\tau < \tau_0$  where  $\tau_0 = \min\{\tau_k^j\}$  and

$$\tau_k^j = \frac{1}{\omega_k} \left[ \cos^{-1} \left( \frac{m^2 \omega_k^{2\alpha} - n^2 \omega_k^{2\alpha} - \omega_k^{4\alpha} + 25n^2}{10mn\omega_k^\alpha + 2n\omega_k^{3\alpha}} \right) - \frac{\alpha\pi}{2} + 2j\pi \right].$$

(ii) The system undergoes a Hopf bifurcation about the equilibrium point  $(u^*, v^*)$  for  $\tau = \tau_0$ .

*Proof.* Assume that the characteristic equation (3.5) has a pair of pure imaginary roots  $s_{1,2} = \pm i\zeta$ ,  $\zeta > 0$ . By putting  $s_1 = i\zeta$  into the equation (3.5), we obtain

$$(i\zeta)^{2\alpha} - m(i\zeta)^\alpha + (n(i\zeta)^\alpha + 5n)e^{-i\zeta\tau} = 0. \quad (3.6)$$

By separating real and imaginary parts of (3.6), one has

$$\begin{aligned} \zeta^{2\alpha} \cos\alpha\pi - m\zeta^\alpha \cos\frac{\alpha\pi}{2} &= -5n\cos\tau\zeta - n\zeta^\alpha \cos\left(\frac{\alpha\pi}{2} - \tau\zeta\right), \\ \zeta^{2\alpha} \sin\alpha\pi - m\zeta^\alpha \sin\frac{\alpha\pi}{2} &= 5n\sin\tau\zeta - n\zeta^\alpha \sin\left(\frac{\alpha\pi}{2} - \tau\zeta\right). \end{aligned} \quad (3.7)$$

Squaring and adding two equations in (3.7) yields to the equality

$$\zeta^{4\alpha} - 2m\zeta^{3\alpha} \cos\frac{\alpha\pi}{2} + \zeta^{2\alpha}(m^2 - n^2) - 10n^2\zeta^\alpha \cos\frac{\alpha\pi}{2} - 25n^2 = 0. \quad (3.8)$$

Since  $-25n^2 < 0$ , the Eq. (3.8) has at least one positive root. Denote this positive root as  $\zeta_k$ . Substituting  $\zeta_k$  in (3.7) gives

$$\begin{aligned} \zeta_k^{2\alpha} \cos\alpha\pi + n\zeta_k^\alpha \cos\left(\frac{\alpha\pi}{2} - \tau\zeta_k\right) &= -5n\cos\tau\zeta_k + m\zeta_k^\alpha \cos\frac{\alpha\pi}{2}, \\ \zeta_k^{2\alpha} \sin\alpha\pi + n\zeta_k^\alpha \sin\left(\frac{\alpha\pi}{2} - \tau\zeta_k\right) &= 5n\sin\tau\zeta_k + m\zeta_k^\alpha \sin\frac{\alpha\pi}{2}. \end{aligned} \quad (3.9)$$

Squaring and adding two equations in (3.9), we obtain

$$\zeta_k^{4\alpha} + \zeta_k^{3\alpha} 2n\cos\left(\frac{\alpha\pi}{2} + \tau\zeta_k\right) + \zeta_k^{2\alpha}(n^2 - m^2) + \zeta_k^\alpha 10mn\cos\left(\frac{\alpha\pi}{2} + \tau\zeta_k\right) - 25n^2 = 0. \quad (3.10)$$

From (3.10),  $\tau_k$  can be obtained as

$$\tau_k^j = \frac{1}{\omega_k} \left[ \cos^{-1} \left( \frac{m^2 \omega_k^{2\alpha} - n^2 \omega_k^{2\alpha} - \omega_k^{4\alpha} + 25n^2}{10mn\omega_k^\alpha + 2n\omega_k^{3\alpha}} \right) - \frac{\alpha\pi}{2} + 2j\pi \right],$$

where  $j=0,1,2, \dots$ . We define  $\tau_0 = \min\{\tau_k^j\}$ . For  $\tau < \tau_0$  all the roots of the characteristic equation (3.5) have negative real parts and the equilibrium point  $(u^*, v^*)$  is locally asymptotically stable.

Now, we check the transversality condition. Let us rewrite the characteristic equation (3.5) as

$$Q_1(s) + Q_2(s)e^{-s\tau} = 0, \quad (3.11)$$

where  $Q_1(s) = s^{2\alpha} - ms^\alpha$  and  $Q_2(s) = ns^\alpha + 5n$ . We differentiate (3.11) with respect to  $\tau$  to get

$$\frac{ds}{d\tau} (Q_1'(s) + Q_2'(s)e^{-s\tau} - Q_2(s)e^{-s\tau}\tau) - Q_2(s)e^{-s\tau}s = 0$$

and

$$\frac{ds}{d\tau} = \frac{Q_2(s)e^{-s\tau}s}{Q_1'(s) + Q_2'(s)e^{-s\tau} - Q_2(s)e^{-s\tau}\tau} = \frac{A(s)}{B(s)},$$

where

$$\begin{aligned} A(s) &= (ns^\alpha + 5n)e^{-s\tau}s = A_1 + iA_2, \\ B(s) &= 2\alpha s^{2\alpha-1} - m\alpha s^{\alpha-1} + n\alpha s^{\alpha-1}e^{-s\tau} - (ns^\alpha + 5n)e^{-s\tau}\tau = B_1 + iB_2. \end{aligned}$$

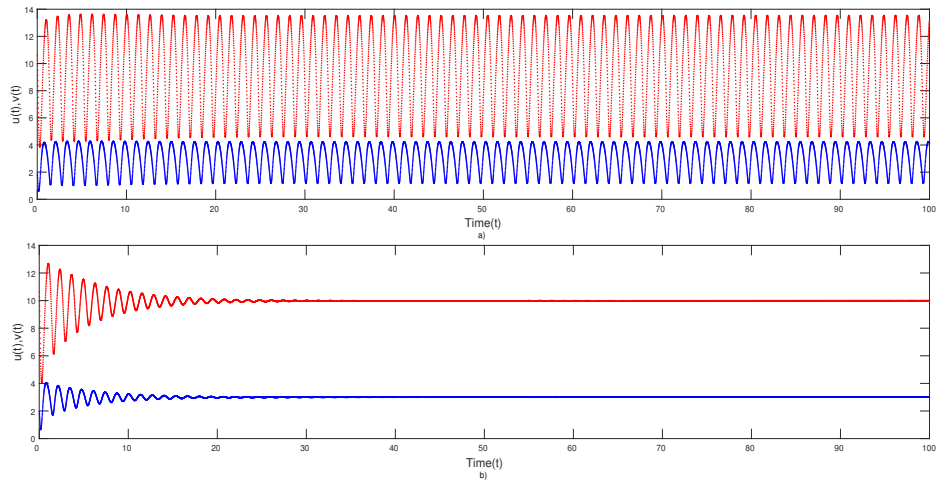
Let  $s(\tau) = v(\tau) + i\zeta(\tau)$  be the root of equation (3.11) with  $v(\tau_j) = 0$ ,  $\zeta(\tau_j) = \zeta_0$ . Then, we can obtain

$$\operatorname{Re} \left[ \frac{ds}{d\tau} \right] \Big|_{(\tau=\tau_0, \zeta=\zeta_0)} = \frac{A_1 B_1 + A_2 B_2}{B_1^2 + B_2^2}.$$

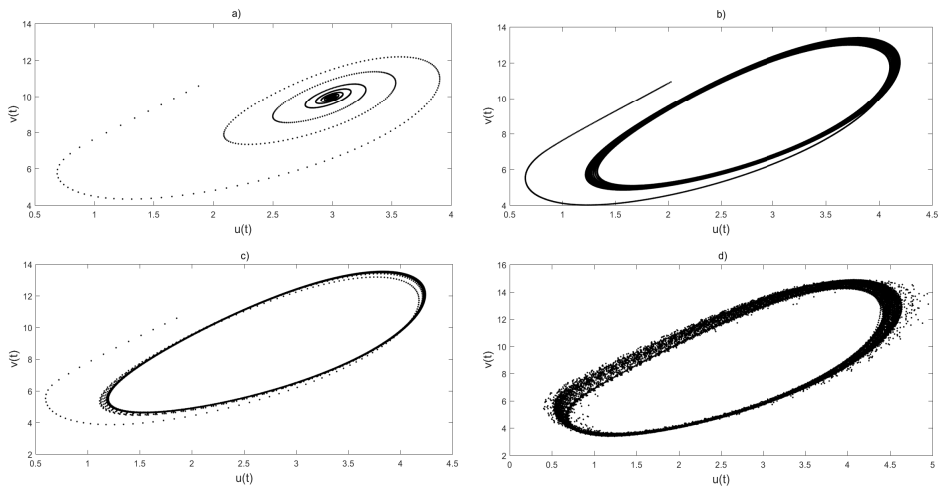
So, under the condition

$$\frac{A_1 B_1 + A_2 B_2}{B_1^2 + B_2^2} \neq 0,$$

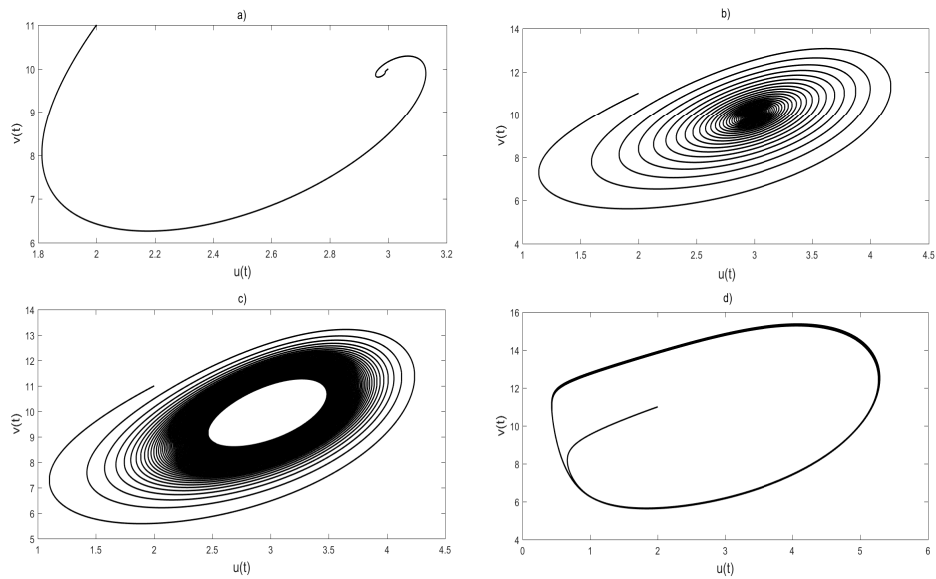
the transversality condition holds.  $\square$



(a) Solution of system (3.1) where  $\alpha = 0.80$ ,  $\tau = 0.11$  in a),  $\tau = 0.10$  in b);  $u(t)$  and  $v(t)$  displayed by blue and red lines resp. with initial condition (2, 11).



(b) Phase portraits of system (3.1) with varying the time delay  $\tau$  as  $\tau = 0.09$  a),  $\tau = 0.103$  b),  $\tau = 0.11$  c),  $\tau = 0.13$  d); where  $\alpha = 0.80$  and initial condition (2, 11).



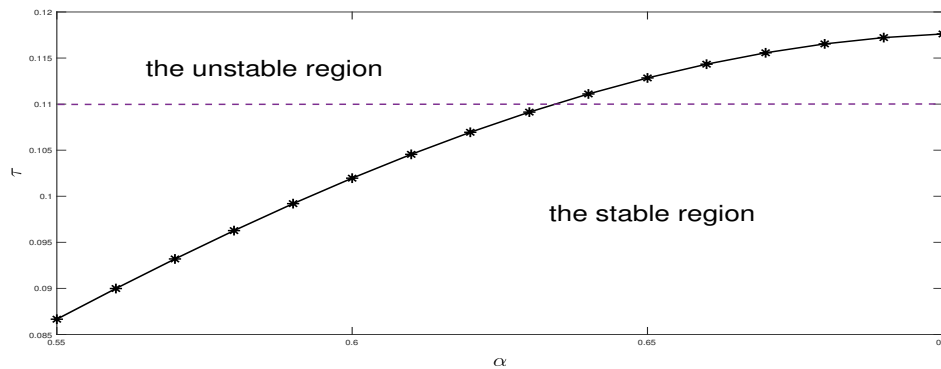
(c) Phase portraits of system (2.1) with varying the parameter  $b$  where  $b = 3$  a),  $b = 0.8$  b),  $b = 0.765879$  c),  $b = 0.4$  d);  $\alpha = 0.90$  and initial condition (2, 11).

Figure 3.1: Numerical simulations of system (3.1)

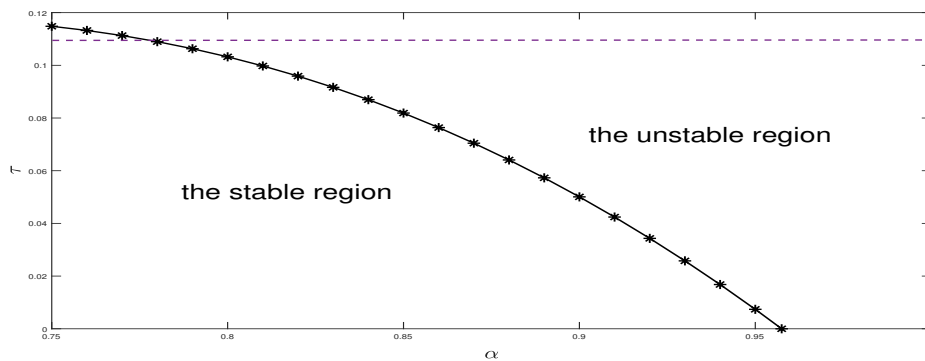
## 4. Numerical Results

In this section, numerical illustrations are displayed to support theoretical results. Firstly, we give numerical simulations about the system (2.1) using predictor corrector (PECE) method. The PECE method, referred to as fractional Adams-Bashforth-Moulton methods [31], has proven to be an accurate and powerful method to find approximate solutions of FDEs.

For numerical simulations, we pick parameter values as  $a = 15$ ,  $b = 1$ ,  $\sigma = 6$ . In Figure 2.1a, we observe that the equilibrium point  $(u^*, v^*) = (3, 10)$  is locally asymptotically stable for  $\alpha = 0.90$ . The critical bifurcation value of fractional order  $\alpha$  in Theorem 2.4 is calculated as  $\alpha^* = 0.9575$ . By setting  $\alpha = \alpha^*$ , the system (2.1) undergoes a Hopf bifurcation. We observe the oscillatory behavior of the solutions (Figure 2.1b).



(a) The curve represent the correlation between the fractional order parameter  $\alpha$  and the critical value of time delay  $\tau_0$  for the system (3.1) with  $0.75 \leq \alpha \leq 1$



(b) The curve represent the correlation between the fractional order parameter  $\alpha$  and the critical value of time delay  $\tau_0$  for the system (3.1) with  $0.50 \leq \alpha \leq 0.70$

**Figure 4.1:** Fractional order parameter  $\alpha$  versus delay parameter  $\tau$  in terms of stability

In Figure 2.1c, we give phase diagrams of the system (2.1) for several values of fractional order  $\alpha$ . There exist a limit cycle for  $\alpha = \alpha^* = 0.9975$  (Figure 2.1c,c). Moreover the system (2.1) is locally asymptotically stable for smaller values of  $\alpha$  (Figure 2.1c,a,b) and unstable otherwise (Figure 2.1c,d). In Figure 2.1d, we display the corresponding bifurcation diagram. In Figure 3.1c, we give phase diagrams of the system (2.1) for different values of  $b$ . We obtain the critical value of  $b$  as 0.765879 for which we obtain a limit cycle (Figure 3.1c,c). The unique positive equilibrium point of the system is locally asymptotically stable for bigger values of  $b$  (Figure 3.1c,a,b) and unstable otherwise (Figure 3.1c,d).

Now, we give numerical simulations of the fractional delayed differential system (3.1). We again pick parameter values as  $a = 15$ ,  $b = 1$ ,  $\sigma = 6$ . For  $\alpha = 0.80$ , the critical bifurcation value is calculated as  $\tau_0 = 0.1032287$ . For  $\tau < \tau_0$ , the system (3.1) shows stable behaviour (Figure 3.1a,b, Figure 3.1b,a). For  $\tau \approx \tau_0$ , we observe a periodic solution caused by Hopf bifurcation (Figure 3.1a,a, Figure 3.1b,b). For  $\tau > \tau_0$ , the system continues to exhibit oscillatory behavior and the equilibrium  $(3, 10)$  of the system (3.1) is unstable (Figure 3.1b,c,d).

Figure 4.1a and Figure 4.1b represent correlation between the fractional order parameter  $\alpha$  and the critical value of time delay  $\tau_0$  for the system (3.1). In general, we can say that the smaller fractional order enlarges the regions of stability for a system without delay. This is due to the stability condition  $|\arg(\lambda_i)| > \frac{\alpha\pi}{2}$  in Theorem 2.1. But, we cannot extend this statement for fractional delayed differential systems. In [11], the authors work on a fractional delayed network system and conclude that the Hopf bifurcation appearance is delayed as the order increases. So, for some values of  $\tau$ , mentioned system exhibit stable behaviour for bigger fractional order and exhibit unstable behaviour for smaller fractional order. On the other hand, in [18], authors conclude that the occurrence of bifurcation can be delayed with the decrease of the fractional order for the introduced fractional delayed predator-prey system. The system (3.1) we are examining in this article comprises both of these situations. For  $0.75 \leq \alpha \leq 0.9575$ , the critical value of time delay parameter  $\tau_0$  decreases while  $\alpha$  increases (Figure 4.1b). On the contrary, for  $0.50 \leq \alpha \leq 0.70$ ,  $\tau_0$  increases while fractional order parameter  $\alpha$  increases (Figure 4.1a). This behavioral change occurs approximately at  $\alpha = 0.707$  due to the characteristic equation (3.5) and the equation (3.8). We call this situation as ‘‘conflict of memory

effects” to emphasize that both fractional derivatives and time delays are using to reflect memory effects in modeling dynamical systems that also depend on past data. To better understand the destabilizing (Figure 4.1b) and stabilizing (Figure 4.1a) effect of increment of fractional order, we draw the line  $\tau = 0.11$  in both figures. For example, for  $\tau = 0.11$ , we observe that the system (3.1) is unstable for  $\alpha = 0.55$  and stable if  $\alpha = 0.65$  (Figure 4.2).

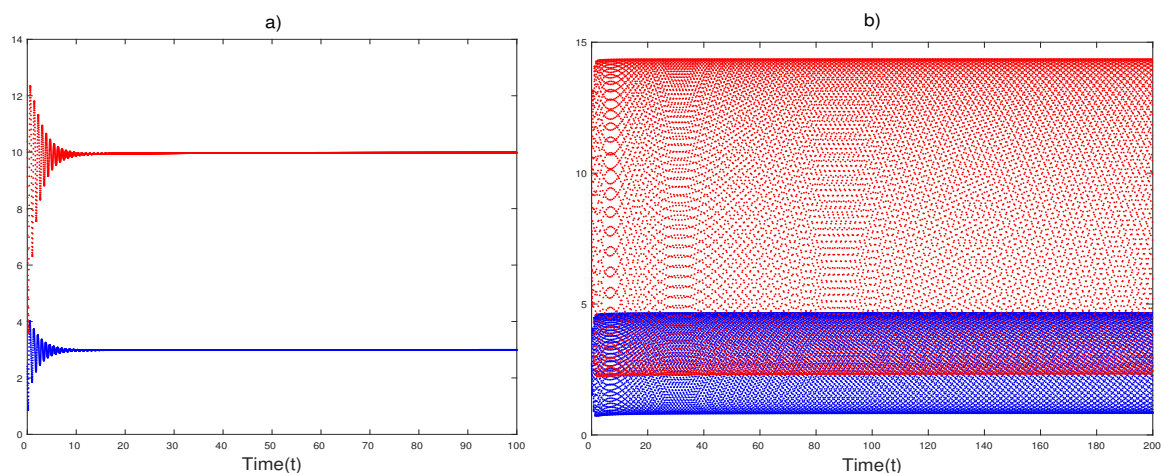


**Figure 4.2:** The equilibrium  $(u^*, v^*) = (3, 10)$  of the system (3.1) is locally asymptotically stable for  $\alpha = 0.65$  in a) and unstable for  $\alpha = 0.55$  in b) where  $\tau = 0.11$ .

## 5. Conclusions

This paper has analyzed local Lengley-Epstein system with fractional delayed differential equations. For the case  $\tau = 0$ , system (2.1) undergoes a Hopf bifurcation depending on  $\alpha$ . The stabilizing influence of the decrement in fractional order for the system (2.1) is exhibited with the help of numerical examples. Then, the impact of time delay parameter on the system (3.1) is investigated. The critical  $\tau_0$  value is determined such that the equilibrium point is locally asymptotically stable for  $\tau < \tau_0$ , and undergoes a Hopf bifurcation for  $\tau = \tau_0$ . Time delays and fractional derivatives are both used to include memory effects to the model if the current state of the system depends on past data. We conclude that for different values of time delay  $\tau$ , the decrement of the fractional order  $\alpha$  has opposite effects on the system (3.1) in terms of stability. We named this situation as ”conflict of memory effects”. Time delays are present in many chemical processes. By incorporating time delays into the local Lengley-Epstein system with the fractional order derivative, we observed the presence of oscillatory behavior, which is also encountered in chemical models, depending on the critical parameters.

## Article Information

**Acknowledgements:** The authors would like to express their sincere thanks to the editor and the anonymous reviewers for their invaluable feedback and insightful recommendations.

**Author’s contributions:** The article has a single author. The author has read and approved the final manuscript.

**Conflict of Interest Disclosure:** No potential conflict of interest was declared by the author.

**Copyright Statement:** Authors own the copyright of their work published in the journal and their work is published under the CC BY-NC 4.0 license.

**Supporting/Supporting Organizations:** No grants were received from any public, private or non-profit organizations for this research.

**Ethical Approval and Participant Consent:** It is declared that during the preparation process of this study, scientific and ethical principles were followed and all the studies benefited from are stated in the bibliography.

**Plagiarism Statement:** This article was scanned by the plagiarism program. No plagiarism detected.

**Availability of data and materials:** Not applicable.

## References

- [1] H. Esmonde, S. Holm, *Fractional derivative modelling of adhesive cure*, Appl. Math. Model., **77**(2) (2020), 1041-1053. doi.org/10.1016/j.apm.2019.08.021
- [2] B. Jamil, M.S. Anwar, A. Rasheed, M. Irfan, *MHD Maxwell flow modeled by fractional derivatives with chemical reaction and thermal radiation*, Chaos Solitons Fractals, **67** (2020), 512-533.
- [3] C. Zu, X. Yu, *Time fractional Schrödinger equation with a limit based fractional derivative*, Chaos Solitons Fractals, **157** (2022), 111941.
- [4] J.L. Echenausía-Monroy, H.E. Gilardi-Velázquez, R. Jaimes-Reátegui, V. Aboites, G. Huerta-Cuellar, *A physical interpretation of fractional-order derivatives in a jerk system: Electronic approach*, Chaos Solitons Fractals, **90** (2020), 105413.

- [5] C.M.A. Pinto, J.T. Machado, *Fractional model for malaria transmission under control strategies*, *Comput. Math. Appl.*, **66**(5) (2013), 908–916.
- [6] E. Balci, I. Ozturk, S. Kartal, *Dynamical behaviour of fractional order tumor model with Caputo and conformable fractional derivative*, *Chaos Solitons Fractals*, **123** (2019), 43-51.
- [7] M.B. Ghorji, P.A. Naik, J. Zu, Z. Eskandari, M. Naik, *Global dynamics and bifurcation analysis of a fractional-order SEIR epidemic model with saturation incidence rate*, *Math. Meth. Appl. Sci.*, **45**(7) (2022), 3665–3688.
- [8] P.A. Naik, M. Ghoreishi, J. Zu, *Approximate solution of a nonlinear fractional-order HIV model using homotopy analysis method*, *Int. J. Numer. Anal. Model.*, **19**(1) (2022), 52-84.
- [9] P.A. Naik, K.M. Owolabi, M. Yavuz, M, J. Zu, *Chaotic dynamics of a fractional order HIV-1 model involving AIDS-related cancer cells*, *Chaos Solitons Fractals*, **140** (2020), 110272.
- [10] P.F. Qu, Q.Z. Zhu, Y.F. Sun, *Elastoplastic modelling of mechanical behavior of rocks with fractional-order plastic flow*, *Int. J. Mech. Sci.*, **163** (2019), 105102.
- [11] C. Huang, J. Cao, M. Xiao, A. Alsaedi, T. Hayat, *Bifurcations in a delayed fractional complex-valued neural network*, *Appl. Math. Comput.*, **292** (2017), 210-227.
- [12] V.E. Tarasov, *No nonlocality. No fractional derivative*, *Commun. Nonlinear Sci. Numer. Simul.*, **62** (2018), 157-163.
- [13] B. Barman, B. Ghosh, B. *Explicit impacts of harvesting in delayed predator-prey models*, *Chaos Solitons Fractals*, **122** (2019), 213-228.
- [14] J. Cermak, J. Hornicek, T. Kisela, T. *Stability regions for fractional differential systems with a time delay*, *Commun. Nonlinear Sci. Numer. Simul.*, **1**(3) (2016), 108-123.
- [15] S. Liu, R. Yang, X.F. Zhou, W. Jiang, X. Li, X.W. Zhao, *Stability analysis of fractional delayed equations and its applications on consensus of multi-agent systems*, *Commun. Nonlinear Sci. Numer. Simul.*, **73** (2016), 351-362.
- [16] M. Lazarevic, *Stability and stabilization of fractional order time delay systems*, *Sci. Tech. Rev.*, **61**(1) (2011), 31-44.
- [17] X. Li, R. Wu, *Hopf bifurcation analysis of a new commensurate fractional-order hyperchaotic system*, *Nonlinear Dyn.*, **78**(1) (2014), 279-288.
- [18] H. Li, C. Huang, T. Li, *Dynamic complexity of a fractional-order predator–prey system with double delays*, *Phys. A*, **526** (2019), 120852.
- [19] J. Alidousti, M.M. Ghahfarokhi, *Stability and bifurcation for time delay fractional predator prey system by incorporating the dispersal of prey*, *Appl. Math. Model.*, **72** (2019), 385-402.
- [20] E. Balci, I. Ozturk, S. Kartal, *Comparison of dynamical behavior between fractional order delayed and discrete conformable fractional order tumor-immune system*, *Math. Model. Nat. Phenom.*, **16**(3) (2021).
- [21] I. Lengyel, I.R. Epstein, *Modeling of Turing structures in the chlorite iodide-malonic acid-starch reaction system*, *Science*, **251** (1991), 650-652.
- [22] I. Lengyel, I.R. Epstein, *A chemical approach to designing Turing patterns in reaction-diffusion system*, *Proc. Nati. Acad. Sci USA*, **89**(9) (1992), 3977-3979.
- [23] F. Yi, J. Wei, J. Shi, *Diffusion-driven instability and bifurcation in the Lengyel–Epstein system*, *Nonlinear Anal. Real World Appl.*, **9**(3) (2008), 1038-1051.
- [24] C. Çelik, H. Merdan, *Hopf bifurcation analysis of a system of coupled delayed-differential equations*, *Appl. Math. Comput.*, **219** (2013), 6605-6617.
- [25] B.D. Hassard, N.D. Kazarinoff, Y.H. Wan, *Theory and Applications of Hopf Bifurcation*, Cambridge University Press;1981.
- [26] D. Mansouri, S. Abdelmalek, S. Bendoukha, *On the asymptotic stability of the time-fractional Lengyel–Epstein system*, *Comput. Math. Appl.*, **78**(5) (2019), 1415-1430.
- [27] I. Petras, *Fractional-Order Nonlinear Systems: Modeling, Analysis and Simulation*, Springer Berlin; 2011.
- [28] K. Baisad, S. Moonchai, *Analysis of stability and Hopf bifurcation in a fractional Gauss-type predator-prey model with Allee effect and Holling type-III functional response*, *Adv. Differ. Equ.*, **2018** (2018), 82.
- [29] W. Deng, C. Li, J. Lu, *Stability analysis of linear fractional differential system with multiple time delays*, *Nonlinear Dyn.*, **48**(4) (2009), 409-416.
- [30] Z. Wang, X. Wang, X. *Stability and Hopf bifurcation analysis of a fractional-Order epidemic model with time delay*, *Math. Probl. Eng.* **2018** (2018), 2308245.
- [31] K. Diethelm, N.J. Ford, A.D. Freed, *A predictor-corrector approach for the numerical solution of fractional differential equations*, *Nonlinear Dyn.*, **29** (2002) 3-22.
- [32] S. Bhalekar, V.A. Daftardar-Gejji, *A predictor-corrector scheme for solving nonlinear delay differential equations of fractional order*, *J. Fract. Calc. Appl.*, **1**(5) (2011), 1-9.

# Qualitative Study of a Discrete-Time Harvested Fishery Model in the Presence of Toxicity

Debasis Mukherjee

Department of Mathematics, Vivekananda College, Thakurpukur, Kolkata-700063, India

## Article Info

**Keywords:** Bifurcation, Chaos control, Global stability, Michaelis-Menten type harvesting, Toxicity

**2010 AMS:** 39A28, 39A30, 92D10, 92D25

**Received:** 19 Sempember 2022

**Accepted:** 17 March 2023

**Available online:** 21 July 2023

## Abstract

This paper analyses a discrete-time Michaelis-Menten type harvested fishery model in the presence of toxicity. Boundary and interior (positive) fixed points are examined. Using an iteration scheme and the comparison principle of difference equations, we determined the sufficient condition for global stability of the interior fixed point. It is shown that the sufficient criterion for Neimark-Sacker bifurcation and flip bifurcation can be established. It is observed that the system behaves in a chaotic manner when a specific set of system parameters is selected, which are controlled by a hybrid control method. Examples are cited to illustrate our conclusions.

## 1. Introduction

In ecological modelling, harvesting is considered as a crucial factor that creates the attention among researchers due to its importance in resource management from the biological and economic point of views. The effect of harvesting on population is a basic problem in fishery theory. How harvesting influences population dynamics depends not only stock structure and ecological parameters but also on fishing strategies. The over-exploitation weakens the conservation of populations and also creates problem for fishery. So optimal harvesting problem should be taken into account within the models describing population dynamics. Optimal harvesting and mathematical models are investigated in [1]. Our main concern on fishery model as fish are one of the most valuable source of protein and many people depend on it and it is one of the most renewable resources in ecological system [2, 3]. Fish populations facing extinction not only for over fishing, but also on other factors such as competition and toxic materials. Industrial waste is a form of toxicity in aquatic ecosystems. In case of open access fishery, harvest by fishermen are unregulated. Under these conditions, there may be possibility of extinction of species. Different types of interactions are observed in fisheries systems. For the objectives of bioeconomic modelling, the most important are biological, harvest and market interactions [4]. In particular, the biological interactions indicate predator-prey, competition between them. The interactions between the fish populations is also significant. However, the impact of toxicity among the fish species emitted by each of them and emerge from factories, agricultural land etc. become problems of major environmental concern. On this issue, several works are done through mathematical models [5–10]. All these studies are mainly confined into one or two species without considering aquatic environment. It creates among researchers to examine the effects of toxicant released by the marine biological species. The toxin emitted by one species not only affects that species, but also affect the growth of the other species.

Maynard-Smith [11] considered the impact of toxic material in a two species Lotka-Volterra system, taking into account that each species produce a chemical toxic to the other but only when the other is present. Kar and Chaudhuri [6] modified the system studied in [11] to a two competing fish species which are commercially exploited. They proposed and analysed the following model:

$$\begin{aligned}\frac{dx}{dt} &= x(k_1 - \alpha_1 x - \beta_{12} y - \gamma_1 xy - q_1 E), \\ \frac{dy}{dt} &= y(k_2 - \alpha_2 y - \beta_{21} x - \gamma_2 xy - q_2 E)\end{aligned}\quad (1.1)$$

where  $x(t), y(t)$  are the densities of two competing fish species at time  $t$ , and  $k_1, k_2$  are intrinsic growth rates,  $\alpha_1, \alpha_2$  are the intra specific competition rates respectively. The constants  $\beta_{12}, \beta_{21}$  are the relative rate of inter specific competition.  $\gamma_1, \gamma_2$  are the coefficients of toxicity.

$E$  denotes the harvesting effort.  $q_1, q_2$  are the catchability coefficients of the two species. Similar type of system (1.1) is investigated in [12]. In studying harvesting phenomena, non-linear Michaelis-Menten harvesting is more realistic in fisheries modelling from the biological and economic point of views. The conventional catch-per-unit effort harvesting faces different unrealistic and insignificant characteristics. It is customary to take catch-per-unit effort harvesting  $h$  in the form  $h = qEx$  where  $q$  stands for the catchability coefficient of harvested population  $x$  and  $E$  denotes the harvesting effort used during the farming process. It is clear that when harvesting effort  $E$  is constant, harvesting activity  $h \rightarrow \infty$  as harvested population  $x \rightarrow \infty$  or when harvested population  $x$  is constant and fixed, harvesting activity  $h \rightarrow \infty$  as the harvesting effort  $E \rightarrow \infty$ . This hypothesis is unrealistic in case of random fishing due to unbounded linear increase of  $h$  with  $E$  and  $x$  [13]. In fact, Michaelis-Menten harvesting can eliminate this unrealistic situation by considering the harvesting term in the form  $\frac{qEx}{d_1E + d_2x}$ . It can be noted that for fixed effort  $E$ ,  $h \rightarrow \frac{qE}{d_1}$  when  $x \rightarrow \infty$  or for fixed harvested population  $x$ ,  $h \rightarrow \frac{qE}{d_1}$  when  $E \rightarrow \infty$ .

The above studies address into continuous capture system. Though, we know that fish distribution is inhomogeneous and it is more appropriate to consider the discrete system's capture which in turn maintains the ecological balance and save time and produce more economic revenue for fishermen. The dynamical behaviour of discrete time system is more complex than those obtained in continuous systems [14–16]. Even discrete time models can show chaotic dynamics [14, 15]. Hening [17] analysed the long-term behaviour of interacting populations in a discrete time stochastic system that can be controlled through harvesting. Ding et al. [18] investigated discrete time harvesting model of fish populations and they derived the necessary and sufficient conditions and the characterizations of the harvesting strategies.

The main aim of this work is to investigate the discrete version of system (1.1) as well as selective non-linear harvesting  $\frac{qEx}{d_1E + d_2x}$  in the first equation of system (1.1) where  $q$  is the catchability coefficient of the first species and  $d_1, d_2$  are the degree of competition in the harvesting business and handling time respectively. As we consider selective harvesting so  $q_2Ey = 0$ .

In this paper, we propose a discrete-time two competing fish species where each species release chemical toxic to another. We study the existence and stability of different fixed points. After then, we identify the system parameters that give Neimark-Sacker and flip bifurcation. Chaos control of the system will be examined. Finally, we examine the global stability of the interior fixed point of the method of iteration scheme.

The paper is formatted as follows. In Section 2, we present a discrete version of system (1.1). The dynamical behaviour of different fixed points is described in Section 3. Chaos control is shown in Section 4. Global stability criterion of interior fixed point is presented in Section 5. In Section 6, the dynamical behaviour of the system is demonstrated when values of parameters are changed. A brief discussion is given in Section 7.

## 2. Discrete Model

Now, we present the following discrete version of system (1.1):

$$\begin{aligned}x_{n+1} &= x_n \exp(k_1 - \alpha_1 x_n - \beta_{12} y_n - \gamma_1 x_n y_n - \frac{qE}{d_1 E + d_2 x_n}), \\y_{n+1} &= y_n \exp(k_2 - \alpha_2 y_n - \beta_{21} x_n - \gamma_2 x_n y_n)\end{aligned}\quad (2.1)$$

where  $x_n$  and  $y_n$  represent population densities of two competing fish species at  $n$ -generation respectively.

## 3. Fixed Points and Their Nature

In this section, we determine the fixed points and their dynamics. Evidently, system (1.1) has at most four non-negative fixed points  $E_0 = (0, 0)$ . If  $q < k_1 d_1$  then the fixed point  $E_1 = (\bar{x}, 0)$  exists uniquely where

$$\bar{x} = \frac{k_1 d_2 - \alpha_1 d_1 + \sqrt{(k_1 d_2 - \alpha_1 d_1)^2 + 4\alpha_1 d_2 E (k_1 d_1 - q)}}{2\alpha_1 d_2}.$$

If  $q > k_1 d_1, k_1 d_2 > \alpha_1 d_1$  and  $(k_1 d_2 - \alpha_1 d_1)^2 + 4\alpha_1 d_2 E (k_1 d_1 - q) > 0$  then multiple fixed points exist  $E_{1\pm} = (x_{\pm}, 0)$  where

$$x_{\pm} = \frac{k_1 d_2 - \alpha_1 d_1 \pm \sqrt{(k_1 d_2 - \alpha_1 d_1)^2 + 4\alpha_1 d_2 E (k_1 d_1 - q)}}{2\alpha_1 d_2} \quad \text{and} \quad E_2 = (0, \frac{k_2}{\alpha_2}).$$

There exists interior fixed point  $E^* = (x^*, y^*)$  where  $x^*$  is a positive root of the equation

$$a_0 x^3 + 3a_1 x^2 + 3a_2 x + a_3 = 0 \quad (3.1)$$

with

$$\begin{aligned}a_0 &= d_2 (\gamma_1 \beta_{21} - \alpha_1 \gamma_2), \\a_1 &= \frac{1}{3} [d_1 E (\gamma_1 \beta_{21} - \alpha_1 \gamma_2) + d_2 (k_1 \gamma_2 - \alpha_1 \alpha_2 + \beta_{12} \beta_{21} - \gamma_1 k_2)], \\a_2 &= \frac{1}{3} [d_1 E (k_1 \gamma_2 - \alpha_1 \alpha_2 + \beta_{12} \beta_{21} - \gamma_1 k_2) - d_2 \beta_{12} k_2 - qE \gamma_2 + d_2 k_1 \alpha_2], \\a_3 &= E (d_1 k_1 \alpha_2 - d_1 \beta_{12} k_2 - q \alpha_2)\end{aligned}\quad (3.2)$$

and  $y^* = \frac{k_2 - \beta_{21} x^*}{\alpha_2}$  provided  $k_2 > \beta_{21} x^*$ . Define

$$G = a_0^2 a_3 - 3a_0 a_1 a_2 + 2a_1^3, H = a_0 a_2 - a_1^2.$$

**Structure of the interior fixed points**

**Theorem 3.1.** Eq. (3.1) has

- (a) a unique positive root  $x^*$  if  $G^2 + H^3 > 0, a_0$  and  $a_3$  are of opposite signs.
- (b) two positive roots  $x_1^*, x_2^*$  if  $G^2 + H^3 < 0, a_0$  and  $a_3$  are of the same signs and  $a_1$  and  $a_2$  are of opposite signs.
- (c) three positive roots  $x_{11}^*, x_{12}^*, x_{13}^*$  if  $G^2 + H^3 < 0, a_0, a_2 > 0$  ( $or < 0$ ) and  $a_1, a_3 < 0$  ( $or > 0$ ).

*Proof.* The positive fixed point of system (2.1) satisfies the equations

$$k_1 - \alpha_1 x - \beta_{12} y - \gamma_1 xy - \frac{qE}{d_1 E + d_2 x} = 0, \tag{3.3}$$

$$k_2 - \alpha_2 y - \beta_{21} x - \gamma_2 xy = 0. \tag{3.4}$$

From the Eq. (3.4), we get  $y = \frac{k_2 - \beta_{21} x}{\alpha_2 + \gamma_2 x}$ . Substituting the value of  $y$  to the equation (3.3) is precisely equation (3.1).

- (a) Assumptions of the theorem implies that (3.1) has one real root and two imaginary roots. Since  $a_0$  and  $a_3$  are of opposite signs so (3.1) has a unique positive root.
- (b) Assumptions of the theorem implies that (3.1) has three real roots and one of them is negative. Consequently, (3.1) has two positive roots.
- (c) Assumptions of the theorem implies that (3.1) has three real roots and there is no negative roots. Consequently, (3.1) has three positive roots. This completes the proof.

To determine the nature of the fixed points, we compute the Jacobian matrix at each fixed point. The Jacobian matrix at an arbitrary fixed point  $(x, y)$  is given by

$$J(x, y) = \begin{pmatrix} m_{11} & m_{12} \\ m_{21} & m_{22} \end{pmatrix} \tag{3.5}$$

where

$$\begin{aligned} m_{11} &= \left\{ 1 - (\alpha_1 + \gamma_1 y - \frac{d_2 q E}{(d_1 E + d_2 x)^2}) x \right\} \exp(k_1 - \alpha_1 x - \beta_{12} y - \gamma_1 xy - \frac{qE}{d_1 E + d_2 x}), \\ m_{12} &= -(\beta_{12} + \gamma_1 x) x \exp(k_1 - \alpha_1 x - \beta_{12} y - \gamma_1 xy - \frac{qE}{d_1 E + d_2 x}), \\ m_{21} &= -(\beta_{21} + \gamma_2 y) y \exp(k_2 - \alpha_2 y - \beta_{21} x - \gamma_2 xy), \\ m_{22} &= \left\{ 1 - (\alpha_2 + \gamma_2 x) y \right\} \exp(k_2 - \alpha_2 y - \beta_{21} x - \gamma_2 xy). \end{aligned}$$

We first present the results which will be required to investigate the nature of fixed points.

**Lemma 3.2.** ([19]) Let the characteristic equation of  $J$  is  $F(\lambda) = \lambda^2 + p\lambda + q = 0$ . Suppose  $\lambda_1$  and  $\lambda_2$  are two roots of  $F(\lambda) = 0$ . Then there are the following definitions.

- 1. If  $|\lambda_1| < 1$  and  $|\lambda_2| < 1$  then the fixed point is called a sink and is locally asymptotically stable.
- 2. If  $|\lambda_1| > 1$  and  $|\lambda_2| > 1$  then the fixed point is called a source and unstable.
- 3. If  $|\lambda_1| > 1$  and  $|\lambda_2| < 1$  then the fixed point is called a saddle.
- 4. If  $|\lambda_1| = 1$  or  $|\lambda_2| = 1$  then the fixed point is called non-hyperbolic.

**Lemma 3.3.** ([19]) Let  $F(\lambda) = \lambda^2 + p\lambda + q$  where  $p$  and  $q$  are constants. Suppose  $F(1) > 0$  and  $\lambda_1$  and  $\lambda_2$  are two roots of  $F(\lambda) = 0$ . Then

- 1.  $|\lambda_1| < 1$  and  $|\lambda_2| < 1$  if and only if  $F(-1) > 0$  and  $q < 1$ ,
- 2.  $|\lambda_1| > 1$  and  $|\lambda_2| > 1$  if and only if  $F(-1) > 0$  and  $q > 1$ ,
- 3.  $|\lambda_1| < 1$  and  $|\lambda_2| > 1$  if and only if  $F(-1) < 0$ ,
- 4.  $\lambda_1 = -1$  and  $|\lambda_2| \neq 1$  if and only if  $F(-1) = 0$  and  $p \neq 0, 2$ ,
- 5.  $\lambda_1$  and  $\lambda_2$  are the conjugate complex roots and  $|\lambda_1| = |\lambda_2| = 1$  if and only if  $p^2 - 4q < 0$  and  $q = 1$ .

**Theorem 3.4.** For all positive parameters, system (2.1) has the fixed point  $E_0 = (0, 0)$  then  $E_0$  is:

- 1. source if  $k_1 > \frac{q}{d_1}$  and hence unstable.
- 2. saddle if  $k_1 < \frac{q}{d_1}$ .
- 3. non-hyperbolic if  $k_1 = \frac{q}{d_1}$ .

*Proof.* The Jacobian matrix of system (2.1) at  $E_0$  is

$$J(E_0) = \begin{pmatrix} \exp(k_1 - \frac{q}{d_1}) & 0 \\ 0 & \exp k_2 \end{pmatrix} \tag{3.6}$$

Here the eigenvalues of  $J(E_0)$  are  $\lambda_1 = \exp(k_1 - \frac{q}{d_1}) > 1$  if  $k_1 > \frac{q}{d_1}$  and  $\lambda_1 < 1$  if  $k_1 < \frac{q}{d_1}$ . If  $k_1 = \frac{q}{d_1}$  then  $\lambda_1 = 1$  and  $\lambda_2 = \exp k_2 > 1$  since  $k_2 > 0$ . Hence  $E_0$  is a source when  $k_1 > \frac{q}{d_1}$  and hence unstable.  $E_0$  is a saddle when  $k_1 < \frac{q}{d_1}$ . Lastly,  $E_0$  is non-hyperbolic when  $k_1 = \frac{q}{d_1}$ . This completes the proof.

**Theorem 3.5.** Assume that  $q < k_1 d_1$ . The fixed point  $E_1 = (\bar{x}, 0)$ .  $E_1$  is

- 1. sink if  $\frac{d_2 q E \bar{x}}{(d_1 E + d_2 \bar{x})^2} < \alpha_1 \bar{x} < q + \frac{d_2 q E \bar{x}}{(d_1 E + d_2 \bar{x})^2}$  and  $k_2 < \beta_{21} \bar{x}$ .
- 2. saddle if one of the following conditions hold:

- (a)  $\alpha_1 \bar{x} > q + \frac{d_2 q E \bar{x}}{(d_1 E + d_2 \bar{x})^2}$  and  $k_2 < \beta_{21} \bar{x}$ .  
 (b)  $\frac{d_2 q E \bar{x}}{(d_1 E + d_2 \bar{x})^2} < \alpha_1 \bar{x} < q + \frac{d_2 q E \bar{x}}{(d_1 E + d_2 \bar{x})^2}$  and  $k_2 > \beta_{21} \bar{x}$ .

3. source if  $\alpha_1 \bar{x} > q + \frac{d_2 q E \bar{x}}{(d_1 E + d_2 \bar{x})^2}$  and  $k_2 > \beta_{21} \bar{x}$ , then  $E_1$  is unstable.

4. non-hyperbolic if  $1 + \frac{d_2 q E \bar{x}}{(d_1 E + d_2 \bar{x})^2} = \alpha_1 \bar{x}$  or  $k_2 = \beta_{21} \bar{x}$ .

*Proof.* The Jacobian matrix of system (2.1) at  $E_1$  is

$$J(E_1) = \begin{pmatrix} 1 - (\alpha_1 - \frac{d_2 q E \bar{x}}{(d_1 E + d_2 \bar{x})^2}) \bar{x} & -(\beta_{12} + \gamma_1 \bar{x}) \bar{x} \\ 0 & \exp(k_2 - \beta_{21} \bar{x}) \end{pmatrix} \quad (3.7)$$

The eigenvalues of  $J(E_1)$  are  $\lambda_1 = 1 - (\alpha_1 - \frac{d_2 q E \bar{x}}{(d_1 E + d_2 \bar{x})^2}) \bar{x}$ ,  $\lambda_2 = \exp(k_2 - \beta_{21} \bar{x})$ . Similar to the proof of Theorem 3.4, the above results can be easily derived.

**Remark.** In case of multiple fixed points  $E_{\pm}$ , we can obtain similar type of conditions as in Theorem 3.5, where  $\bar{x}$  is replaced by  $x_{\pm}$  for determining the nature of  $E_{1\pm}$ .

**Theorem 3.6.** System (2.1) always has the fixed point  $E_2 = (0, \frac{k_2}{\alpha_2})$ .  $E_2$  is

- sink if  $k_2 < 2$  and  $k_1 < \frac{d_1 \beta_{12} k_2 + q \alpha_2}{\alpha_2 d_1}$ .
- saddle if one of the following conditions hold:
  - $k_2 > 2$  and  $k_1 < \frac{d_1 \beta_{12} k_2 + q \alpha_2}{\alpha_2 d_1}$ .
  - $k_2 < 2$  and  $k_1 > \frac{d_1 \beta_{12} k_2 + q \alpha_2}{\alpha_2 d_1}$ .
- source if  $k_2 > 2$  and  $k_1 > \frac{d_1 \beta_{12} k_2 + q \alpha_2}{\alpha_2 d_1}$ , then  $E_1$  is unstable.
- non-hyperbolic if  $k_2 = 2$  or  $k_1 = \frac{d_1 \beta_{12} k_2 + q \alpha_2}{\alpha_2 d_1}$ .

*Proof.* The proof is similar to the proof of Theorem 3.4 and is omitted here.

**Theorem 3.7.** Assume that the conditions of Theorem 3.1 be hold and also suppose that  $a > 0$ . Then the fixed point  $E^*$  is

- sink if  $a < b \leq 2$  or  $b > 2$  and  $2b - 4 < a < b$ ,
- source if  $b \leq 2$  and  $a > b$  or  $b > 2$  and  $a > \max\{b, 2b - 4\}$ ,
- saddle if  $b > 2$  and  $a < 2b - 4$ ,
- non-hyperbolic if  $a < 2b - 4$ , where

$$a = x^* y^* \left\{ (\alpha_1 + \gamma_1 y^* - \frac{d_2 q E}{(d_1 E + d_2 x^*)^2}) (\alpha_2 + \gamma_2 x^*) - (\beta_{12} + \gamma_1 x^*) (\beta_{21} + \gamma_2 y^*) \right\} \quad (3.8)$$

$$b = (\alpha_1 + \gamma_1 y^* - \frac{d_2 q E}{(d_1 E + d_2 x^*)^2}) x^* + (\alpha_2 + \gamma_2 x^*) y^* \quad (3.9)$$

*Proof.* The Jacobian matrix at  $E^*$  is

$$J(E^*) = \begin{pmatrix} 1 - (\alpha_1 + \gamma_1 y^* - \frac{d_2 q E}{(d_1 E + d_2 x^*)^2}) x^* & -(\beta_{12} + \gamma_1 x^*) x^* \\ -(\beta_{21} + \gamma_2 y^*) y^* & 1 - (\alpha_2 + \gamma_2 x^*) y^* \end{pmatrix} \quad (3.10)$$

so the characteristic equation of the above matrix can be written as

$$F(\lambda) = \lambda^2 + p\lambda + q = 0 \quad (3.11)$$

where  $p = -2 + b$  and  $q = 1 - b + a$ . After simple calculation, we get

$$\begin{aligned} F(1) &= 1 + p + q = a, \\ F(-1) &= 1 - p + q = 4 - 2b + a, \\ q - 1 &= a - b. \end{aligned}$$

Now  $F(1) > 0$  if  $a > 0$ .  $F(-1) > 0$  if  $b \leq 2$  and  $a > 0$  or  $b > 2$  and  $a > 2b - 4$ ,  $F(-1) < 0$  if  $b > 2$  and  $a < 2b - 4$ ,  $q - 1 < 0$  if  $a < b$ . According to Lemma 3.2 and 3.3,  $E^*$  is a sink and it is stable, if the conclusion (1) of Theorem 3.7 holds. Next, if the other conditions of Theorem 3.7 hold separately,  $E^*$  is a source, saddle and non-hyperbolic, respectively, at which  $E^*$  is unstable. This completes the proof.

### 3.1. Bifurcation around the interior fixed point

System (2.1) has at most an unique fixed point  $E^*$ , hence the system does not admit fold bifurcation. So we are interested in examining the Neimark-Sacker bifurcation and flip bifurcation.

**Theorem 3.8.** The fixed point  $E^*$  changes from the stable state to Neimark-Sacker bifurcation if the following conditions are satisfied:  $a = b$  and  $b < 4$  where  $a$  and  $b$  are defined in (3.8) and (3.9).

*Proof.* If the Jacobian matrix  $J(E^*)$  has two complex conjugate eigenvalues with modulus 1, Neimark-Sacker bifurcation appears [20]. This requires that  $\det(J(E^*)) = q = 1$  and  $-2 < \text{tr}(J(E^*)) = -p < 2$ . Replacing  $p$  and  $q$ , we have  $a = b$  and  $b < 4$ . This completes the proof.

**Theorem 3.9.** The fixed point  $E^*$  changes from the stable state to flip bifurcation if the following conditions are satisfied:

$$a + 4 = 2b.$$

*Proof.* System (1.1) admits flip bifurcation when a single eigenvalue  $-1$ . Thus the condition for flip bifurcation can be written in the form  $1 - p + q = 0$ . Replacing  $p$  and  $q$ , we have  $a + 4 = 2b$ . This completes the proof.

### 4. Chaos Control

In discrete dynamical system, one can observe chaotic behaviour for certain choices of the system parameters and controlling chaos is an important issue. There are different methods for controlling chaos. We use mainly use hybrid control technique [21] to stabilize a chaotic orbit at an unstable fixed point of system (2.1). Define the following controlled system with respect to (2.1):

$$\begin{aligned} x_{n+1} &= \rho x_n \exp(k_1 - \alpha_1 x_n - \beta_{12} y_n - \gamma_1 x_n y_n - \frac{qE}{d_1 E + d_2 x_n}) + (1 - \rho)x_n, \\ y_{n+1} &= \rho y_n \exp(k_2 - \alpha_2 y_n - \beta_{21} x_n - \gamma_2 x_n y_n) + (1 - \rho)y_n \end{aligned} \tag{4.1}$$

where  $0 < \rho < 1$  is taken as a control parameter. The Jacobian matrix of controlled system (4.1) evaluated at  $E^*$  is given by

$$J(x^*, y^*) = \begin{pmatrix} 1 - \rho x^* (\alpha_1 + \gamma_1 y^* - \frac{qE d_2}{(d_1 E + d_2 x^*)^2}) & -\rho x^* (\beta_{12} + \gamma_1 x^*) \\ -\rho y^* (\beta_{21} + \gamma_2 y^*) & 1 - \rho y^* (\alpha_2 + \gamma_2 x^*) \end{pmatrix} \tag{4.2}$$

The fixed point  $E^*$  of the controlled system (4.1) is locally asymptotically stable if all the roots of the characteristic polynomial of (4.2) lie in an unit open disk.

### 5. Global Stability

In this section, we will utilize the process of iteration scheme and the comparison principle of difference equation to investigate the global stability of the positive fixed point of system (2.1). To establish global stability result, we require the following lemmas.

**Lemma 5.1.** ([19]) Let  $f(u) = u \exp(\delta - \eta u)$ , where  $\delta$  and  $\eta$  are positive constants. Then  $f(u)$  is nondecreasing for  $u \in (0, \frac{1}{\eta}]$ .

**Lemma 5.2.** ([19]) Assume that the sequence  $u_n$  satisfies  $u_{n+1} = u_n \exp(\delta - \eta u_n)$ ,  $n = 1, 2, 3, \dots$  where  $\delta$  and  $\eta$  are positive constants and  $u_0 > 0$ . Then;

1. If  $\delta < 2$ , then  $\lim_{n \rightarrow \infty} u_n = \frac{\delta}{\eta}$ .
2. If  $\delta \leq 1$ , then  $u_n \leq \frac{1}{\eta}$ ,  $n = 2, 3, \dots$

**Lemma 5.3.** ([22]) Suppose that functions  $f, g : \mathbb{Z}_+ \times [0, \infty)$  satisfy  $f(n, x) \leq g(n, x)$  ( $f(n, x) \geq g(n, x)$ ) for  $n \in \mathbb{Z}_+$  and  $g(n, x)$  is nondecreasing with respect to  $x$ . If  $u_n$  are the nonnegative solutions of the difference equations

$$\begin{aligned} x_{n+1} &= f(n, x_n), \\ u_{n+1} &= g(n, u_n) \end{aligned}$$

respectively, and  $x_0 \leq u_0$  ( $x_0 \geq u_0$ ) then  $x_n \leq u_n$  ( $x_n \geq u_n$ ) for all  $n \geq 0$ .

**Theorem 5.4.** Assume that  $\frac{k_2 d_1 (\beta_{12} \alpha_1 + \gamma_1 k_1) + q \alpha_1 \alpha_2}{d_1 \alpha_1 \alpha_2} < k_1 \leq 1$  and  $\frac{k_1 (\beta_{21} \alpha_2 + \gamma_2 k_2)}{\alpha_1 \alpha_2} < k_2 \leq 1$  then the fixed point  $E^*(x^*, y^*)$  of system (2.1) is globally asymptotically stable.

*Proof.* Assume that  $(x_n, y_n)$  is any solution of system (2.1) with initial values  $x_0 > 0, y_0 > 0$ . Let

$$\begin{aligned} U_1 &= \limsup_{n \rightarrow \infty} x_n, \quad V_1 = \liminf_{n \rightarrow \infty} x_n, \\ U_2 &= \limsup_{n \rightarrow \infty} y_n, \quad V_2 = \liminf_{n \rightarrow \infty} y_n. \end{aligned}$$

In the following, we will prove that  $U_1 = V_1 = x^*, U_2 = V_2 = y^*$ .

First we show that  $U_1 \leq M_1^x, U_2 \leq M_1^y$ . From the first equation of system (2.1), we get

$$x_{n+1} \leq x_n \exp(k_1 - \alpha_1 x_n), \quad n = 0, 1, 2, \dots$$

Considering the auxiliary equation

$$u_{n+1} = u_n \exp(k_1 - \alpha_1 u_n) \tag{5.1}$$

by Lemma 5.2 (ii), because of  $k_1 \leq 1$ , we get  $u_n \leq \frac{1}{\alpha_1}$  for all  $n \geq 2$ . By Lemma 5.1, we obtain  $f(u) = u \exp(k_1 - \alpha_1 u)$  is nondecreasing for  $u \in (0, \frac{1}{\alpha_1}]$ . Thus from Lemma 5.3, we get  $x_n \leq u_n$  for all  $n \geq 2$ , where  $u_n$  is the solution of Eq. (5.1) with initial value  $u_2 = x_2$ . By Lemma 5.2 (i), we get

$$U_1 = \limsup_{n \rightarrow \infty} x_n \leq \lim_{n \rightarrow \infty} u_n = \frac{k_1}{\alpha_1}.$$

Hence, for any sufficiently small  $\varepsilon > 0$ , there exists a  $n_1 > 2$  such that if  $n \geq n_1$ , then

$$x_n \leq \frac{k_1}{\alpha_1} + \varepsilon = M_1^x.$$

Similarly, from the second equation of system (2.1), we obtain,

$$U_2 = \limsup_{n \rightarrow \infty} y_n \leq \lim_{n \rightarrow \infty} u_n = \frac{k_2}{\alpha_2} \quad \text{as } k_2 \leq 1.$$

Hence, for any sufficiently small  $\varepsilon > 0$ , there exists a  $n_2 > n_1$  such that if  $n \geq n_2$ , then

$$y_n \leq \frac{k_2}{\alpha_2} + \varepsilon = M_1^y.$$

Next we show that  $V_1 \geq N_1^x$  and  $V_2 \geq N_1^y$ . From the first equation of system (2.1), we have

$$x_{n+1} \geq x_n \exp(k_1 - \alpha_1 x_n - \beta_{12} M_1^y - \gamma_1 M_1^x M_1^y - \frac{q}{d_1})$$

Consider the auxiliary equation

$$u_{n+1} = u_n \exp(k_1 - \frac{q}{d_1} - \alpha_1 u_n - \beta_{12} M_1^y - \gamma_1 M_1^x M_1^y). \quad (5.2)$$

Since we have  $k_1 - \frac{q}{d_1} - \beta_{12} M_1^y - \gamma_1 M_1^x M_1^y < 1$ , by Lemma 5.2 (ii), we have,  $u_n \leq \frac{1}{\alpha_1}$  for  $n \geq n_2$ . By Lemma 5.1, we obtain  $f(u) = u \exp(k_1 - \frac{q}{d_1} - \beta_{12} M_1^y - \gamma_1 M_1^x M_1^y - \alpha_1 u)$  is nondecreasing for  $u \in (0, \frac{1}{\alpha_1}]$ . Thus from Lemma 5.3, we get  $x_n \geq u_n$  for all  $n \geq n_2$ . By Lemma 5.2 (i), we get

$$V_1 = \liminf_{n \rightarrow \infty} x_n \geq \lim_{n \rightarrow \infty} u_n = \frac{d_1(k_1 - \beta_{12} M_1^y - \gamma_1 M_1^x M_1^y) - q}{d_1 \alpha_1}.$$

Hence for any sufficiently small  $\varepsilon > 0$ , there exists  $n_3 > n_2$  such that for  $n \geq n_3$ ,

$$x_n \geq \frac{d_1(k_1 - \beta_{12} M_1^y - \gamma_1 M_1^x M_1^y) - q}{d_1 \alpha_1} - \varepsilon = N_1^x.$$

From the second equation of system (2.1), we have

$$y_{n+1} \geq y_n \exp(k_2 - \alpha_2 y_n - \beta_{21} M_1^x - \gamma_2 M_1^x M_1^y).$$

Since we have  $0 < k_2 - \beta_{21} M_1^x - \gamma_2 M_1^x M_1^y < 1$ , a similar argument as above, we can get

$$V_2 = \liminf_{n \rightarrow \infty} y_n = \frac{k_2 - \beta_{21} M_1^x - \gamma_2 M_1^x M_1^y}{\alpha_2}.$$

Hence for any sufficiently small  $\varepsilon > 0$ , there exists  $n_4 > n_3$  such that for  $n \geq n_4$ ,

$$y_n \geq \frac{k_2 - \beta_{21} M_1^x - \gamma_2 M_1^x M_1^y}{\alpha_2} - \varepsilon = N_1^y.$$

Now we show that  $U_1 \leq M_2^x, U_2 \leq M_2^y$  where  $M_2^x \leq M_1^x, M_2^y \leq M_1^y$  respectively. From the first equation of system (2.1) for  $n > n_4$ , we get

$$x_{n+1} \leq x_n \exp(k_1 - \alpha_1 x_n - \beta_{12} N_1^y - \gamma_1 N_1^x N_1^y - \frac{qE}{d_1 E + d_2 M_1^x}).$$

Since  $M_1^x > N_1^x$  and  $M_1^y > N_1^y$ , we get

$$k_1 - \frac{q}{d_1} - \beta_{12} M_1^y - \gamma_1 M_1^x M_1^y < k_1 - \beta_{12} N_1^y - \gamma_1 N_1^x N_1^y - \frac{qE}{d_1 E + d_2 M_1^x} \leq k_1 \leq 1.$$

Using the similar argument as in above, we can get

$$U_1 = \limsup_{n \rightarrow \infty} x_n \leq \frac{1}{\alpha_1} [k_1 - \beta_{12} N_1^y - \gamma_1 N_1^x N_1^y].$$

Hence for any sufficiently small  $\varepsilon > 0$ , there exists  $n_5 > n_4$  such that for  $n \geq n_5$ ,

$$x_n \leq \frac{1}{\alpha_1} [k_1 - \beta_{12} N_1^y - \gamma_1 N_1^x N_1^y - \frac{qE}{d_1 E + d_2 M_1^x}] + \frac{\varepsilon}{2} = M_2^x \leq M_1^x.$$

Similarly, from the second equation of system (2.1) for  $n > n_5$ , we get

$$y_{n+1} \leq y_n \exp[k_2 - \alpha_2 y_n - \beta_{21} N_1^x - \gamma_2 N_1^x N_1^y],$$

since

$$k_2 - \beta_{21} M_1^x - \gamma_2 M_2^x M_2^y < k_2 - \beta_{21} N_1^x - \gamma_2 N_1^x N_1^y \leq k_2 \leq 1.$$

Using the similar argument as in above, we can get

$$U_2 = \limsup_{n \rightarrow \infty} y_n \leq \frac{1}{\alpha_2} [k_2 - \beta_{21} N_1^x - \gamma_2 N_1^x N_1^y],$$

Hence for any sufficiently small  $\varepsilon > 0$ , there exists  $n_6 > n_5$  such that for  $n \geq n_6$ ,

$$y_n \leq \frac{1}{\alpha_2} [k_2 - \beta_{21} N_1^x - \gamma_2 N_1^x N_1^y] + \frac{\varepsilon}{2} = M_2^y \leq M_1^y.$$

Now we show that  $V_1 \geq N_2^x$  and  $V_2 \geq N_2^y$ . Further, from the first of system (2.1) for  $n > n_6$ , we get

$$x_{n+1} \geq x_n \exp\left[k_1 - \frac{qE}{d_1E + d_2N_1^x} - \alpha_1x_n - \beta_{12}M_2^y - \gamma_1M_2^xM_2^y\right].$$

Since  $M_1^y \geq M_2^y, M_1^x \geq M_2^x$ , we have

$$0 < k_1 - \frac{q}{d_1} - \beta_{12}M_1^y - \gamma_1M_1^xM_1^y < k_1 - \frac{qE}{d_1E + d_2N_1^x} - \beta_{12}M_2^y - \gamma_1M_2^xM_2^y.$$

Using a similar argument, we get

$$V_1 = \liminf_{n \rightarrow \infty} x_n \geq \frac{1}{\alpha_1} \left[ k_1 - \frac{qE}{d_1E + d_2N_1^x} - \beta_{12}M_2^y - \gamma_1M_2^xM_2^y \right].$$

Hence for any sufficiently small  $\varepsilon > 0$ , there exists  $n_7 > n_6$  such that for  $n \geq n_7$ ,

$$x_n \geq \frac{1}{\alpha_1} \left[ k_1 - \frac{qE}{d_1E + d_2N_1^x} - \beta_{12}M_2^y - \gamma_1M_2^xM_2^y \right] - \frac{\varepsilon}{2} = N_2^x.$$

Similarly, from the second equation of system (2.1) for  $n > n_7$ , we have

$$y_{n+1} \geq y_n \exp[k_2 - \alpha_2y_n - \beta_{21}M_2^x - \gamma_2M_2^xM_2^y].$$

Since

$$0 < k_2 - \beta_{21}M_1^x - \gamma_2M_1^xM_1^y < k_2 - \beta_{21}M_2^x - \gamma_2M_2^xM_2^y \leq k_2 \leq 1$$

we have

$$V_2 = \liminf_{n \rightarrow \infty} y_n \geq \frac{1}{\alpha_2} [k_2 - \beta_{21}M_2^x - \gamma_2M_2^xM_2^y].$$

Hence for any sufficiently small  $\varepsilon > 0$ , there exists  $n_8 > n_7$  such that for  $n \geq n_8$ ,

$$y_n \geq \frac{1}{\alpha_2} [k_2 - \beta_{21}M_2^x - \gamma_2M_2^xM_2^y] - \frac{\varepsilon}{2} = N_2^y.$$

Repeating the above process, we ultimately get four sequences  $\{M_n^x\}, \{M_n^y\}, \{N_n^x\}, \{N_n^y\}$  such that for all  $n \geq 2$ ,

$$\begin{aligned} M_n^x &= \frac{1}{\alpha_1} \left[ k_1 - \beta_{12}N_{n-1}^y - \gamma_1N_{n-1}^xN_{n-1}^y - \frac{qE}{d_1E + d_2M_{n-1}^x} \right] + \frac{\varepsilon}{n}, \\ M_n^y &= \frac{1}{\alpha_2} [k_2 - \beta_{21}N_{n-1}^x - \gamma_2N_{n-1}^xN_{n-1}^y] + \frac{\varepsilon}{n}, \\ N_n^x &= \frac{1}{\alpha_1} \left[ k_1 - \beta_{12}M_n^y - \gamma_1M_n^xM_n^y - \frac{qE}{d_1E + d_2N_{n-1}^x} \right] - \frac{\varepsilon}{n}, \\ N_n^y &= \frac{1}{\alpha_2} [k_2 - \beta_{21}M_n^x - \gamma_2M_n^xM_n^y] - \frac{\varepsilon}{n}. \end{aligned} \tag{5.3}$$

Clearly, we have for any integer  $n > 0, N_n^x \leq V_1 \leq U_1 \leq M_n^x$  and  $N_n^y \leq V_2 \leq U_2 \leq M_n^y$ .

In the following, we will prove that  $\{M_n^x\}$  and  $\{M_n^y\}$  are monotonically decreasing and  $\{N_n^x\}$  and  $\{N_n^y\}$  are monotonically increasing, with the help of mathematical induction. Firstly, when  $n = 2$ , it is clear that

$$M_2^x \leq M_1^x, M_2^y \leq M_1^y, N_2^x \geq N_1^x \quad \text{and} \quad N_2^y \geq N_1^y.$$

For  $n = k (k \geq 2)$ , we assume that

$$M_k^x \leq M_{k-1}^x, M_k^y \leq M_{k-1}^y, N_k^x \geq N_{k-1}^x \quad \text{and} \quad N_k^y \geq N_{k-1}^y.$$

Now

$$\begin{aligned} M_{k+1}^x - M_k^x &= \frac{1}{\alpha_1} \left[ k_1 - \beta_{12}N_k^y - \gamma_1N_k^xN_k^y - \frac{qE}{d_1E + d_2M_k^x} \right] + \frac{\varepsilon}{k+1} - \frac{1}{\alpha_1} \left[ k_1 - \beta_{12}N_{k-1}^y - \gamma_1N_{k-1}^xN_{k-1}^y - \frac{qE}{d_1E + d_2M_{k-1}^x} \right] - \frac{\varepsilon}{k} \\ &= -\frac{\beta_{12}}{\alpha_1} [N_k^y - N_{k-1}^y] - \frac{\gamma_1}{\alpha_1} [N_k^xN_k^y - N_{k-1}^xN_{k-1}^y] + \frac{qEd_2(M_k^x - M_{k-1}^x)}{\alpha_1(d_1E + d_2M_k^x)(d_1E + d_2M_{k-1}^x)} - \frac{\varepsilon}{k(k+1)} \leq 0. \\ M_{k+1}^y - M_k^y &= \frac{1}{\alpha_2} [k_2 - \beta_{21}N_k^x - \gamma_2N_k^xN_k^y] + \frac{\varepsilon}{k+1} - \frac{1}{\alpha_2} [k_2 - \beta_{21}N_{k-1}^x - \gamma_2N_{k-1}^xN_{k-1}^y] - \frac{\varepsilon}{k} \\ &= -\frac{\beta_{21}}{\alpha_2} [N_k^x - N_{k-1}^x] - \frac{\gamma_2}{\alpha_2} [N_k^xN_k^y - N_{k-1}^xN_{k-1}^y] - \frac{\varepsilon}{k(k+1)} \leq 0 \\ N_{k+1}^x - N_k^x &= \frac{1}{\alpha_1} \left[ k_1 - \beta_{12}M_{k+1}^y - \gamma_1M_{k+1}^xM_{k+1}^y - \frac{qE}{d_1E + d_2N_k^x} \right] - \frac{\varepsilon}{k+1} - \frac{1}{\alpha_1} \left[ k_1 - \beta_{12}M_k^y - \gamma_1M_k^xM_k^y - \frac{qE}{d_1E + d_2N_{k-1}^x} \right] + \frac{\varepsilon}{k} \\ &= -\frac{\beta_{12}}{\alpha_1} [M_{k+1}^y - M_k^y] - \frac{\gamma_1}{\alpha_1} [M_{k+1}^xM_{k+1}^y - M_k^xM_k^y] + \frac{qEd_2(N_k^x - N_{k-1}^x)}{\alpha_1(d_1E + d_2N_k^x)(d_1E + d_2N_{k-1}^x)} + \frac{\varepsilon}{k(k+1)} \geq 0 \\ N_{k+1}^y - N_k^y &= \frac{1}{\alpha_2} [k_2 - \beta_{21}M_{k+1}^x - \gamma_2M_{k+1}^xM_{k+1}^y] - \frac{\varepsilon}{k+1} - \frac{1}{\alpha_2} [k_2 - \beta_{21}M_k^x - \gamma_2M_k^xM_k^y] + \frac{\varepsilon}{k} \\ &= -\frac{\beta_{21}}{\alpha_2} [M_{k+1}^x - M_k^x] - \frac{\gamma_2}{\alpha_2} [M_{k+1}^xM_{k+1}^y - M_k^xM_k^y] + \frac{\varepsilon}{k(k+1)} \geq 0. \end{aligned}$$

This shows that  $\{M_n^x\}$  and  $\{M_n^y\}$  are monotonically decreasing and  $\{N_n^x\}$  and  $\{N_n^y\}$  are monotonically increasing. Therefore, by the criterion of monotonic bounded, we have established that every one of this four sequences has a limit.

Let  $\lim_{n \rightarrow \infty} M_n^x = x_1$ ,  $\lim_{n \rightarrow \infty} M_n^y = y_1$ ,  $\lim_{n \rightarrow \infty} N_n^x = x_2$ ,  $\lim_{n \rightarrow \infty} N_n^y = y_2$ . Passing to the limit as  $n \rightarrow \infty$  in (5.3), we get

$$\begin{aligned} x_1 &= \frac{1}{\alpha_1} \left[ k_1 - \beta_{12} y_2 - \gamma_1 x_2 y_2 - \frac{qE}{d_1 E + d_2 x_1} \right], \\ y_1 &= \frac{1}{\alpha_2} [k_2 - \beta_{21} x_2 - \gamma_2 x_2 y_2], \\ x_2 &= \frac{1}{\alpha_1} \left[ k_1 - \beta_{12} y_1 - \gamma_1 x_1 y_1 - \frac{qE}{d_1 E + d_2 x_2} \right], \\ y_2 &= \frac{1}{\alpha_2} [k_2 - \beta_{21} x_1 - \gamma_2 x_1 y_1]. \end{aligned} \quad (5.4)$$

It is clear that  $x_1 = x_2$  and  $y_1 = y_2$ . Thus we obtain  $x_1 = x_2 = x^*$ ,  $y_1 = y_2 = y^*$  as a solution of (5.3). Hence, the global asymptotic stability of  $E^*(x^*, y^*)$  is obtained. This completes the proof of the theorem.

## 6. Numerical Simulation

In this section, we present some numerical simulation to illustrate the usefulness of the obtained results as well as for giving direction to find desirable bifurcations and chaos of the discrete time system (2.1).

**Example 6.1.** Suppose  $k_1 = 0.8, k_2 = 0.6, \alpha_1 = 1, \alpha_2 = 1, \beta_{12} = 0.1, \beta_{21} = 0.01, \gamma_1 = 1, \gamma_2 = 1, E = 4, q = 0.1, d_1 = 1, d_2 = 1$ . It follows from Theorem 5.4 that the fixed point (0.478, 0.4027) is globally stable (see Figure 6.1a and 6.1b) for initial points (0.1, 0.1) and (0.5, 0.2) respectively.

**Example 6.2.** Suppose  $k_1 = 2, k_2 = 2.8, \alpha_2 = 1.5, \beta_{12} = 1, \beta_{21} = 1.1, \gamma_1 = 0.5, \gamma_2 = 1.4, E = 1, q = 0.1, d_1 = 1, d_2 = 1$  and the initial point (0.5, 0.5) for system (2.1). We draw the bifurcation diagram with respect to the parameter  $\alpha_1$  in the interval (0.75, 1.5). As  $\alpha_1$  increases, we observe a transition phase from stability to bifurcation within a limit cycle, to a periodic window and ultimately to chaos (see Figure 6.2).

**Example 6.3.** Suppose  $k_1 = 2, k_2 = 2.8, \alpha_1 = 1, \alpha_2 = 1.5, \beta_{12} = 1, \beta_{21} = 1.1, \gamma_1 = 0.5, E = 1, q = 0.1, d_1 = 1, d_2 = 1$  and the initial point (0.5, 0.5) for system (2.1). We draw the bifurcation diagram with respect to the parameter  $\gamma_2$  in the interval (0.7, 1.5). As  $\gamma_2$  increases, we observe a transition phase from chaotic behaviour to stable state (see Figure 6.3).

**Example 6.4.** Suppose  $k_1 = 1.1, \alpha_1 = 0.1, \alpha_2 = 0.5, \beta_{12} = 0.1, \beta_{21} = 0.1, \gamma_1 = 0.5, \gamma_2 = 0.1, E = 1, q = 0.1, d_1 = 1, d_2 = 1$  and the initial point (0.5, 0.5) for system (2.1). We draw the bifurcation diagram with respect to the parameter  $k_2$  in the interval (1.5, 3). As  $k_2$  increases, we observe a transition phase from stability to bifurcation within a limit cycle, to a periodic window and ultimately to chaos (see Figure 6.4).

**Example 6.5.** Suppose  $k_1 = 2.2, k_2 = 3.2, \alpha_1 = 1, \alpha_2 = 1.5, \beta_{12} = 1, \beta_{21} = 0.5, \gamma_1 = 0.01, \gamma_2 = 2, E = 1, d_1 = 1, d_2 = 1, q = 0.1$  and the initial point (0.1, 0.1) for system (2.1) showing chaotic dynamics. The condition (3) of Theorem 3.7 is satisfied and the fixed point (1.664, 0.4905) is saddle in nature and hence unstable. Chaotic dynamics is observed (see Figure 6.5a). The chaotic system is controlled when we choose  $\rho = 0.5$  for system (4.1) (see Figure 6.5b).

**Example 6.6.** Suppose  $k_1 = 2.2, k_2 = 3.5, \alpha_1 = 1, \alpha_2 = 1.5, \beta_{12} = 1, \beta_{21} = 2.1, \gamma_1 = 0.04, \gamma_2 = 0.62, q = 0.1, d_1 = 1, d_2 = 1$  and the initial point (0.5, 0.5) for system (2.1). We draw the bifurcation diagram with respect to the parameter  $E$  in the interval (0.1, 1.5). As  $E$  increases, we observe a transition phase from stability to bifurcation within a limit cycle, to a periodic window and ultimately to chaos (see Figure 6.6).

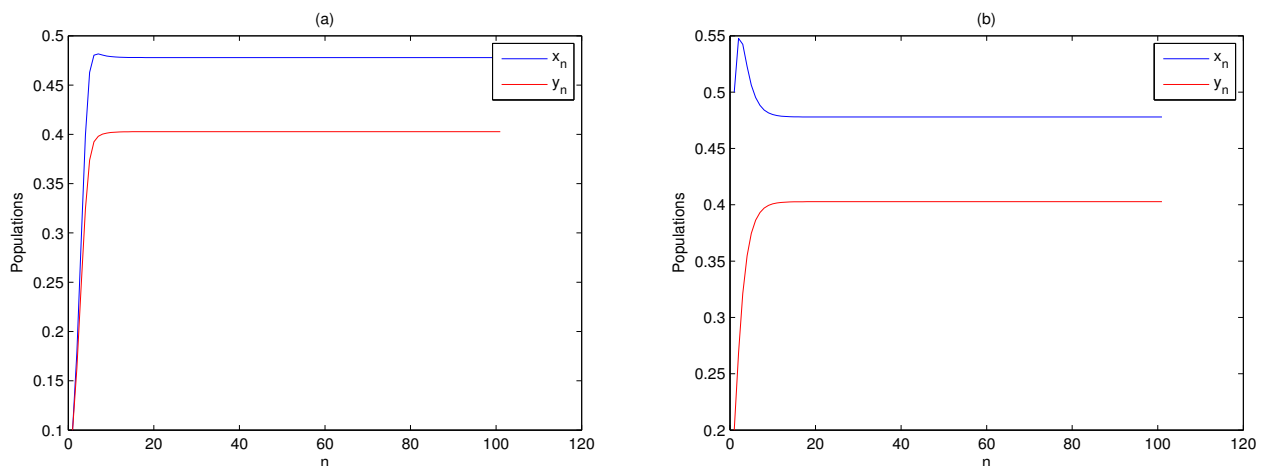


**Figure 6.1:** Time series plots of system (2.1) for  $k_1 = 0.8, k_2 = 0.6, \alpha_1 = 1, \alpha_2 = 1, \beta_{12} = 0.1, \beta_{21} = 0.01, \gamma_1 = 1, \gamma_2 = 1, E = 4, q = 0.1, d_1 = 1, d_2 = 1$  with initial points (0.1, 0.1) and (0.5, 0.2) respectively

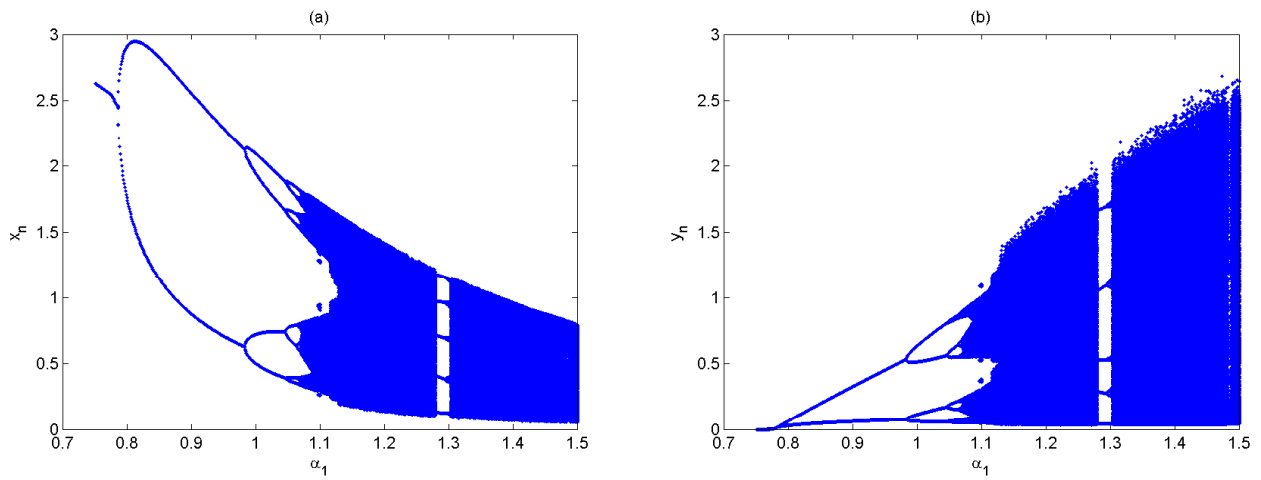


**Figure 6.2:** Bifurcation diagram for two competing fish species with  $\alpha_1$  of system (2.1) for fixed values  $k_1 = 2, k_2 = 2.8, \alpha_2 = 1.5, \beta_{12} = 1, \beta_{21} = 1.1, \gamma_1 = 0.5, \gamma_2 = 1.4, E = 1, q = 0.1, d_1 = 1, d_2 = 1$ .

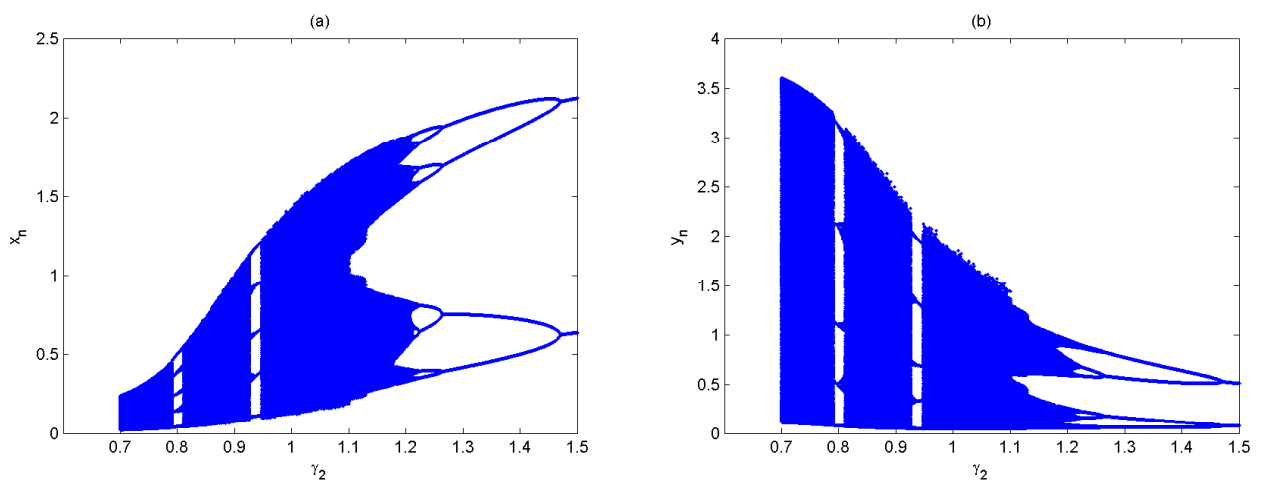


**Figure 6.3:** Bifurcation diagram for competing fish species  $\gamma_2$  of system (1.1) for fixed values  $k_1 = 2, k_2 = 2.8, \alpha_1 = 1, \alpha_2 = 1.5, \beta_{12} = 1, \beta_{21} = 1.1, \gamma_1 = 0.5, E = 1, q = 0.1, d_1 = 1, d_2 = 1$ .

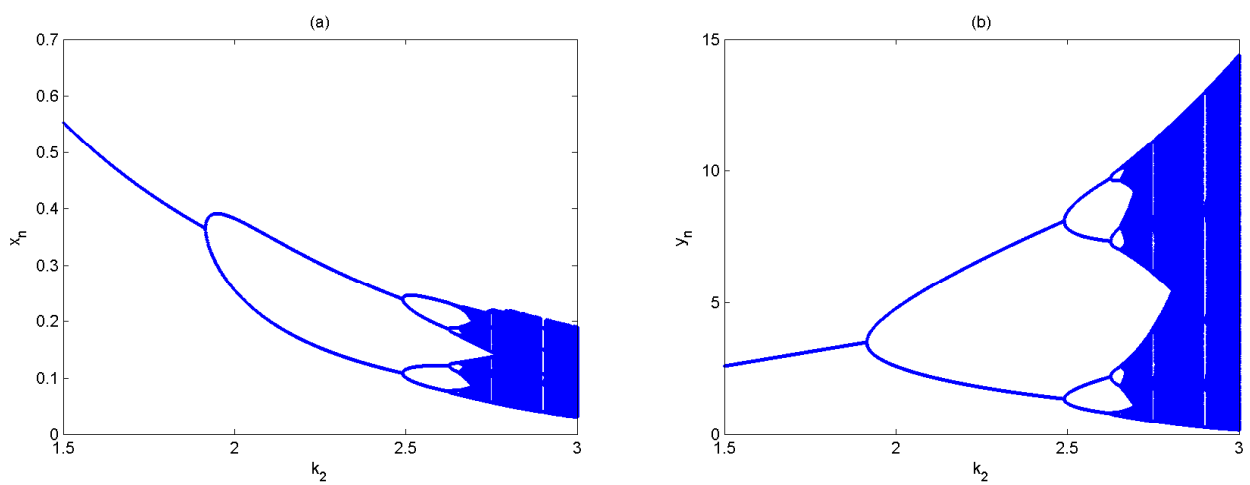


**Figure 6.4:** Bifurcation diagram for competing fish species with  $k_2$  of system (2) for fixed values  $k_1 = 1.1, \alpha_1 = 0.11, \alpha_2 = 0.5, \beta_{12} = 0.1, \beta_{21} = 0.1, \gamma_1 = 0.5, \gamma_2 = 1, E = 1, q = 0.1, d_1 = 1, d_2 = 1$ .

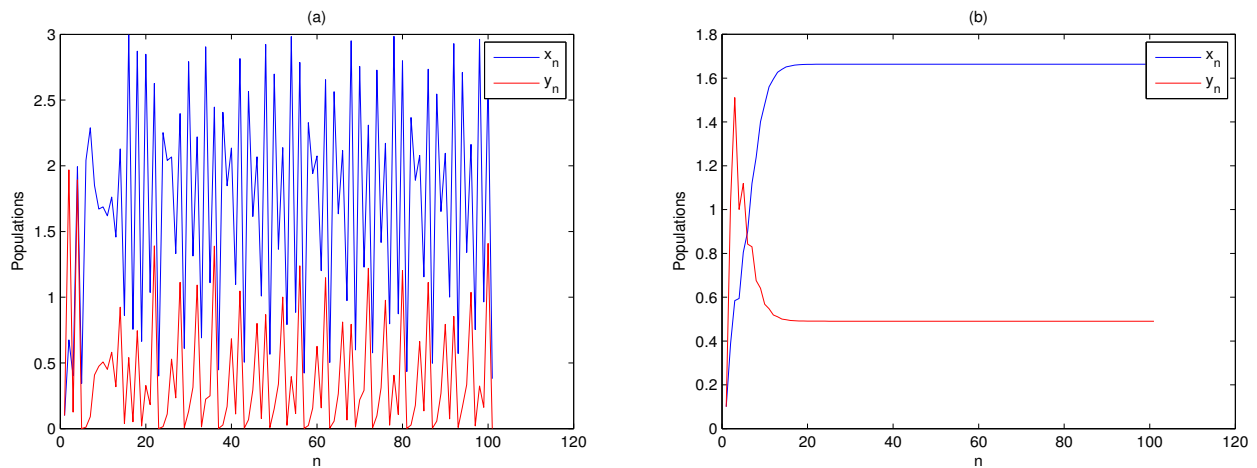


**Figure 6.5:** Time series plots for two competing fish species of system (2.1) fixed values  $k_1 = 2.2, k_2 = 3.2, \alpha_1 = 1, \alpha_2 = 1.5, \beta_{12} = 1, \beta_{21} = 0.5, \gamma_1 = 0.01, \gamma_2 = 2, E = 1, d_1 = 1, d_2 = 1, q = 0.1$  and for system (14) with  $\rho = 0.5$ .

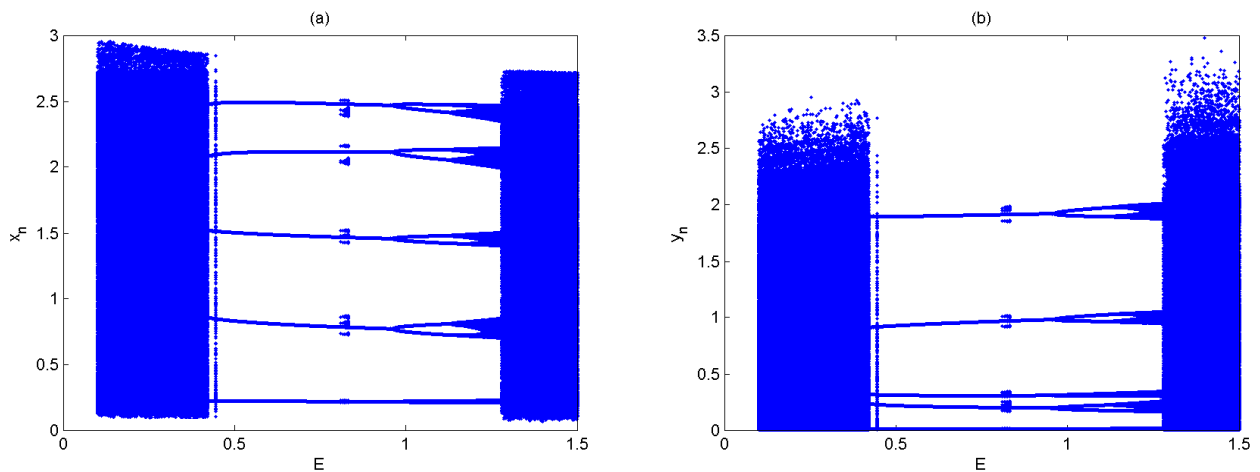


**Figure 6.6:** Bifurcation diagram for competing fish species with  $E$  of system (2.1) for fixed values  $k_1 = 2.2, k_2 = 3.5, \alpha_1 = 1, \alpha_2 = 1.5, \beta_{12} = 1, \beta_{21} = 1.1, \gamma_1 = 0.4, \gamma_2 = 0.62, d_1 = 1, d_2 = 1, q = 0.1$

## 7. Discussion

Kar and Chaudhuri [6] proposed system (1.1) and showed global stability and existence of biometric equilibrium under certain conditions. The main novelty in our study is to introduce the non-linear Michaelis-Menten type harvesting in the first equation of system (1.1) and examine the dynamical behaviour of discrete version of the continuous system. Discrete-time harvesting models studied in [17, 18] did not consider the effect of toxicity of the interacting populations. Michaelis-Menten harvesting of the first species plays a significant role in determining the dynamics and bifurcations of the system. We discover interesting oscillations in the population size which are not observed in the continuous system. The parameters  $q$  and  $d_1$  in the harvesting term influence the number and stability of the fixed points. The stability of boundary and interior fixed points is examined. As the trivial fixed point always exists and unstable when the intrinsic growth rate of the first fish species exceeds a certain threshold value, which in turn implies that the two species cannot go to extinction together. Neimark-Sacker and flip bifurcation, chaos control is investigated. Furthermore, the detailed mathematical proof of the global stability of the positive fixed point is given by using iteration scheme and the comparison principle of difference equations. Conditions of Theorem 5.4 indicate that if the intrinsic growth rates remain below one, then the global stability of the system may occur. But if we increase these rates, then the chaotic behaviour will appear (see Figure 6.5 a). The chaotic nature of the system is controlled by the hybrid control technique (see Figure 6.5b). In investigating bifurcation, we have identified that intra specific competition rate ( $\alpha_1$ ), toxicity rate ( $\gamma_2$ ) and the intrinsic growth rate ( $k_2$ ) have a major role in the system dynamics. It is observed that if the value of one of the parameters  $\alpha_1$  or  $k_2$  are increased we find a transition phase from stability to bifurcation within a limit cycle, to a periodic window and ultimately to chaos (see Figure 6.2 and Figure 6.4) whereas the opposite holds when we increase the value of the toxic inhibition rate (see Figure 6.3). Thus, the increase amount toxicity level can enhance the stability of the system. According to Figure 6.6, we can observe that the system is under control when harvesting effort  $E$  is low and chaotic when it is increased. Bifurcating behaviour and chaos have always been considered as an unwanted situation in biology. There will be a high risk of extinction of the species due to chaos. So, to prevent such extinction of the species, one can consider the application of a hybrid control method. It is to be noted that the competition terms used in (1.1) are instantaneous. In other words, two different species that compete for a given resource require a certain amount of time to get the resource. So the interference term of the model will be in the form of

a Holling type II. Also, both the species can be harvested in the form mentioned above. Therefore, the model (2.1) can be reformulated as:

$$\begin{aligned}x_{n+1} &= x_n \exp\left(k_1 - \alpha_1 x_n - \frac{\beta_{12} y_n}{1 + a_1 x_n} - \gamma_1 x_n y_n - \frac{q_1 E}{d_1 E + d_2 x_n}\right), \\y_{n+1} &= y_n \exp\left(k_2 - \alpha_2 y_n - \frac{\beta_{21} x_n}{1 + a_2 y_n} - \gamma_2 x_n y_n - \frac{q_2 E}{d_3 E + d_4 y_n}\right)\end{aligned}\quad (7.1)$$

Stability, bifurcation analysis and chaos control for model (7.1) is our future work for investigation.

## Article Information

**Acknowledgements:** The author is grateful to the anonymous reviewers for their helpful comments for improving the paper.

**Author's contributions:** The author contributed solely to the writing of this paper. The author read and approved the final manuscript.

**Conflict of Interest Disclosure:** No potential conflict was declared by the author.

**Copyright Statement:** Authors own copyright of his work published and his work is published under the CC BY-NC 4.0 license.

**Ethical Approval and Participant Consent:** It is declared that during the preparation process of this study, scientific and ethical principles were followed and all the studies benefited from are stated in the bibliography.

**Supporting/Supporting Organizations:** This research received no specific grant from any funding agency in the public, commercial or not-for-profit sectors.

**Plagiarism Statement:** This article was scanned by the plagiarism program. No plagiarism detected.

**Availability of data and materials:** Not applicable.

## References

- [1] C. W. Clark, *Mathematical Bioeconomics: The Optimal Management of Renewable Resources*, Wiley, New York, 1976.
- [2] M. Mesterton-Gibbons, *On the optimal policy for the combined harvesting of predator and prey*, Nat. Resour. Model., **3** (1988), 63-90.
- [3] M. Mesterton-Gibbons, *A technique for finding optimal two species harvesting policies*, Ecol. Model., **92** (1996), 235-244.
- [4] O. Flaaten, *On the bioeconomics of predator prey fishery*, Fish. Res., **37** (1998), 179-191.
- [5] T. G. Hallam, C. W. Clark, *Non-autonomous logistic equations as models of populations in a deteriorating environment*, J. Theoret. Biol., **93** (1982), 303-313.
- [6] T. K. Kar, K. S. Chaudhuri, *On non-selective harvesting of two competing fish species in the presence of toxicity*, Ecol. Model., **161** (2003), 125-137.
- [7] J. Chattopadhyay, *Effect of toxic substances on a two species competitive system*, Ecol. Model., **84** (1996), 287-289.
- [8] T. G. Hallam, J. T. De Luna, *Effects of toxicants on populations : a qualitative approach 3. Environmental and food chain pathways*, J. Theoret. Biol., **199** (1984), 411-429.
- [9] H. I. Freedman, J. B. Shukla, *Models for the effect of toxicant in a single species and predator prey systems*, J. Math. Biol., **30** (1990), 15-30.
- [10] D. Mukherjee, *Persistence and global stability of a population in a polluted environment with delay*, J. Biol. Syst., **10**(3) (2002), 1-8.
- [11] J. M. Smith, *Mathematical Models in Biology*, Cambridge University Press. Cambridge, 1968.
- [12] M. Haque, S. Sarwardi, *Effect of toxicity on a harvested fishery model*, Model. Earth Syst. Environ., **2** (2016), 122.
- [13] D. Hu, H. Cao, *Stability and bifurcation analysis in a predator-prey system with Michaelis-Menten type predator harvesting*, Nonlinear Anal. Real World Appl., **33** (2017), 58-82.
- [14] H. N. Agiza, E. M. Elabbasy, El-Metwally, A. A. Elasadany, *Chaotic dynamics of a discrete predator-prey model with Holling type II*, Nonlinear Anal. Real World Appl., **10** (2009), 116-129.
- [15] Q. Din, *Complexity and chaos control in a discrete time prey-predator model*, Commun. Nonlinear Sci. Numer. Simul., **49** (2017), 113-134.
- [16] M. E. Elettreby, T. Nabil, A. Khawagi, *Stability and bifurcation analysis of a discrete predator-prey model with mixed Holling interaction*, Computer Modeling in Engineering and Sciences., **122** (2020), 907-921.
- [17] A. Hening, *Coexistence, extinction, and optimal harvesting in discrete-time stochastic population models*, J. Nonlinear Sci., **31** (2021), 1-50.
- [18] W. Ding, S. Lenhart, H. Behncke, *Discrete time optimal harvesting of fish populations with age structure*, Lett. Biomath., **1** (2014), 193-207.
- [19] G. Y. Chen, Z. D. Teng, *On the stability in a discrete two species competition system*. J. Appl. Math. Comput., **38** (2012), 25-39.
- [20] S. Elaydi, *Discrete Chaos with Applications in Science and Engineering*, Chapman and Hall/CRC, Boca Raton, Fla, USA, 2000.
- [21] X. S. Luo, G. Chen, B. H. Wang, J. Q. Fang, *Hybrid control of period-doubling bifurcation and chaos in discrete nonlinear dynamical systems*, Chaos Solitons and Fractals, **18** (2003), 775-783.
- [22] L. Wang, M. Wang, *Ordinary Difference Equations*, Xin Jiang University Press, Urumqi, 1989.

# Quantitative Aeroelastic Stability Prediction of Wings Exhibiting Nonlinear Restoring Forces

Aykut Tamer

Department of Mechanical Engineering, University of Bath, Bath / UK

## Article Info

**Keywords:** Aeroelasticity, Lyapunov Exponents, Nonlinear Dynamical Systems

**2010 AMS:** 74F10, 74H55

**Received:** 5 December 2022

**Accepted:** 31 March 2023

**Available online:** 22 July 2023

## Abstract

In engineering practice, eigen-solution is used to assess the stability of linear dynamical systems. However, the linearity assumption in dynamical systems sometimes implies simplifications, particularly when strong nonlinearities exist. In this case, eigen-analysis requires linearisation of the problem and hence fails to provide a direct stability estimation. For this reason, a more reliable tool should be implemented to predict nonlinear phenomena such as chaos or limit cycle oscillations. One method to overcome this difficulty is the Lyapunov Characteristic Exponents (LCEs), which provides quantitative indications of the stability characteristics of dynamical systems governed by nonlinear time-dependent differential equations. Stability prediction using Lyapunov Characteristic Exponents is compatible with the eigen-solution when the problem is linear. Moreover, LCE estimations do not need a steady or equilibrium solution and they can be calculated as the system response evolves in time. Hence, they provide a generalization of traditional stability analysis using eigenvalues. These properties of Lyapunov Exponents are very useful in aeroelastic problems possessing nonlinear characteristics, which may significantly alter the aeroelastic characteristics, and result in chaotic and limit cycle behaviour. A very common nonlinearity in flexible systems is the nonlinear restoring force such as cubic stiffness, which would substantially benefit from using LCEs in stability assessment. This work presents the quantitative evaluation of aeroelastic stability indicators in the presence of nonlinear restoring force. The method is demonstrated on a two-dimensional aeroelastic problem by comparing the system behaviour and estimated Lyapunov Exponents.

## 1. Introduction

Linear system aeroelasticity is extensively studied in literature as presented in Ref. [1]. Stability indicators of linear, time-invariant (LTI) problems are evaluated by conducting eigen-analysis and extracting the real part of the eigenvalues of its state space matrix, which is a constant matrix by definition. This solution provides a spectrum of the system's orthogonal behaviour, namely modes. Stability evaluation is more complex if the linear problem is time-dependent, i.e. the elements in the state space matrix explicitly depend on time. A specific time-dependent problem is when these matrices are periodic. In this case, confirming to Floquet method, the stability properties of the system can be evaluated using eigen-solution. However, this time the real parts of the logarithm of the eigenvalues of the state transition matrix separated by the system's period (monodromy matrix) are defined as the stability indicators.

Nonlinearities always arise in aeroelastic systems, which sometimes become non-negligible. Typical sources of the nonlinearities are structure, aerodynamics, joints (bolts, fasteners etc), friction and control systems. When nonlinearities dominate, unique phenomena arise, which cannot be predicted using linear stability theory. Among them, self-sustained oscillations, also referred to as limit cycle oscillations (LCO), occur without needing external input [2]. Additionally, more complex responses may exist, such as chaotic motion [3]. Many experiments and observations on aeroelasticity problems mention phenomena of nonlinear origin. Therefore, understanding and analyzing nonlinearities in aeroelasticity is crucial for safer, more efficient, and advanced designs [4]. Nonlinear aeroelastic problems can be analyzed using theoretical and numerical methods such as wind tunnel experiments, nonlinear simulations or conducting flight tests [5].

For nonlinear, time-invariant dynamical systems, the eigenvalues and eigenvectors of the linear model computed at points on the phase plane related to a steady-state solution provide localized information on the stability in the vicinity of those points. If enough points are considered and a sufficiently large phase plane is constructed, it is possible to reach a geometric and qualitative understanding of a system's stability. However, these methods are not as practical and useful as eigen-solution, which provides a spectrum and stability characteristics of each branch (corresponding to modes in a linear system). Especially, for systems having higher degrees of freedom, geometric identification is not straightforward; thus, a quantitative method would be more useful.

A method, which gives insight into the stability characteristics of the system and, simultaneously, provides a practical means for its analysis would be very useful in nonlinear time-dependent system dynamics. Such a method is expected to: i) work without a special reference or steady-state solution (i.e. equilibrium point or a stable orbit); and ii) provide indications about the existence of nonlinear characteristics (such as an attractor, a periodic orbit or a higher-order solution), during computation of the system's evolution in time. Lyapunov Characteristic Exponents (LCEs in short) are indicators of the stability characteristics of the solutions of differential equations [6, 7]. In other words, LCEs identify the spectrum of the corresponding initial value problem [8]. LCEs can be applied to a wide range of dynamical systems, including those governed by nonlinear time-dependent differential equations.

The use of LCEs is suggested as a technique for predicting the stability of nonlinear aeroelastic problems [5]. Mostly, the LCEs estimates based on time series were studied in the literature [9]. Ref. [10] presented the aeroelastic response of a wing section with nonlinearities of structural origin; where LCO and chaotic response were identified and compared with estimates of Lyapunov Exponents based on time series analysis. In Ref. [11], chaos and chaotic transients were shown to exist in aeroelastic systems. In another work, nonlinearities originated from aerodynamics and physical parameters were investigated for an airfoil under supersonic flow by Ref. [12], where bifurcations were identified using First Lyapunov Quantity. While the above literature estimate LCEs from time series, the LCE stability indication working directly on system differential equation rather than calculating them using time series, was recently introduced into rotorcraft stability assessment in Ref. [13], where accurate predictions of nonlinear phenomena were observed. In addition to research on LCEs, their analytical sensitivity was also investigated in Ref. [14]. The extension of the LCE approach to multi-body dynamics is under investigation and would be a promising contribution to the stability assessment of problems formulated using differential-algebraic equations [15–17].

With the improved nonlinear analysis tools, the nonlinearities can be tolerated and even intentionally included in the design [18]. Use of as the use of extremely flexible wings [19] is an example where nonlinearities arise. In particular, cubic restoring forces are commonly encountered and can induce a substantial effect on the system stability, which is characterized by the presence of a quadratic term in the stiffness coefficient [4]. In the literature, this problem has been investigated numerically and experimentally to determine the effects of the cubic spring on the aeroelastic stability of airfoils. Depending on the characteristics of the cubic spring, namely a soft or a hard one, the flutter characteristics of the system can change significantly and depend on the initial conditions [20]. It is also observed that the limit cycle oscillations is a common consequence of a cubic restoring moment (See for example Refs. [10, 21–23]). Therefore, quantitative means of estimations of stability indicators could be useful in the design phases of aircraft when analyzing possible outcomes due to cubic stiffness effects.

An aeroelastic system needs to operate in a stable region without exhibiting chaotic or divergent behaviour. This work presents quantitative stability estimation of aeroelastic problems involving cubic restoring force nonlinearity. LCEs are implemented along with the differential equations governing the system. The LCEs and simulations have been used to show that the nonlinear term provides stability to the aeroelastic system examined and, the system would be unstable without it. In other words, the system's state transition matrix is directly used rather than first simulating the system and later working on time series. LCE estimation is obtained using the discrete QR method along with simulating the problem in time.

This work is organized as follows. The next section discussed the stability problem of nonlinear systems and Lyapunov characteristic exponents including practical means of estimating LCEs. Then, a two-degree-of-freedom nonlinear aeroelastic problem with unsteady aerodynamics was explained. The stability of the aeroelastic model to perturbations was calculated using LCEs. The stability indications of LCEs were verified by comparing them with the evolution of the system response to initial perturbations.

## 2. Method

This section presents the nonlinear time-dependent problems and introduces Lyapunov Characteristic Exponents for predicting and quantifying their stability characteristics. In addition, the numerical procedure for their practical estimation of LCEs was also presented with a set of criteria that would help to interpret the LCEs of a dynamical system.

### 2.1. Stability of dynamical systems

Engineering systems that are governed by differential equations of the form:

$$\dot{\mathbf{x}} = \mathbf{f}(\mathbf{x}, t) \quad \text{for} \quad \mathbf{x}(t_0) = \mathbf{x}_0, \quad (2.1)$$

often arise in engineering practice. The linear time-variant problem is one of the special cases:

$$\dot{\mathbf{x}}(t) = \mathbf{A}(t)\mathbf{x}(t),$$

where the state space matrix is not constant but changes with time. In many other cases, the state space matrix is constant, hence the system is time-invariant (LTI). In other words:

$$\dot{\mathbf{x}} = \mathbf{A}\mathbf{x}$$

with  $\mathbf{A}$  being constant in time.

The stability of LTI problems is determined by calculating the eigenvalues of constant state space matrix  $\mathbf{A}$ , also referred to as the system's spectrum. Stability is identified by the real part of the eigenvalues: stable if negative, marginally stable if zero, and unstable if positive.

Stability prediction is more complicated if the system is linear time-dependent. The most common time dependence is periodicity. If the system is linear time periodic (LTP), the state space matrix  $\mathbf{A}$  has periodic coefficients and repeats itself at time steps separated by period  $T$ :

$$\dot{\mathbf{x}} = \mathbf{A}(t)\mathbf{x} \quad \text{where} \quad \mathbf{A}(t+T) = \mathbf{A}(t).$$

In this case, LTP system stability is evaluated using the real part of the logarithm of the eigenvalues of the monodromy matrix  $\mathbf{H}$ . The monodromy matrix  $\mathbf{H}$  is defined as the state transition matrix  $\mathbf{Y}$  between two temporal states separated by one period ( $T$ ):

$$\mathbf{H} = \mathbf{Y}(T, 0)$$

and the state transition matrix  $\mathbf{Y}$  is the solution to the problem:

$$\dot{\mathbf{T}} = \mathbf{A}(t)\mathbf{Y}, \quad \mathbf{Y}(0) = \mathbf{I}$$

where  $\mathbf{I}$  is the identity matrix, which denotes an initial perturbation with unit magnitude along all the degrees of freedom of the system. Both linearity and periodicity could mean simplifications to the real behaviour, which is represented by the most general form in Eq. (2.1). The stability prediction in the most general sense (nonlinear and time-dependent) cannot be directly predicted using eigen-analysis, which requires simplifications or assumptions on the real system behaviour.

## 2.2. Lyapunov characteristic exponents

The formulation of stability is less intuitive for nonlinear time-dependent dynamical systems. Yet, stability has the same interpretation, which can be defined as the decaying rate of the response amplitude after a perturbation. Stability is indicated by the solution of eigen-analysis for linear systems as explained in the previous section. For non-linear time-variant systems, the Lyapunov Exponents can be considered as an extension of linear eigen-analysis to nonlinear time-dependent systems and LCEs provide a more reliable and general indicator of suitability. Consider the problem in Eq. (2.1), with state vector  $\mathbf{x}$ , and time  $t$ , and the nonlinear time-dependent function  $\mathbf{f}(\mathbf{x}, t)$  with a solution  $\mathbf{x}(t)$  for prescribed initial conditions  $\mathbf{x}(t_0) = \mathbf{x}_0$ . The Lyapunov Characteristic Exponents ( $\lambda_i$ ) of this system are defined as:

$$\lambda_i = \lim_{t \rightarrow \infty} \frac{1}{t} \log \frac{\|{}_i\mathbf{x}(t)\|}{\|{}_i\mathbf{x}(t_0)\|},$$

In the above equation,  ${}_i\mathbf{x}(t)$  is geometrically defined as the solution that describes the exponential evolution of the  $i$ -th axis of the ellipsoid that grows from an initially infinitesimal  $n$ -sphere (representing unit perturbations along each axis) according to the Jacobian  $\mathbf{f}'_{\mathbf{x}}$  tangent to  $\mathbf{f}$  along the fiducial trajectory  $\mathbf{x}(t)$ . That is,  ${}_i\mathbf{x}(t)$  is the solution to the linear, time-dependent problem  ${}_i\dot{\mathbf{x}}(t) = \mathbf{f}'_{\mathbf{x}}(\mathbf{x}, t){}_i\mathbf{x}(t)$ , with  ${}_i\mathbf{x}(t_0) = {}_i\mathbf{x}_0$ . This is graphically represented in Figure 2.1.

In engineering-related terms, LCEs provide a measure of the rate of growth of perturbed solutions. The LCE formula involves an unbounded limit for time  $t$  approaches infinity. As a result, in practice, the LCEs can only be numerically calculated for a sufficiently large value of  $t$  such that the calculations are truncated for converged LCEs. For this reason, the LCEs usually, except for very simple problems, mean that they are numerically estimated for a large enough value of  $t$ , where the LCEs converge to a value.

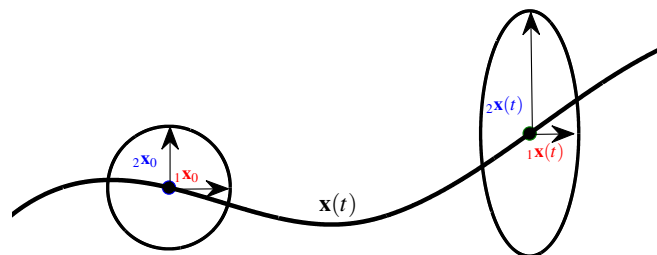


Figure 2.1: Evolution of a perturbation of a solution of a differential equation.

## 2.3. Numerical estimation of LCEs

Practical calculation of LCEs faces the difficulty of operating on matrices with coefficients quickly diverging (instability) or converging to zero (exponential stability). To solve this problem, several approaches were developed. Continuous formulations for the prediction of the LCEs can be achieved using singular value decomposition (SVD) or through QR decomposition [24]. An alternative technique is the Schur decomposition, which could provide better results in the case of multiple LCEs [25], which is especially advantageous when LCEs appear in multiples. Discrete methods are more practical than continuous ones as they can be more computationally feasible and can be applied to more complex problems in engineering. Among the available methods of LCE estimation, a famous one is the Discrete QR Method. It is derived from incrementally calculating the QR decomposition applied on the state transition matrix at every time step of numerical integration. For its practicality, the discrete QR approach is selected as the LCE computation method in this study and explained hereafter.

## 2.4. Discrete QR method

The discrete QR method computes LCEs by updating the LCEs estimates with the diagonal elements of the upper-triangular matrix  $\mathbf{R}$  gathered from incremental QR decompositions of the state transition matrix between two successive time steps. Considering the previously defined state transition matrix  $\mathbf{Y}(t, t_j)$  from time  $t_{j-1}$  to time  $t$ , the state transition matrix is defined as  $\mathbf{Y}_j = \mathbf{Y}(t, t_j)$ . Then, compute

the QR decomposition of  $\mathbf{Y}_j \mathbf{Q}_{j-1}$ , starting from  $\mathbf{Q}_0 = \mathbf{I}$  (representing a perturbation on each system degree of freedom), which implies  $\mathbf{Q}_j \mathbf{R}_j = \mathbf{Y}_j \mathbf{Q}_{j-1}$ . After defining  $\mathbf{R}_{\Pi_j} = \prod_{k=0}^j \mathbf{R}_{j-k}$ , ( $\Pi$  is the product operator), it can be shown that:

$$\mathbf{Y}_j \mathbf{Q}_{j-1} \mathbf{R}_{\Pi_{j-1}} = \mathbf{Q}_j \mathbf{R}_{\Pi_j}.$$

Then,  $\mathbf{Y}_j \mathbf{Q}_{j-1} \mathbf{R}_{\Pi_{j-1}}$  can be utilized to form  $\mathbf{R}_j$  by implementing incremental QR decompositions of  $\mathbf{Y}_j \mathbf{Q}_{j-1}$ . Thanks to the limited contraction/expansion due to the small time step, matrices do not have rapidly diverging or vanishing elements. The LCEs are then calculated using  $\mathbf{R}_{P_{i_j}}$  as:

$$\lambda_i = \lim_{j \rightarrow \infty} \frac{1}{t_j} \log r_{ii}(t_j), \quad (2.2)$$

where  $r_{ii}(t_j)$  represents the diagonal elements of  $\mathbf{R}_j = \mathbf{R}_{\Pi_j}$  matrix. Eq. (2.2) can further be arranged by considering that the logarithm involving multiplication can be converted to summation, which leads to:

$$\lambda_i = \lim_{j \rightarrow \infty} \frac{1}{t_j} \sum_{k=0}^j \log(r_{kii}).$$

## 2.5. Quantitative stability assessment

In practice, the obtained LCEs are indicators of the stability properties of a dynamical system. If the system is linear, then the LCEs are equivalent to the real part of the eigenvalues of the state-space matrix. In the case of the nonlinear system, the following criteria could be used to interpret the LCEs:

- The solution is exponentially stable if all LCEs are negative.
- If at least one of the LCEs is positive, the solution is unstable or leads to a chaotic attractor.
- When the largest LCE is zero, or the largest LCEs are zero, a limit cycle oscillation is expected; i.e., the solution neither expands nor contracts.

## 3. Aeroelastic Problem

This section presents a two-degree-of-freedom aeroelastic problem and its quantitative stability assessment to demonstrate the LCE approach in stability assessment. The example is related to a cubic representation of the restoring pitch moment of an airfoil, which can be seen as a simplification of a wing or control surface.

### 3.1. Flutter of aircraft wings

Aeroelasticity deals with the interaction of aerodynamic forces and elastic deformations and investigates the influences of wing deformations on airloads [26]. The major problems are divergence and flutter. While the former is static unstable feedback between the deformations and loads; the latter also involves inertial forces and results in an unstable condition where the streamlined body extracts energy from the airflow [27].

A typical aeroelastic system starts with total positive damping coming from the structure aerodynamics at low airspeed, meaning that the system stabilizes itself after perturbations. The damping increases up to a maximum, after which it starts reducing due to aeroelastic interactions. As the flight speed is further increased damping becomes zero and eventually negative, which indicates that the structure extracts energy from the flow. The result is an unstable system where the perturbations grow in amplitude with the extracted energy. The flutter analysis is therefore required to determine at which airspeed the damping becomes zero (onset of instability) and then leave a safety margin below that speed to assess the maximum safe flight speed.

### 3.2. Model

The most proper method to analyze flutter is to build the full finite element model with unsteady aerodynamics. Having said this, the first bending and first torsion modes of the wing couple interact with unsteady aerodynamics in the most common flutter problem. For this reason, two degrees of freedom models reduced from detailed models or identified through experiments are frequently used in flutter calculations to gain more insight into the physics of the problem during preliminary design and/or reduce computation time [28]. With the same motivation, this work follows the classical two-degree of freedom aeroelastic wing model representing the wing plunging and pitching motions coupled with unsteady aerodynamics.

Figure 3.1 presents the cross-section of a wind-tunnel model of a wing with chord length  $2b$ . The pitch ( $\alpha$ ), and plunge ( $w$ ) degrees of freedom are supported by springs and dampers (dampers not shown for clarity but are connected exactly at the same points where springs are attached). The positions of the elastic axis  $a$  and the centre of gravity  $x_\alpha$  are normalized by half-chord length  $b$ . The mass of the wing is represented by  $m_w$ , and the total mass including wing and support is denoted by  $m_T$ .  $S$  and  $I$  are the first and second moments of inertia with respect to the rotation axis. In the equations, subscripts  $\alpha$  and  $w$  indicate the parameters corresponding to that motion.

### 3.3. Equations of motion

The mathematical representation of the model presented in Figure 3.1 was obtained from Ref. [29], with parameters reported in Table 3.1. The model is linear except for the pitch spring which has cubic restoring force. For this reason, the problem is separated into linear state space form and nonlinear forcing:

$$\mathbf{M}\ddot{\mathbf{x}} + \mathbf{C}\dot{\mathbf{x}} + \mathbf{K}\mathbf{x} = \mathbf{f}_{nl}$$

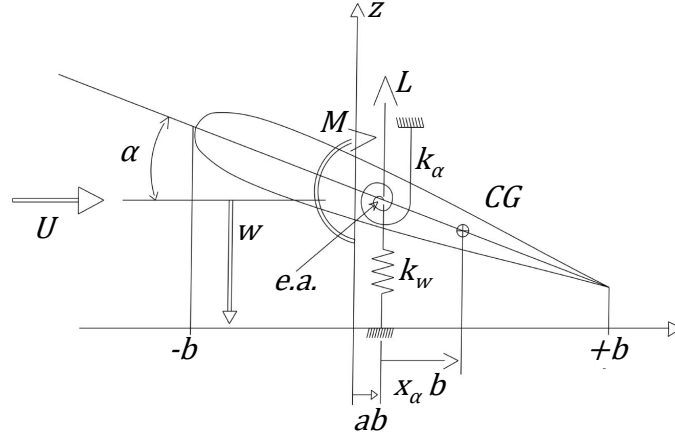


Figure 3.1: Two degrees of freedom aeroelastic wing.

Variable Description	Value
Span, $s$	0.6 m
Semi-chord, $b$	0.0325 m
Position of elastic axis normalized by semi-chord, $a$	-0.5
Centre of gravity normalized by semi-chord, $x_\alpha$	0.5
Air density, $\rho$	1.225 kg/m <sup>3</sup>
Mass of the wing, $m_w$	1.0662 kg
Mass of wing and supports, $m_T$	3.836 kg
Moment of inertia about elastic axis, $I_\alpha$	4067.5 N m s rad <sup>-1</sup>
Pitch and plunge damping coefficients, $c_\alpha, c_h$	0.0115, 0.011 kg m s <sup>-2</sup>
Stiffness in pitch and plunge, $k_\alpha, k_h$	0.942, 0.895 N m <sup>-1</sup>
Stiffness constants of nonlinear damper, $k_{\alpha 1}, k_{\alpha 2}$	3.95, 107.0 N m

Table 3.1: Parameters of aeroelastic model [22]

In the above equation,  $\mathbf{x} = [w \ \alpha \ \xi]^T$  is the state vector for plunging  $w$ , pitching  $\alpha$  and augmented state  $\xi$ .  $\mathbf{f}_{nl}$  is the nonlinear forcing due to cubic spring force. and  $\mathbf{K}$ ,  $\mathbf{C}$ , and  $\mathbf{M}$  are linear stiffness, damping, and mass matrices including unsteady aerodynamics. For the linear part, the mass, stiffness and damping matrices are given as:

$$\mathbf{M} = \mathbf{M}_{structural} + \mathbf{M}_{aero} = \begin{bmatrix} m_T & m_w x_\alpha b & 0 \\ m_w x_\alpha b & I_\alpha & 0 \\ 0 & 0 & 0 \end{bmatrix} + \begin{bmatrix} \pi \rho b^2 & -a \pi \rho b^3 & 0 \\ -a \pi \rho b^3 & \pi (\frac{1}{8} + a^2) \rho b^4 & 0 \\ 0 & 0 & 1 \end{bmatrix}$$

$$\mathbf{C} = \mathbf{C}_{structural} + \mathbf{C}_{aero} = \begin{bmatrix} c_h & 0 & 0 \\ 0 & c_\alpha & 0 \\ 0 & 0 & 0 \end{bmatrix} + \begin{bmatrix} 2\pi \rho b c_5 U & (1+c_5)(1-2a)\pi \rho b^2 U & 2\pi \rho U^2 b c_6 \\ -2\pi(a+\frac{1}{2})\rho b^2 c_5 U & (\frac{1}{2}-a)(1-c_5(1+2a))\pi \rho b^3 U & -2\pi \rho b^2 U^2 (a+\frac{1}{2})c_6 \\ \frac{-1}{b} & a-\frac{1}{2} & (c_2+c_4)\frac{U}{b} \end{bmatrix}$$

$$\mathbf{K} = \mathbf{K}_{structural} + \mathbf{K}_{aero} = \begin{bmatrix} k_h & 0 & 0 \\ 0 & k_{\alpha 0} & 0 \\ 0 & 0 & 0 \end{bmatrix} + \begin{bmatrix} 0 & 2\pi \rho b c_5 U^2 & 2\pi \rho U^3 c_2 c_4 (c_1+c_3) \\ 0 & -2\pi(\frac{1}{2}+a)\rho c_5 b^2 U^2 & -2\pi \rho b U^2 (a+\frac{1}{2})c_2 c_4 (c_1+c_3) \\ 0 & -\frac{U}{b} & c_2 c_4 \frac{U^2}{b^2} \end{bmatrix}$$

where the subscripts refer to the structural and aerodynamic contribution to the matrices. The structural matrices are symmetric as expected, but the aerodynamic terms spoil the symmetry in the matrices.

It should be emphasized here that the system has two degrees of freedom, but an augmented state ( $\xi$ ) was added based on Wagner's function for arbitrary (i.e. not only valid for simple harmonic motion) airfoil motion. The use of the formulation for arbitrary motion allows us to identify damping at any flight speed. Since this work aims to provide a generalized method, arbitrary motion is more suitable than the harmonic motion formulation which is only valid when damping is zero and hence invalid except for flutter speed [1]. The constants are given as  $c_0 = 1.0$ ,  $c_1 = 0.165$ ,  $c_2 = 0.0455$ ,  $c_3 = 0.335$ ,  $c_4 = 0.3$ , and the dependent variables  $c_5 = c_0 - c_1 - c_3$ ,  $c_6 = c_1 c_2 + c_3 c_4$ .

The cubic restoring force is added to the pitching motion in this example, which has a stiffness coefficient of  $k(\alpha) = k_{\alpha 0} + k_{\alpha 1} \alpha + k_{\alpha 2} \alpha^2$ . The linear stiffness term  $k_{\alpha 0}$  is already included in the linear part function, so the nonlinear term can be stated as:

$$\mathbf{f}_{nl} = [0 \ (k_{\alpha 1} \alpha + k_{\alpha 2} \alpha^2) \alpha \ 0]^T$$

The above matrices can be blended into a state space form as:

$$\dot{\mathbf{x}} = \mathbf{A}\mathbf{x} + \mathbf{g}$$

where

$$\mathbf{x}_s = [\mathbf{x} \ \dot{\mathbf{x}}], \quad \mathbf{A} = \begin{bmatrix} \mathbf{0} & \mathbf{I} \\ -\mathbf{M}^{-1}\mathbf{K} & -\mathbf{M}^{-1}\mathbf{C} \end{bmatrix}, \quad \mathbf{g} = [\mathbf{0} \ -\mathbf{M}^{-1}\mathbf{f}_{nl}]^T. \quad (3.2)$$

The above equation can now be solved numerically for the given initial conditions and LCEs can be calculated as the simulation continues. Note that when  $\mathbf{g} = \mathbf{0}$ , the system is linear. In the nonlinear form, the presence of  $\alpha$  on the right-hand side spoils the linearity and dominates the response depending on the value of spring constants and  $\alpha$ .

### 4. Results

The linear flutter speed can be calculated by tracking the real part of the eigenvalues of linear state space matrix  $\mathbf{A}$  of Eq. (3.2) as flight speed is changed and by omitting the nonlinearities in the pitch stiffness. By doing so, the flutter speed was numerically found to be  $U_f = 10.90 \text{ m s}^{-1}$  by using the speed-damping (V-g) curve for the lowest damping ( $\lambda_1$ : real part of the largest eigenvalue) as shown in Figure 4.1. At speeds below the flutter speed, the wing is stable. On the contrary, the wing is unstable at flight speeds higher than the flutter speed. The flutter speed is in agreement with the results of Ref. [22].

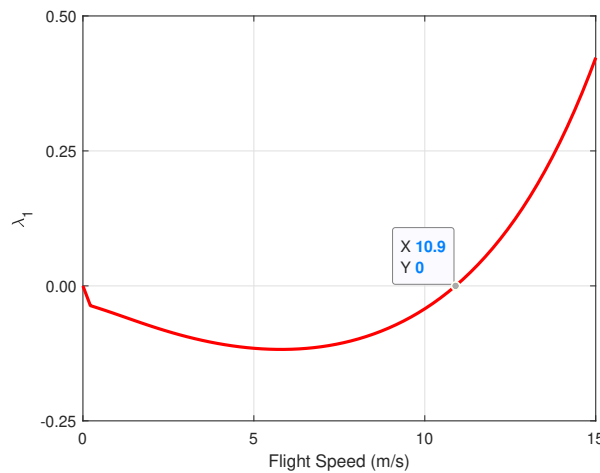


Figure 4.1: Linear flutter analysis finds the flutter speed at  $10.9 \text{ m s}^{-1}$  where the damping is zero.

The response of the system lower than the flutter speed is not of interest since the oscillations die out with time due to the positive damping (negative maximum  $\lambda$ ). An example is presented in Figure 4.2, where the oscillations die out as indicated by positive damping in Figure 4.1. The nonlinearity under flutter speed does not affect system stability since the proposed nonlinearity is of polynomial type and vanishing oscillations mean the higher-order nonlinear contributions would be smaller than linear damping.

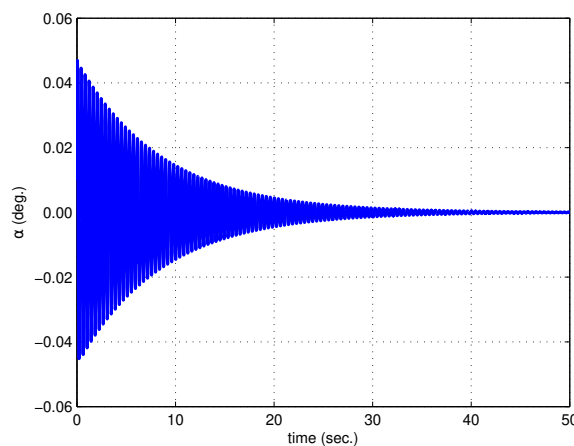


Figure 4.2: Convergent pitch response to perturbation at  $5 \text{ m s}^{-1}$ .

On the other hand, post-flutter behaviour would be more interesting since the higher-order restoring forces can alter the linear divergent behaviour. Two air-stream values above flutter speed were selected at  $U = 1.25U_f$  and  $U = 1.40U_f$ . For both cases first, the pitch responses were presented in Figure 4.3 and Figure 4.5 to show the divergent behaviour after the flutter. Then the pitch response of the nonlinear system is presented in Figure 4.4 and Figure 4.6 respectively, along with the corresponding non-dimensional phase plane plots, which indicate the topological properties of the state space. The initial conditions of the systems in the phase plane plots are marked with a solid dot. It should be noted that the plots involve only pitching motion; the intersections observed in the phase-plane plots (which do not happen when the full model in four dimensions is considered) are due to the projection of the variable and its time derivative on a 2D plane.

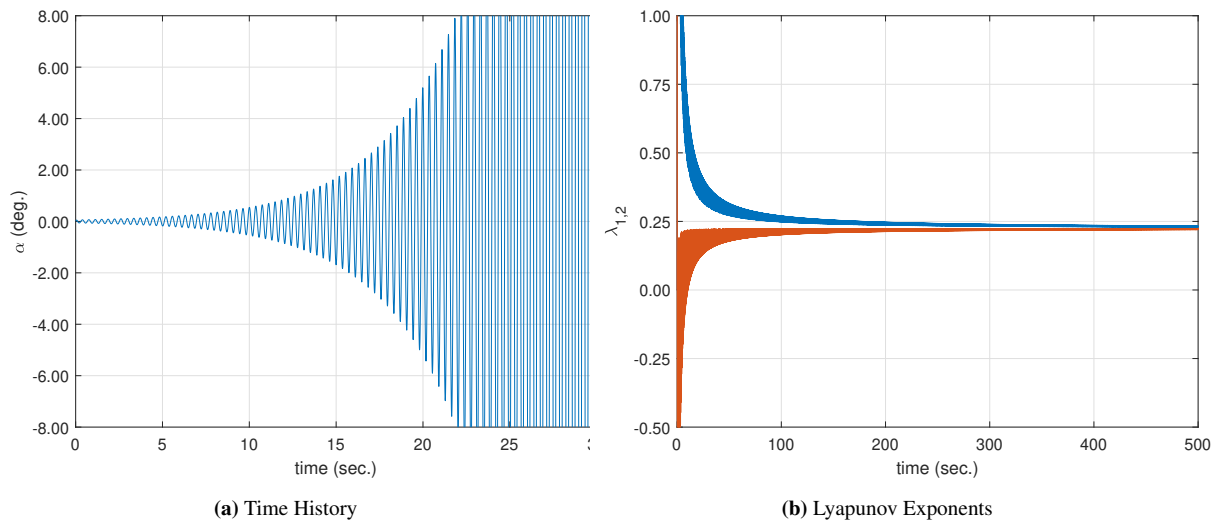


Figure 4.3: Time history, and LCEs for the linear problem after a perturbation at  $U = 1.25U_f$

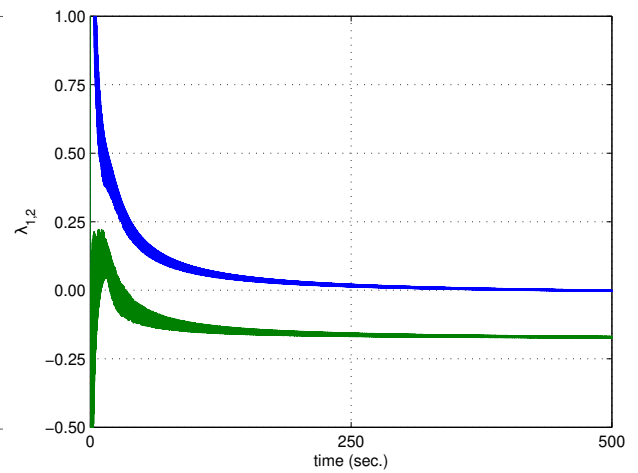
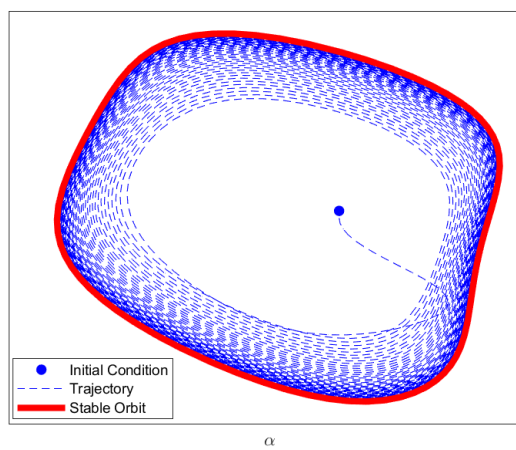
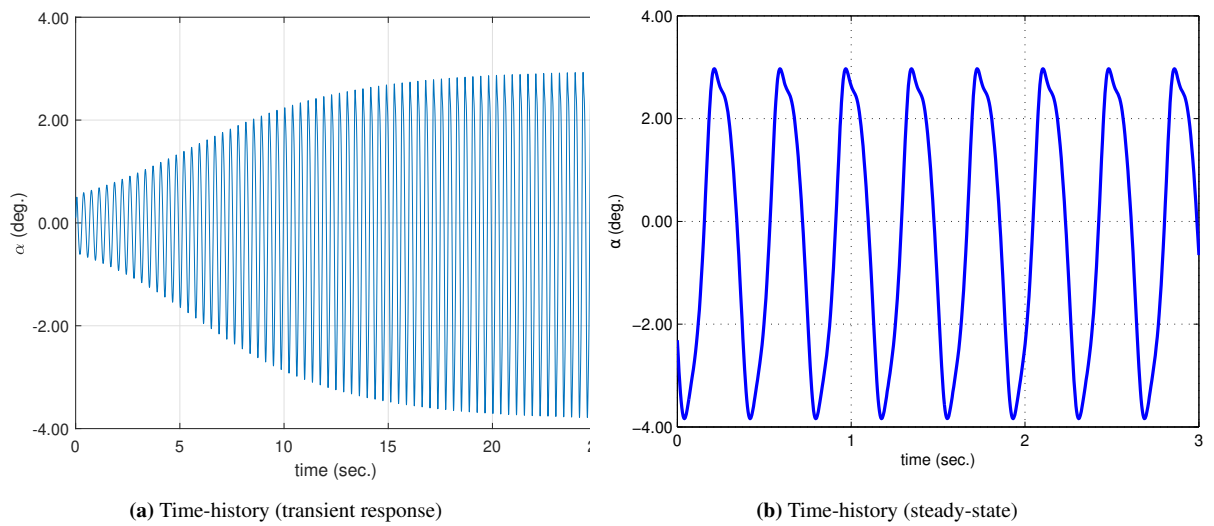


Figure 4.4: Time history, phase plane and LCEs for the nonlinear problem after a perturbation at  $U = 1.25U_f$

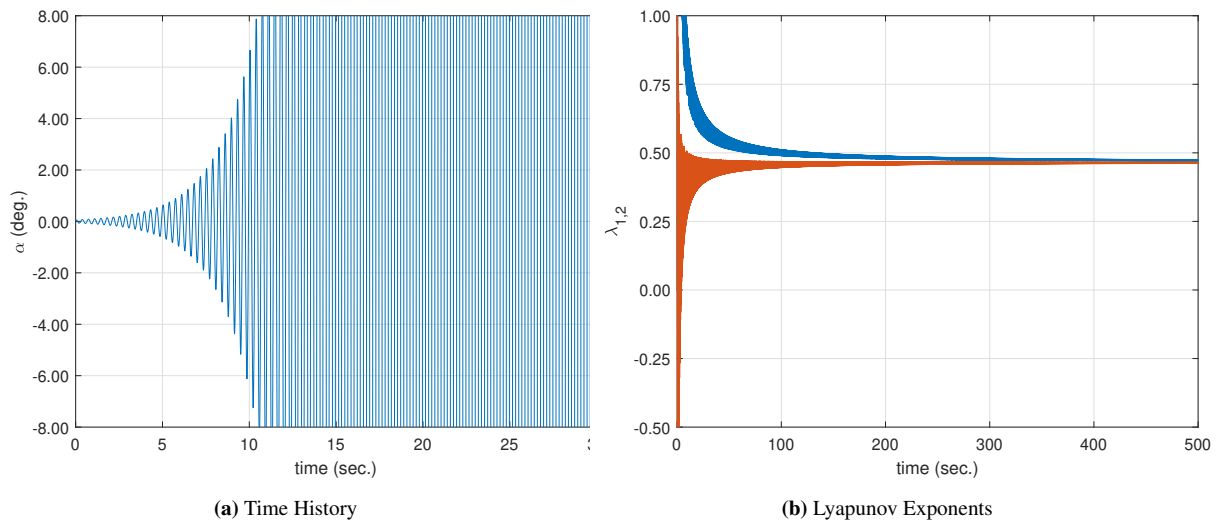


Figure 4.5: Time history, and LCEs for the linear problem after a perturbation at  $U = 1.40U_f$

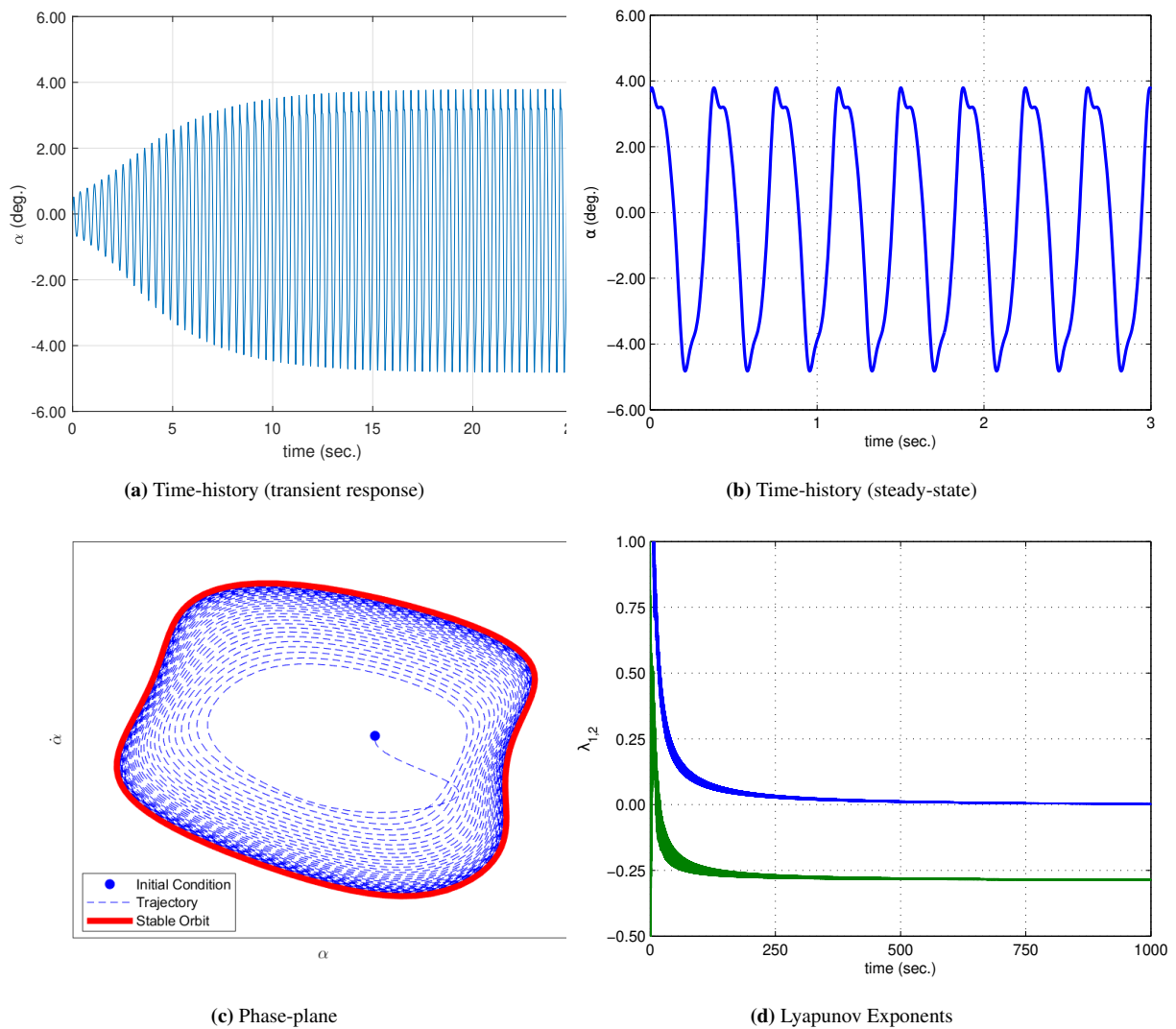


Figure 4.6: Time history, phase plane and LCEs for the nonlinear problem after a perturbation at  $U = 1.40U_f$

When the airstream speed exceeds the flutter speed for a linear system, any perturbation from its equilibrium condition would lead to a divergent response as presented in Figure 4.3 and Figure 4.5. Their LCE estimates are also positive confirming the observed behaviour. However, this did not happen in the presence of a cubic nonlinear restoring force. As a consequence of nonlinearity in stiffness, the system experiences periodic motion (Figure 4.4b and Figure 4.6b) after the transients (Figure 4.4a and Figure 4.6a) die out. The phase portraits converge to an orbit regardless of the initial condition, thus an LCO occurs, as illustrated in Figure 4.4c and Figure 4.6c for flight speeds significantly higher than flutter speed. The amplitude and phase portraits of the responses are in agreement with those of Ref. [22]. From a nonlinear aeroelasticity perspective and within the scope of this work, the periodic orbits of Figure 4.4c and Figure 4.6c are of particular interest. When a nonlinear system has a periodic attractor (for example LCO), zero-valued largest LCE estimates (or converging to zero from a numerical estimation point of view) are expected [30]. This can be observed in Figure 4.4d and Figure 4.6d, which present the time evolution of LCEs for the corresponding flight speed values of  $U = 1.25U_f$  and  $U = 1.40U_f$ . The largest LCE branch converges to zero, while the other tends to be a negative value. Thus, the LCE estimates are compatible with the periodic motion of the system shown in Figure 4.4b and Figure 4.6b. Therefore, the use of LCEs in predicting the nonlinear post-flutter airfoil motion was successfully demonstrated. It is also worth noting that using LCEs as stability indicators can provide two additional benefits. First, LCEs allow us to track the change in the other mode with more damping, which is not possible to extract from time responses. In this particular example, the converging mode damping increased 50% ( $\lambda$  increased from 0.2 at  $1.25U_f$  to 0.30 at  $1.40U_f$ ). The second benefit comes from tracking the lowest damping mode for a larger flight speed range. If LCE estimations are extended to cover from zero flight speed to  $1.40U_f$ , Figure 4.7 is obtained that presents the stability indicators for linear spring (real part of the eigenvalue) and cubic spring (LCEs) cases. Since LCEs are a generalization of linear stability using eigenvalues, it is possible to compare both linear and nonlinear cases. This allows us to understand the impact of nonlinearity before and after the flutter speed. In Figure 4.7 for example, it can be observed that under flutter speed the linear and nonlinear systems have almost equal damping, indicating that the nonlinearities can be neglected. On the other hand, above the flutter speed, the linear system loses stability indicated by the positive real part of the eigenvalues. However, the nonlinear system remains at zero damping ( $\lambda = 0$ ), resulting in an isolated periodic orbit (LCO) rather than a divergent behaviour, showing a completely distinct behaviour as compared to the linear system.

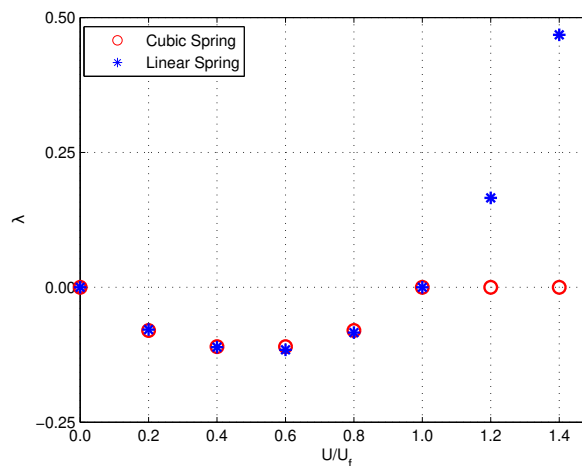


Figure 4.7: Comparison of stability indicators of the linear model and nonlinear model with cubic stiffness.

## 5. Conclusions

Quantitative stability prediction for aeroelastic problems possessing nonlinear restoring force was presented. The spectrum of the nonlinear aeroelastic systems was estimated using Lyapunov Characteristic Exponents to show that i) nonlinearities can stabilize an otherwise chaotic or divergent system; and ii) the nonlinear behaviour can be identified using LCEs. The Discrete QR decomposition method was used for the practical estimation of Lyapunov Characteristic Exponents. The LCEs are compatible with the real part of the eigenvalues of Linear Time Invariant and Linear Time Periodic problems. Therefore, LCEs are considered to be a natural generalization of stability indicators that are used in conventional engineering practice, including nonlinear aeroelastic stability problems.

A two-dimensional wind tunnel wing model was used to demonstrate the use of LCEs in estimating the nonlinear stability of aeroelastic problems. A cubic restoring force is defined on the spring supporting pitching motion. The behaviours indicated by the resulting LCEs were verified with time marching simulations. The results were compared with the linear model in the post-flutter region. It was shown that the use of LCEs can provide several advantages such as quantitatively tracking the change of stability indicators and comparing the system damping with a linear model, as LCEs are a generalization of the eigenvalue solution for nonlinear problems. Therefore the chaotic and divergent phenomena could better be identified and prevented in the design of aeroelastic systems.

Finally, it should be noted that practical aeroelastic analysis usually involves more complex models. The proposed method can directly be applied directly to high-fidelity models but the convergence of the exponents in a high-fidelity nonlinear model will be computationally demanding, hence limiting the practicality of the method. In this case, the proposed method can be applied to reduced-order models of complex systems. This requires the identification of nonlinear properties, therefore nonlinear model reduction techniques should be implemented before starting the quantitative stability analysis.

## Nomenclature

$a$	position of elastic axis
$b$	semi-chord
$c$	viscous damping acting on pitching and plunging
$c_i$	$i=1:6$ , Unsteady aerodynamic constants
$\mathbf{f}_{nl}$	Nonlinear force due to cubic spring
$k$	spring stiffness acting on pitching and plunging
$m_w$	wing mass
$m_T$	total mass
$s$	span
$w$	plunging degree of freedom
$\mathbf{A}$	State space matrix
$\mathbf{C}$	Damping matrix
$I_\alpha$	Moment of inertia about elastic axis
$\mathbf{H}$	Monodromy matrix
LCE	Lyapunov Characteristic Exponents
$\mathbf{K}$	Stiffness matrix
$\mathbf{M}$	Mass matrix
$U$	Flight Speed
$U_f$	Flutter Speed
$\mathbf{Y}$	State transition matrix
$\alpha$	pitching degree of freedom
$\xi$	Augmented State of unsteady flow
$\lambda$	Converged value of LCEs
$\rho$	air density

## Article Information

**Acknowledgements:** The authors would like to express their sincere thanks to the editor and the anonymous reviewers for their invaluable feedback and insightful recommendations.

**Author's contributions:** The article has a single author. The author has read and approved the final manuscript.

**Conflict of Interest Disclosure:** No potential conflict of interest was declared by the author.

**Copyright Statement:** Author owns the copyright of their work published in the journal and their work is published under the CC BY-NC 4.0 license.

**Supporting/Supporting Organizations:** No grants were received from any public, private or non-profit organizations for this research.

**Ethical Approval and Participant Consent:** It is declared that during the preparation process of this study, scientific and ethical principles were followed and all the studies benefited from are stated in the bibliography.

**Plagiarism Statement:** This article was scanned by the plagiarism program. No plagiarism detected.

**Availability of data and materials:** Not applicable.

## References

- [1] R. L. Bisplinghoff, H. Ashley, R. L. Halfman, *Aeroelasticity*, Dover, New York, 1996.
- [2] S. H. Strogatz, *Nonlinear Dynamics and Chaos: With Applications to Physics, Biology, Chemistry, and Engineering*, Perseus Books, Reading, Massachusetts, 1994.
- [3] E. Dowell, J. Edwards, T. Strganac, *Nonlinear aeroelasticity*, *J. Aircraft*, **40**(5)(2003), 857-874.
- [4] B.H.K. Lee, S.J. Price, Y.S. Wong, *Nonlinear aeroelastic analysis of airfoils: bifurcation and chaos*, *Prog. Aero. Sci.*, **35**(3)(1999), 205-334.
- [5] X. Jinwu, Y. Yongju, L. Daochun, *Recent advance in nonlinear aeroelastic analysis and control of the aircraft*, *Chin J. Aeronaut.*, **27**(1)(2014), 12-22.
- [6] L. Adrianova, *Introduction to Linear Systems of Differential Equations*, Translations of Mathematical Monographs, American Mathematical Society, Providence, Rhode Island, 1995.
- [7] G. Benettin, L. Galgani, A. Giorgilli, J. Strelcyn, *Lyapunov characteristic exponents for smooth dynamical systems and for Hamiltonian systems; a method for computing all of them part 1: Theory*, *Meccanica*, **15**(1)(1980), 9-20.
- [8] L. Dieci, *Jacobian free computation of Lyapunov exponents*, *J. Dynam. Differential Equations*, **14**(3)(2002), 697-717.
- [9] A. Wolf, J. B. Swift, H. L. Swinney, J. A. Vastano, *Determining Lyapunov exponents from a time series*, *Phys. D.*, **16**(3)(1985), 285-317.
- [10] S. J. Price, H. A. Ghanbari, B. H. K. Lee, *The aeroelastic response of a two dimensional airfoil with bilinear and cubic structural nonlinearities*, *J. Fluids Struct.*, **9**(1995), 175-193.
- [11] H. Dai, X. Yue, D. Xie, S. N. Atluri, *Chaos and chaotic transients in an aeroelastic system*, *J. Sound Vib.*, **333**(2014), 7267-7285.
- [12] L. Librescu, G. Chiochia, P. Marzocca, *Implications of cubic physical/aerodynamic non-linearities on the character of the flutter instability boundary*, *Int. J. Non Linear Mech.*, **38**(2)(2003), 173-199.
- [13] A. Tamer, P. Masarati, *Stability of nonlinear, time-dependent rotorcraft systems using Lyapunov characteristic exponents*, *J. Am. Helicop. Soc.*, **61**(2)(2016), 14-23.
- [14] P. Masarati, A. Tamer, *Sensitivity of trajectory stability estimated by Lyapunov characteristic exponents*, *Aerosp. Sci. Technol.*, **47**(2015), 501-510.
- [15] N. D. Cong, H. Nam, *Lyapunov's inequality for linear differential algebraic equation*, *Acta Math. Vietnam.*, **28**(1)(2003), 73-88.
- [16] A. Tamer, P. Masarati, *Generalized quantitative stability analysis of time-dependent comprehensive rotorcraft systems*, *Aerospace*, **9**(1)(2022), 10.
- [17] P. Masarati, *Estimation of Lyapunov exponents from multibody dynamics in differential-algebraic form*, *Proceedings of the Institution of Mechanical Engineers, Part K: Journal of Multi-body Dynamics*, **227**(1)(2013), 23-33.
- [18] G. Dimitriadis, *Introduction to Nonlinear Aeroelasticity*, Aerospace, Wiley, Chichester, West Sussex, U.K., 2017.

- [19] A. Tamer, *Aeroelastic response of aircraft wings to external store separation using flexible multibody dynamics*, *Machines*, **9**(3)(2021), 61.
- [20] B. H. K. Lee, L. Y. Jiang, Y. S. Wong, *Flutter of an airfoil with a cubic restoring force*, *J. Fluids Struct.*, **13**(1999), 75–101.
- [21] D. Li, S. Guo, J. Xiang, *Aeroelastic dynamic response and control of an airfoil section with control surface nonlinearities*, *J. Sound Vib.*, **329**(2010), 4756–4771.
- [22] A. Abdelkefi, R. Vasconcellos, A. H. Nayfeh, M. R. Hajj, *An analytical and experimental investigation into limit-cycle oscillations of an aeroelastic system*, *Nonlinear Dyn.*, **71**(2013), 159–173.
- [23] B.H.K. Lee, L. Liu, K.W. Chung. *Airfoil motion in subsonic flow with strong cubic nonlinear restoring forces*, *J. Sound Vib.*, **281**(2005), 699–717.
- [24] K. Geist, U. Parlitz, W. Lauterborn, *Comparison of different methods for computing Lyapunov exponents*, *PTEP. Prog. of Theor. Phys*, **83**(5)(1990), 875–893.
- [25] P. Masarati, A. Tamer, *The real schur decomposition estimates Lyapunov characteristic exponents with multiplicity greater than one*, *Proceedings of the Institution of Mechanical Engineers, Part K: Journal of Multi-body Dynamics*, **230**(4)(2016), 568–578.
- [26] D. Hodges, G. A. Pierce, *Introduction to Structural Dynamics and Aeroelasticity*, Cambridge University Press, Cambridge, England, 2002.
- [27] J. R. Wright, J. E. Cooper, *Introduction to Aircraft Aeroelasticity and Loads*, John Wiley & Sons, 2007.
- [28] W.A. Silva, R.E. Bartels, *Development of reduced-order models for aeroelastic analysis and flutter prediction using the cf3dv6.0 code*, *J. Fluids Struct.*, **19**(6)(2004), 729–745.
- [29] J. W. Edwards, H. Ashley, J. V. Breakwell, *Unsteady aerodynamic modeling for arbitrary motions*, *AIAA Journal*, **17**(4)(1979), 365–374.
- [30] A. Medio, M. Lines, *Nonlinear Dynamics — A Primer*, Cambridge University Press, 2001.